STUDIES ON THE SCATTERING OF STEADY STATE AND TRANSIENT ELECTROMAGNETIC WAVES BY IMPERFECTLY CONDUCTING AND COATED STRUCTURES

by

ABDELRAZIK A. SEBAK

B.Sc. E.E., Cairo University, 1976
B.Sc. Appl. Math., Ain-Shams University, 1978
M.Eng. E.E., University of Manitoba, 1982

A thesis
presented to the University of Manitoba
in partial fulfillment of the
requirements for the degree of
Doctor of Philosphy
in
Electrical Engineering

Winnipeg, Manitoba, 1984

STUDIES ON THE SCATTERING OF STEADY STATE AND TRANSIENT ELECTROMAGNETIC WAVES BY IMPERFECTLY CONDUCTING AND COATED STRUCTURES

by

Abdelrazik A. Sebak

A thesis submitted to the Faculty of Graduate Studies of the University of Manitoba in partial fulfillment of the requirements of the degree of

DOCTOR OF PHILOSOPHY

ABSTRACT

Impedance boundary conditions are used with the method of moment to develop a simple and efficient numerical procedure for treating problems of electromagnetic scattering from finite, imperfectly conducting and coated objects. Both electric and magnetic type integral equations are obtained and used to formulate a combined integral equation. The accuracy of the solutions using these methods is studied for bodies of revolution and the superiority of the combined form is pointed out. The problem of internal resonances is also investigated. For both electric and magnetic integral equations, the inaccuracy of the solutions near resonances depends on the magnitude and phase of the surface impedance. The combined formulation is found to give stable solutions throughout. It is then used to generate scattering data for various objects, and the effect of the object parameters and the field polarization on the results is discussed.

An approximate numerical method for treating the problem of scattering from arbitrarily-shaped objects is then presented. Initially, the electric surface current is determined from the solution of the magnetic field integral equation and neglecting the effect of the magnetic surface current. The impedance boundary conditions are then used to obtain the magnetic surface current from the computed electric current. The method is applied to different objects of varying shapes and surface impedances and the computed results are compared with the direct integral equation solutions. It is found that the accuracy of

the results is reasonable, but depends both on the object's geometry and its surface impedance. The results also show that the method predicts the backscattered field accurately for all surface impedance types.

The frequency domain data obtained using the above method is then transformed to the time domain. The transform technique is used to determine the transient response of imperfectly conducting and permeable objects. The excitation is assumed in this part to be due to a periodic pulse train and generated by a small loop antenna. Representative computed data for the induced voltage in a receiver loop antenna are presented for spheroids with different geometrical parameters and surface impedances. The dependence of the response forms on the spheroid parameters and orientation are also discussed.

ACKNOWLEDGEMENTS

I wish to express my heart felt gratitude to Dr. L. Shafai for both his academic and personal assistance, advice and encouragement throughout the course of this investigation. I am also indebted to him for taking the time to read and evaluate my thesis through his invaluable suggestions.

Special thanks are due to Professor E. Bridges and Dr. D. Trim, the members of my advisory committee, for many valuable comments during my Ph.D. program.

I am grateful to Dr. Yogadhish Das of the Defence Research Establishment Suffield, Alberta, for his valuable advice and discussions and who responded generously to all requests for information in regard to the time domain study. I also wish to thank Dr. A. Mohsen of Cairo University, for his suggestions at the beginning of this study.

I also express my deep appreciation to my colleague Dr. G. Kumar for his expert reviewing of the first manuscript of this thesis and for long hours of helpful discussions.

Extended thanks to my mother for her constant support and encouragement and for her willingness to postpone her own plans for my education. Unfortunately, she was not able to see the completion of the thesis as she died in a tragic situation two years ago. I would like to dedicate this thesis to her memory.

Thank you, Karima, for never asking why it was taking so long and for patience to stay nights waiting for me.

This research has been carried out in part with funds granted by the Defence Research Establishment Suffield, Alberta. Their support is gratefully acknowledged. I also acknowledge the financial assistance provided by the University of Manitoba through a Graduate Fellowship. Full recognition and thanks are due to the National Sciences and Engineering Research Council of Canada and Department of Electrical Engineering, University of Manitoba for their financial assistance. I also wish to thank Ms. L. Ramsay and the general office staff of the Department of Electrical Engineering, University of Manitoba for their kind help and cooperation.

TABLE OF CONTENTS

LIST OF FIGURES

LIST OF TABLES

Chapter One

INTRODUCTION

The problem of electromagnetic scattering from finite bodies has been studied by many investigators. In the past, the frequency domain analysis was the primary means of analyzing and solving electromagnetic scattering problems. However, the widescale introduction of computers, capable of performing rapid computations involving large numbers of iterations, soon made time domain analysis feasible.

For target identification problems, the transient or impulse response is particularly useful, since it contains electromagnetic scattering information about the target. More importantly, it is closely related to the target geometry. Much of the work on the electromagnetic transient solutions [1]-[5] came from programs for object identification using short pulse radars or electromagnetic pulsation. The measurements or calculations were carried out by illuminating the target with a pulse train (or smooth impulse) waveform. The resulting response contains most of the information about the electromagnetic scattering properties of the target over the frequency band that is defined by the spectrum of the incident waveform.

The decision to employ the frequency or time domain solution for scattering problems depends on several factors. One of these factors is the type of data required to be analyzed, while others are required computer time, memory and their cost. To compare these two approaches

and their relative advantages and disadvantages, particularly in terms of computer memory and execution time, consider a general scattering problem. When an electromagnetic wave is incident on a scatterer, it induces currents on the surface. These currents radiate and produce the scattered fields. This problem may be solved, in either the frequency domain [6]-[8] or time domain [9] by constructing integral equations for the currents on the surface of the body. The theoretical formulations and solution procedure have been summarized in [10]. Once these currents are determined, the problem is essentialy solved, since the scattered fields can be computed directly from the surface currents. Because the system matrix in the frequency domain is independent of the incident wave, considerable saving results if the solution for a large number of incident waves arriving from different directions is desired. In contrast, the time domain solution for a scattering problem is constructed by marching on in time [9]. Thus, the solution obtained is clearly valid only for an incident wave arriving from a particular direction. If scattering data at a single frequency is desired, then the frequency domain is the most efficient one. On the other hand, when the scattering data for early times is desired, then all the frequency domain solutions up to the maximum effective frequency must be transformed. In such a case, the time domain approach will be more efficient, since the response for only a short time period need be evaluated.

From a computer storage point of view, and except for very small bodies, the time domain approach is always more efficient. It normally requires less computer memory.

The electromagnetic transient of an object may be obtained either through transformation of the frequency domain scattering data (transform technique), or through direct solutions of space-time dependent integral equations in the time domain (direct technique). A comparative study for both techniques is given by Mittra [9], which describes the relative merit of each technique in the transient response computation. One of the objectives of this thesis is to consider a procedure for efficient computation of the transient electromagnetic response of imperfectly conducting bodies with an impedance boundary condition. The transient behaviour of a body is obtained from the Fourier series of its corresponding frequency domain characteristics (i.e., using the transform technique). It is shown how the computed data can be exploited to relate the transient response of an object to its geometrical parameters and material constitutions.

The selection of the transform technique using the frequency domain solution is based on the fact that no expression is available for the concept of impedance boundary conditions (*IBC*) in the time domain. In addition, for target identification applications, more than one incident wave is required which also improves the efficiency of the computation. A method of approximating the exact solution to electromagnetic scattering problems for any source frequency is presented. It is based on obtaining the induced surface currents from those induced on the surface of a perfectly conducting one, through the use of *IBC*.

Chapter Two

SURVEY OF LITERATURE

2.1 SCATTERING BY IMPERFECTLY CONDUCTING OBJECTS:

The problem of scattering of electromagnetic waves by imperfect conductors of irregular geometrical shape is of great interest to many investigators. Most of the analytic solutions of such a problem are restricted to cases where the scatterer has a complete cylindrical [11], spherical [12] or spheroidal [13] symmetry. These solutions have been obtained using the classical method of separation of variables to solve the wave equation inside and outside the body. The complete electromagnetic field in the exterior region consists of the sum of the given incident fields $(\vec{E}^i, \vec{H}^i)$ and the fields scattered by the object $(\vec{E}^s, \vec{H}^s)$, wherein the total fields generated within the object are given by the transmitted fields which are denoted by $(\vec{E}^t, \vec{H}^t)$ in Fig. 2.1. Both the scattered and transmitted fields must obey the vector Helmholtz equation of the form

$$\nabla^2 \vec{E} + k'^2 \vec{E} = 0 \qquad (2-1)$$

$$\nabla^2 \vec{H} + k'^2 \vec{H} = 0 \qquad (2-2)$$

with k' being the propagation constant of the medium.

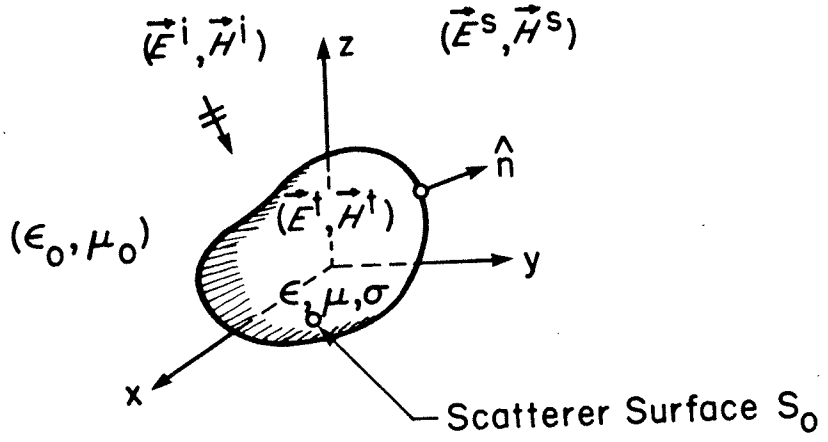

Figure 2.1: Scattering geometry.

For simple geometries, both the scattered and transmitted fields may be expanded in terms of vector wave functions (cylindrical or spherical) with unknown expansion coefficients. These unknown coefficients are determined by application of the boundary conditions which must be satisfied at each point on the scattering surface. In this case, the boundary conditions take the form,

$$\hat{n} \times (\vec{E}^i + \vec{E}^s - \vec{E}^t) = 0 \qquad (2-3)$$

$$\hat{n} \times (\vec{H}^i + \vec{H}^s - \vec{H}^t) = 0 \qquad (2-4)$$

where $\hat{n}$ is any unit vector normal to the surface S_o at each point.

These solutions are well-known for certain simple bodies such as cylinders [11], spheres [12] and ellipsoids [13] and have been used for evaluation of newly developed approximate and numerical techniques. To treat objects of more general shape, asymptotic and numerical approaches are the most attractive ones. At two extreme frequency limits, the Rayleigh approximation [14] is used at low-frequencies and the geometrical theory of diffraction [15] is utilized at high-frequencies. However, both techniques are often unsatisfactory in the so called resonance region (the range of frequencies for which the largest dimension of the body is comparable with the wavelength λ) which requires the rigorous solution of Maxwell's equations. On the other hand, numerical methods such as the extended boundary condition [16], finite element method [17], characteristic modes [18] and the method of moment [19],[20] have proven their effectiveness over a wide range of frequencies. Most of these methods are based on obtaining eletromagnetic sources on the object's surface (i.e., an electric current $\vec{J}$ and a magnetic current $\vec{M}$) which can be used to compute the scattered field. Limitations of these type of solutions are the electrical size of the scatterer and the degree of its geometrical complexity. In this thesis, a general approach for bodies with impedance boundary conditions is presented. It uses the method of moment to solve integral equations on the surface of the body which supports unknown surface currents. Derivation of such integral equations and their numerical solution procedure are presented in detail in *Chapters Three and Four.*

2.2 IMPEDANCE BOUNDARY CONDITIONS APPROXIMATIONS:

The calculation of scattering of electromagnetic waves by penetrable objects can be simplified considerably by solving the wave equation only exterior to the body's surface and subject to the impedance boundary conditions. The impedance boundary conditions, which are widely used in scattering problems, in which it is desirable to take into account the material constitution and/or surface characteristics of the body, are based on the assumption that there is no penetration of the fields inside the scatterer. They relate the tangential components of the electric field to those of the magnetic field through an impedance factor, which is a function of the object's geometry and material.

2.2.1 Physical Implementation Of The Impedance Boundary Conditions:

Consider an electromagnetic wave incident upon a highly conducting body surrounded by free space as shown in Fig. 2.1. Let $\varepsilon_o, \mu_o, z_o = \sqrt{\mu_o/\varepsilon_o}$ and $k = \omega\sqrt{\varepsilon\mu}$ be respectively, the permittivity, permeability, intrinsic impedance and propagation constant of free space; let ε, μ and σ be the permittivity, permeability and conductivity of the body material, and a time-dependence $exp(j\omega t)$ is assumed throughout. The propagation constant of the body $k' = \sqrt{-j\omega\mu(j\omega\varepsilon+\sigma)}$ is then much larger than that of the surrounding medium k. This implies that the wavelength $\lambda' = 2\pi/|\mathrm{Im}(k')|$ inside the body is very much smaller than the wavelength outside. Thus, the field distribution at any point inside the body is determined by the field distribution over the body's surface. As λ' is much smaller than the wavelength outside the body,

the changes of the outside field over a distance λ' is very small. Thus, when considering the field inside a highly conducting body, one may assume that the generating field over the body's surface is approximately constant (i.e., the surface of the conductor is approximately an equiphase surface). This means that the structure of the field inside the body is approximately the same as that of a plane wave propagating perpendicularly to the object's surface. However, for a plane wave inside a homogeneous medium, the ratio of the tangential components of electric and magnetic fields over a plane normal to the propagation direction is constant and equal to the intrinsic impedance of the medium. Consequently, in this approximation, the surface of the body will manifest a surface impedance Z_s equal to the intrinsic impedance Z_c of the body

$$Z_c = \sqrt{\frac{j\omega\mu}{j\omega\varepsilon + \sigma}} \qquad (2\text{-}5)$$

The concept of the impedance surface is, of course, not new and has long been used in varieties of electromagnetic wave scattering problems and was first described by Leontovich in 1948. The concept of Leontovich boundary condition or *IBC* can be written (on the surface S_o of a body) as [21],

$$\vec{E} - (\hat{n} \cdot \vec{E})\hat{n} = Z_s(\hat{n} \times \vec{H}) \qquad (2\text{-}6)$$

Here, $\hat{n}$ is a unit vector along the outward normal to S_o, and $\vec{E}$ and $\vec{H}$ are the total electric and magnetic fields respectively on S_o. The quantity

Z_S is the surface impedance of the body. Leontovich approximation for Z_S is a constant value over S_o, and is equal to the intrinsic impedance Z_C of the object. Another form of Equ. (2-6) may be expressed in its simplest form as [22],

$$\vec{M} = Z_S(\vec{J} \times \hat{n}) \tag{2-7}$$

where the tangential field components at the surface S_o of the body have been expressed in terms of the effective electric and magnetic surface currents

$$\vec{M} = - \hat{n} \times \vec{E} \tag{2-8}$$

$$\vec{J} = + \hat{n} \times \vec{H} \tag{2-9}$$

In terms of the normal components of the fields on S_o, Senior [23],[24] has pointed out that the form of the *IBC* on closed curved surfaces may be written as:

$$\frac{\partial E_n}{\partial n} = jkZ_S/Z_o \; E_n \tag{2-10}$$

$$\frac{\partial H_n}{\partial n} = jkZ_o/Z_S \; H_n \tag{2-11}$$

where E_n and H_n are the field components normal to the boundary. However, this is true only at boundaries for which the metric coefficient

$$h_u = \left| \frac{\partial r}{\partial u} \right| \tag{2-12}$$

in a general coordinate system (u,v,n) is constant. This implies that Equ. (2-10) and (2-11) are true on spherical and right circular cylindrical surfaces but not for example, on spheroidal surfaces.

For closed bodies, the *IBC* method gives good results for scattering problems provided that the following restrictions are satisfied [23]:

a) the skin depth δ is very small compared with the radii of curvature of the body and the effective wavelength inside the body λ',

b) the smallest radius of curvature at any point on the body's surface is large compared with λ', and

c) $| Z_s/Z_o | << 1$.

Garbacz [25] has investigated a special case of bistatic scattering from a class of lossy dielectric spheres and has derived expressions for the bistatic cross sections of these spheres in terms of a fixed surface impedance. Using the same approach, Wait and Jackson [26] have presented many numerical results of the scattering by an impedance sphere assuming various surface conditions. An integral equation for the scattering by a metallic cylinder with arbitrary cross section and using *IBC* has been obtained by Andreasen [27] but no numerical results have been presented. Godzinski [28] has investigated the concept of the *IBC* as applied to the theory of radio-wave propagation over an inhomogeneous earth. He has represented the earth by many homogeneous spherical layers having constant electrical parameters, which are independent of frequency. Due to the analytical complications, he has

only presented his computed results for the case where the earth is approximated by two layers.

The usefulness of the impedance boundary conditions to determine the scattered field has been studied previously for circular cylindrical [29],[30] and spherical [25],[26] objects. The scattering of electromagnetic waves from bodies composed of electrically dissimilar material [31] and from entirely or partially corrugated surfaces [22],[32]-[35] has been solved by representing their surfaces by variable surface impedances. The results of these investigations indicated that the representation of imperfectly conducting objects with impedance boundary conditions is reasonable and has proven to be a very useful tool in obtaining solutions to exterior electromagnetic scattering problems.

2.2.2 *Curvature Dependent Surface Impedance:*

A modification of the method to treat the problem of homogeneous imperfectly conducting objects, with small radii of curvature, has been pointed out by Mitzner [30]. An integral equation was obtained to relate the induced surface currents on the boundary which includes curvature dependent factors. The corrected form of the boundary conditions are

$$M_u(\vec{r}) = -(1 - q(\vec{r}))\, Z_c J_v(\vec{r}) \tag{2-13}$$

$$M_v(\vec{r}) = +(1 + q(\vec{r}))\, Z_c J_u(\vec{r}) \tag{2-14}$$

where (M_u, M_v) and (J_u, J_v) are the (u,v) components of the magnetic and electric surface currents, respectively. The parameter $q(\vec{r})$ is defined by

$$q(\vec{r}) = \tfrac{1}{4}(1 - j)\ \delta\ (\kappa_v(\vec{r}) - \kappa_u(\vec{r})) \qquad (2\text{-}15)$$

and u and v are principal curvature coordinates such that

$$\hat{u} \times \hat{v} = \hat{n} \qquad (2\text{-}16)$$

and κ_u and κ_v are principal curvatures. Excellent agreement with the exact solutions is obtained when this corrected form is utilized.

2.2.3 *Source Dependent Surface Impedance:*

Wait has considered the exact analysis for the field associated with the external excitation of both homogeneous cylinders of infinite length [36] and spheres [37]. He has shown that the impedance matrix Z depends explicitly on the sources. However, if the conductivity of the body is sufficiently high, the elements of the impedance matrix tend to depend primarily on the body structure. Idemen [38] has pointed out that at certain critical frequencies, which are functions of the body characteristics, a certain impedance relation becomes exact, which does not depend on the source.

2.3 *ELECTROMAGNETIC TRANSIENT:*

Since more information may be obtained by transient analysis than from steady state results, the electromagnetic transient analysis has received increasing attention in recent years [39]-[47]. The use of transient response waveforms to describe the scattering properties of objects offers certain advantages over the conventional frequency domain analysis. For example, the geometrical and physical properties of a scatterer may be related to certain features of the backscattering waveforms.

The transient behaviour of a scatterer is conventionally obtained from a Fourier transform of its corresponding frequency domain characteristics (transform technique), or through the solution of a space-time dependent integral equation directly in the time domain (direct technique). Numerical methods for deriving the frequency and time responses of perfectly conducting bodies are now routinely used for a variety of practical problems, thus making them tractable approaches for the transient analysis. The following two sub-sections review the electromagnetic integral equations, for both techniques when applied to perfectly conducting objects.

2.3.1 *Transform Technique:*

The general scattering problem is depicted in Fig. 2.1. The incident magnetic field $\vec{H}^i$ sets up currents on the surface of the scattering body. These currents radiate and produce the scattered fields. In the frequency domain, the integral equation for the surface current $\vec{J}$, on a perfectly conducting surface S_o, is given by [10],

$$\vec{J}(\vec{r}) = 2\hat{n}(\vec{r}) \times \vec{H}^{i}(\vec{r}) + 2\hat{n}(\vec{r}) \times \int_{S_o} \vec{J}(\vec{r}') \times \nabla' G(\vec{r},\vec{r}')\, ds' \tag{2-17}$$

where

$\vec{r}$ = position vector to the observation point

$\vec{r}'$ = position vector to the source point

$G(\vec{r},\vec{r}') = \exp(-jk|\vec{r} - \vec{r}'|)/(4\pi|\vec{r} - \vec{r}'|)$

and $\int$ denotes the principal value integral near the Green's function singularities.

The first term of the right hand side of Equ. (2-17) may be considered as the source term and represents the direct influence of the incident field on the current at the observation point $\vec{r}$. The integral term in Equ. (2-17) represents the influence of currents at the surface points on the current at $\vec{r}$.

The frequency domain integral equation is solved by geometrically representing the scatterer by N discrete grid patches and solving the equation using matrix methods. In matrix notation, Equ. (2-17) can be represented as

$$[J] = [J^{inc}] + [a_{ij}]\ [J] \tag{2-18}$$

where $[J]$ is related to the unknown surface current matrix, $[J^{inc}]$ is related to the contribution of the incident field and $[a_{ij}]$ is the scattering matrix. The solution is obtained by inverting the matrix to solve for the surface current $\vec{J}$.

To obtain the transient responses of a scatterer in this method, the frequency response of the scatterer must be obtained over a wide range of frequencies and the results transformed to the time domain. This can be carried out by solving Equ. (2-18) at the required frequency values. An effective approach in obtaining the transient response using this technique is making use of the fact that for lower frequencies, less current samples are needed which allows the patch configuration to vary with frequency. In this case, there is some minimum number of patches to realistically represent the scatterer. This configuration may be kept constant for all frequencies up to some value f_n, after which the number of patches must be increased with the frequency up to the maximum desired frequency.

2.3.2 *Direct Technique:*

In the time domain, the integral equation for the surface currents on a perfectly conducting surface S_o, takes a form similar to Equ. (2-17), namely [10]

$$\vec{J}(\vec{r},t) = 2\hat{n} \times \vec{H}^i(\vec{r},t) + \frac{1}{2\pi}\hat{n}(r) \times \oint_{S_o} L\hat{J}(\hat{r}',\tau) \times \hat{R}\, ds' \qquad (2\text{-}19)$$

where

$$R = |\vec{r} - \vec{r}'|$$

t = time in units of light-meters (where one light-meter is the time taken by light to travel one meter)

$$\tau = t - R$$

$$\hat{R} = \vec{R}/|\vec{R}|$$

and

$$L = \frac{1}{R^2} + \frac{1}{R} \frac{\partial}{\partial t}$$

The first term in the right-hand side of Equ. (2-19) may be considered as the source term and represents the direct influence of the incident field on the current at the observation point $(\vec{r},t)$. The integral term on the right-hand side of Equ. (2-19) represents the influence of currents at other surface points at earlier points in time on the currents at $(\vec{r},t)$. It is this delay in time by R that allows the equation to be solved by a 'marching on in time' procedure. Details of the numerical solutions of Equ. (2-19) are given in [10]. Again the scatterer surface is represented by discrete grid patches. The currents are computed by starting at a point in time, before the incident field has arrived at the scatterer, and simply stepping on in time. The time step is chosen to not exceed the minimum spacing between patches so that all terms on the right-hand side of Equ. (2-19) have either been specified or previously computed. As can be seen, the numerical solution does not involve a matrix inversion which is an advantage. A disadvantage is that the computation has to be repeated for a different angle of incidence.

2.4 *INVERSE SCATTERING:*

The inverse scattering problem consists of determining the material constitution and the geometry of an unknown scatterer from the given information about the incident field upon the scatterer and the measured response of the scatterer due to that field. Most early attempts to solve inverse scattering problems were carried out in the frequency domain. For perfectly conducting objects, the geometrical parameters

which characterize the scatterer can be determined from the transverse components of the far-zone scattered electric field measured at different aspect angles. This approach has been used to calculate the electric radius of a cylinder [48], sphere [49] and the interfocal distance and the eccentricity of a prolate spheriod [50]. In all these cases, it was assumed that the scatterer is a perfect conductor and its shape is known prior to the computation.

Time domain techniques for inverse scattering problems were first introduced by Kennaugh and Cosgriff [51]. They used the physical optics approximation to calculate the impulse response of a scatterer that was simply the second derivative of the projected area function of the scatterer. Using the projected area in a plane normal to the line of sight, Das and Boerner [52] used a general theory of Radon transform to reconstruct the shape of perfectly conducting convex targets from their ramp responses. Time domain techniques and others are also studied in a special issue of the IEEE Transaction on Antennas and Propagation on Inverse Methods in Electromagnetics [53].

A special case was considered by Bennett [54], for a rotationally symmetric target under the influence of an axial incident ramp electromagnetic wave. An exact expression which relates the contour of the target ρ as a function of z and the far scattered ramp response field H_R measured at $(\vec{r},t)$ is given by

$$\rho(z,t) = \left[2r_o H_R(\vec{r},t) - \frac{1}{2\pi} \int_{S_o} \left(\vec{J}(\vec{r}',t) - 2\hat{n}(\vec{r}') \times \vec{H}_R^i(\vec{r}',t) \right) \times \hat{r}\, ds' \right]^{\frac{1}{2}} \tag{2-20}$$

where r_o is the distance of the observer from the target. Iterative solutions of Equ. (2-20) and examples are given in [54].

2.5 *OVERVIEW:*

The objective of this thesis is to study the analytical and numerical solutions of steady state electromagnetic scattering problems and make use of the obtained solutions to compute the transient response. The main effort has been conducted toward the analysis of the transient response of imperfectly conducting bodies, and the formulation and numerical solutions of the frequency domain integral equations.

In *Chapters Three and Four* the steady state solutions for scattering from imperfectly conducting bodies of revolution and objects of arbitrary shape are considered. Initially, the surface integral equations involving the unknown surface fields or currents on the boundary are derived. Next, the concept of the impedance boundary conditions is used to reduce the order of the matrix equation, in the numerical solution of the problem. The method of moment is then used to compute the surface field distributions. After the unknown surface fields or currents are found, the scattered fields at any point outside the object are determined and the results are compared to the exact eigenfunction solutions for a sphere. The method is initially applied to rotationally symmetric bodies. The approach is then generalized to handle scattering by arbitrarily shaped objects.

Chapter Five presents the formulation of the transient response of imperfectly conducting bodies using the transform technique. The frequency domain data is generated using the method developed in

Chapters Three and Four. For small spheroids, the induced voltages in receive coils are given, as a function of time, at different points in space. The incident fields are generated by a transmit loop carrying an oscillating current at low-frequencies. Application to target identification with the aid of the obtained data is also illustrated.

The ideas presented in this work are summarized in *Chapter Six* which also lists the contributions resulting from the present study. New problems arising out of this work are pointed out and some suggestions are made for their possible solution.

Appendix A briefly reviews eigenfunction solutions for scattering of plane waves by an imperfectly conducting sphere. Both exact and *IBC* solutions are presented. These solutions are used throughout the thesis for testing the numerical method and its applicability to objects of arbitrary shape.

The radiated fields by a small circular current loop are derived in *Appendix B.*

Appendix C gives an example of the oscillation occuring near a discontinuity when a partial sum of the Fourier series is used to represent a square wave.

The most commonly used symbols in this thesis are listed in *Appendix D.*

Chapter Three

SCATTERING FROM IMPERFECTLY CONDUCTING AND IMPEDANCE OBJECTS: BODIES OF REVOLUTION

3.1 INTRODUCTION:

Exact analytic solutions for the problem of electromagnetic wave scattering by perfectly conducting objects are known for a limited number of shapes. These solutions, which are readily known for circular [11] and elliptic [55] cylinders, and spherical [12] and spheroidal [13],[56] objects, play an important role in the investigation of scattering problems. Aside from providing exact solutions for their respective geometries, they are invaluable in the evaluation of approximate and numerical solutions. Unfortunately, some of these solutions, in particular those for spheroidal objects, are complex in form and are difficult to evaluate. For spheroidal objects, not only is the evaluation of the spheroidal functions difficult [57]-[59], but also the solution needs a matrix inversion of the same order as that of the matrix equation in a numerical solution of the problem using the method of moment [60].

For an object of arbitrary shape, such an analytic solution is usually not feasible and an approximate or numerical solution must be obtained. The problem becomes even more difficult to solve when the object is neither perfectly conducting nor perfectly dielectric. In such cases, the integral equation method can be utilized to generate a

useful formulation. An application of the method to objects that are not perfectly conducting involves the integral representation of the field vectors for both the interior and exterior to the body. Enforcing the boundary conditions provides a set of integral equations for the unknown surface electric and magnetic fields. These integral equations can be solved by a variety of methods and are widely used in the investigation of scattering by axisymmetric objects [61]-[65] and bodies of arbitrary shape [8],[66]. Each method has a range of applicability which is generally limited by the form of the incident field and the size and complexity of the geometry.

One of the most successful methods is the method of moment [19],[20], where the integral equations are solved by expanding the unknown surface current distributions in series of suitable basis functions. Utilizing a set of testing functions, together with the evaluation of their moments, the integral equations can be reduced to a set of simultaneous linear equations, a solution of which gives the required surface current distribution. The method, while being generally applicable to any scattering problem, is limited by the storage and computation time of available computers. This limitation is most severe for penetrable bodies wherein existence of both equivalent electric and magnetic surface currents increases the size of the resulting matrix compared with the perfectly conducting case. In such a case and for a given object size, this larger matrix size results in more costly solutions or, alternatively, in less accurately calculated surface currents. However, if only far field patterns are desired, and not currents, then less accuracy may be tolerated in the solution of the

matrix system. This is due to the fact that the accuracy of the far field data is generally better than that of the surface currents.

Another method of the scattering matrix formulation, which could be classified as an integral equation method, has been developed by Waterman [68]. It is called the extended boundary condition method, and provides a general formulation for scattering from bodies of arbitrary size and shape, with sizes from the Rayleigh region to the geometrical optics limit. This method originally published for perfectly conducting bodies [67] was later extended by Waterman himself to dielectric bodies [68].

Both of the above methods can be applied successfuly to problems that involve a finite space region. For open region space problems, the boundary element method [69] is one of the most successful methods. It is an extension of the finite element method and is more attractive in the structure engineering research areas.

Another method dealing with the numerical solutions of integral equations in field problems has been introduced by Mei [70]. It is known as the unimoment method. It is a combination of finite elements and method of moment and is based on replacing the integral equations by finite difference or finite element equations. Its ability to formulate inhomogeneous structure problems [71] is one of its advantages in engineering applications.

In this chapter, the scattering of an electromagnetic wave by a homogeneous penetrable body of revolution is investigated. An integral equation formulation is utilized and the concept of impedance boundary conditions is used to simplify the formulation and reduce the

computational efforts. For imperfectly conducting objects with a relatively thin coating, the impedance boundary conditions are reasonable and eliminate the need for the inclusion of the integral equation interior to the body. The problem is solved by three different formulations: the electric field integral equation, the magnetic field integral equation and a linear combination of both.

3.2 *PROBLEM STATEMENT:*

Figure 3.1 shows the scattering structure to be considered. The scattering object is a homogeneous body and has a conductivity σ, permeability μ and permittivity ε and bounded by a closed surface S_o. It is illuminated by an incident electromagnetic wave represented by its electric and magnetic fields $\vec{E}^i$ and $\vec{H}^i$, respectively. The permeability, permittivity and intrinsic impedance of the surrounding medium are respectively, μ_o, ε_o and $Z_o = \sqrt{\mu_o/\varepsilon_o}$.

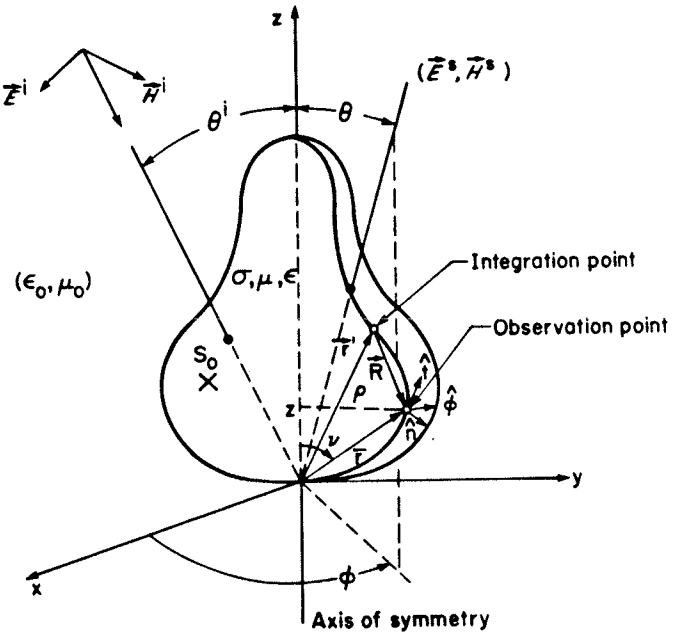

Figure 3.1: Geometry of an imperfectly conducting body of revolution.

The scattered electric field $\vec{E}^s$ and magnetic field $\vec{H}^s$ outside the body surface can be computed in terms of equivalent surface currents $\vec{J}$ and $\vec{M}$ using

$$\vec{E}^s = - j\omega\mu_o \vec{A}(\vec{J}) + \frac{1}{j\omega\varepsilon_o} \nabla\Phi(\vec{J}) - \nabla \times \vec{F}(\vec{M}) \tag{3-1}$$

$$\vec{H}^s = - j\omega\varepsilon_o \vec{F}(\vec{M}) + \frac{1}{j\omega\mu_o} \nabla\Psi(\vec{M}) + \nabla \times \vec{A}(\vec{J}) \tag{3-2}$$

with the magnetic vector potential $\vec{A}$ and electric vector potential $\vec{F}$ defined as

$$\vec{A}(\vec{J}) = \int_{S_o} \vec{J}\, G\, ds' \tag{3-3}$$

$$\vec{F}(\vec{M}) = \int_{S_o} \vec{M}\, G\, ds' \tag{3-4}$$

and the scalar potential Φ and Ψ as

$$\Phi(\vec{J}) = \int_{S_o} (\nabla'_s \cdot \vec{J})\, G\, ds' \tag{3-5}$$

$$\Psi(\vec{M}) = \int_{S_o} (\nabla'_s \cdot \vec{M})\, G\, ds' \tag{3-6}$$

where $G = exp(-jkR)/4\pi R$ is the free space scalar Green's function, $R = |\vec{r} - \vec{r}'|$ is the distance from a source point $\vec{r}'$ on S_o to a field point $\vec{r}$, and $\vec{J}$ and $\vec{M}$ are the equivalent surface electric and magnetic currents, yet to be determined. A harmonic time-dependence $exp(j\omega t)$ is assumed and suppressed, and $k = \omega\sqrt{\mu_o \varepsilon_o} = 2\pi/\lambda$, where λ is the wavelength.

For objects of arbitrary material constitution, where fields penetrate inside the object, the internal fields are given by

$$\vec{E}^t = -j\omega\mu\vec{A}(\vec{J}') + \frac{1}{j\omega\varepsilon'}\nabla\Phi(\vec{J}') - \nabla \times \vec{F}(\vec{M}') \tag{3-7}$$

$$\vec{H}^t = -j\omega\varepsilon'\vec{F}(\vec{M}') + \frac{1}{j\omega\mu}\nabla\Psi(\vec{M}') + \nabla \times \vec{A}(\vec{J}') \tag{3-8}$$

where $\varepsilon' = \varepsilon + \sigma/j\omega$ and $\vec{J}'$ and $\vec{M}'$ are equivalent surface current sources for the internal fields and should satisfy the conditions

$$\vec{J} + \vec{J}' = 0 \tag{3-9}$$

$$\vec{M} + \vec{M}' = 0 \tag{3-10}$$

The integral equations for $\vec{J}$ and $\vec{M}$ are derived by enforcing the boundary conditions

$$\hat{n} \times (\vec{E}^i + \vec{E}^s - \vec{E}^t) = 0 \tag{3-11}$$

$$\hat{n} \times (\vec{H}^i + \vec{H}^s - \vec{H}^t) = 0 \tag{3-12}$$

which satisfy the continuity of the tangential electric and magnetic field components on S_o. Substituting from Equs. (3-1) through (3-10) for $\vec{E}$'s and $\vec{H}$'s in Equs. (3-11) and (3-12), and taking the limits as $\vec{r}$ approaches $\vec{r}'$ from outside in the R.H.S. of Equs. (3-11) and (3-12) and limits as $\vec{r}$ approaches $\vec{r}'$ from inside in the L.H.S., results in a set of coupled integral equations for $\vec{J}$ and $\vec{M}$. They are

$$\hat{n} \times \vec{E}^{i}(\vec{r}) = \hat{n} \times \oint_{S_o} \Big(j\omega\mu_o \vec{J}(\vec{r}\,')G(\vec{r},\vec{r}\,') - \frac{1}{j\omega\varepsilon_o}(\nabla'_s \cdot \vec{J}(\vec{r}\,'))$$

$$\cdot\nabla G(\vec{r},\vec{r}\,') - \vec{M}(\vec{r}\,') \times \nabla G(\vec{r},\vec{r}\,') + j\omega\mu\vec{J}(\vec{r}\,')G'(\vec{r},\vec{r}\,')$$

$$- \frac{1}{j\omega\varepsilon'}(\nabla'_s \cdot \vec{J}(\vec{r}\,'))\nabla G'(\vec{r},\vec{r}\,') - \vec{M}(\vec{r}\,') \times \nabla G'(\vec{r},\vec{r}\,') \Big)\, ds' \tag{3-13}$$

and

$$\hat{n} \times \vec{H}^{i}(\vec{r}) = \hat{n} \times \oint_{S_o} \Big(\vec{J}(\vec{r}\,') \times \nabla G(\vec{r},\vec{r}\,') + j\omega\varepsilon_o \vec{M}(\vec{r}\,')G(\vec{r},\vec{r}\,')$$

$$- \frac{1}{j\omega\mu_o}(\nabla'_s \cdot \vec{M}(\vec{r}\,'))\nabla G(\vec{r},\vec{r}\,') + \vec{J}(\vec{r}\,') \times \nabla G'(\vec{r},\vec{r}\,')$$

$$+ j\omega\varepsilon'\vec{M}(\vec{r}\,')G'(\vec{r},\vec{r}\,') - \frac{1}{j\omega\mu}(\nabla'_s \cdot \vec{M}(\vec{r}\,'))\nabla G'(\vec{r},\vec{r}\,') \Big)\, ds' \tag{3-14}$$

where G' is the scalar Green's function inside the object. In derivation of Equs. (3-13) and (3-14), the following relations [72] are employed in the limiting process

1) The integrals

$$\int_{S_o} \vec{J}(\vec{r}\,')G(\vec{r},\vec{r}\,')\, ds' \text{ and } \int_{S_o} (\nabla'_s \cdot \vec{J}(\vec{r}\,'))\nabla G(\vec{r},\vec{r}\,')\, ds'$$

are continuous for all $\vec{r}$.

2) $$-\hat{n}(\vec{r}) \times \lim_{\vec{r}\to\vec{r}'} \int_{S_o} \vec{J}(\vec{r}\,') \times \nabla G(\vec{r},\vec{r}\,')\, ds' = \pm\tfrac{1}{2}\vec{J}(\vec{r}) - \oint_{S_o} \hat{n}(\vec{r}) \times [\vec{J}(\vec{r}\,') \times \nabla G(\vec{r},\vec{r}\,')]\, ds'$$

The plus and minus signs in Equ. (3-15) correspond, respectively, to approaches from the outside and inside of S_o along the normal $\hat{n}(\vec{r})$. The integral equations (3-13) and (3-14) constitute four coupled two dimensional scalar integral equations and are substantially more difficult to handle than the case of S_o being a perfect conductor.

The solutions of (3-13) and (3-14) may be carried out using the method of moment. However, since both $\vec{J}$ and $\vec{M}$ are nonzero, the resulting matrix equation will be twice as large as that for a perfectly conducting object. This larger size of the matrix is, of course, undesirable and its solution requires excessive storage and computation time. In practice therefore, it is desirable to reduce the matrix size by any suitable approximation to the field equations or the boundary conditions. A useful approximation which considerably simplifies the problem is the use of the impedance boundary conditions to represent a certain class of scattering objects. It is known that imperfectly conducting objects can effectively be represented by impedance boundary conditions on their surfaces, provided that the field penetration is reasonably small [30]. The concept can also be used satisfactorily for perfectly conducting objects with a thin material coating.

The simplification of the matrix equation, due to the impedance boundary conditions, arises because the surface impedance relates the magnetic current $\vec{M}$ to the electric current $\vec{J}$. Using this relationship, one of the surface currents can be eliminated and the matrix equation can be expressed in terms of either $\vec{M}$ or $\vec{J}$ alone. In particular, if the surface impedance is represented in a dyadic form $\bar{\bar{Z}}$, the boundary conditions provide

$$\vec{M}(\vec{r}) = \bar{\bar{Z}}(\vec{r}) \cdot \vec{J}(\vec{r}) \times \hat{n}(\vec{r}) \qquad (3\text{-}16)$$

which can be used in the scattered field expression to eliminate $\vec{M}$. In this case, the order of the coefficients matrix equation is reduced by a factor of two. This means that the numerical solution of the problem using the impedance boundary conditions is more efficient by a factor of four in terms of both computer time[1] and storage[2] than the classical solutions. The resulting uncoupled equations can be solved independently to obtain $\vec{J}$ and are generally referred to as the electric field integral equation (*EFIE*) and the magnetic field integral equation (*MFIE*).

EFIE

For bodies with impedance boundary conditions, the electric field integral equation is obtained by setting the tangential components of the total electric field equal to zero just inside S_o. In this case, since there are no internal fields, the following condition should be satisfied on S_o

$$\frac{1}{Z_o}\left[\vec{E}^s + \vec{E}^i\right]_{tan} = 0 \qquad (3\text{-}17)$$

The subscript *tan* denotes tangential components on S_o. Substituting for $\vec{E}^s$ from (3-1) to (3-6) in (3-17) and for $\vec{M}$ from (3-16), and taking the limit as $\vec{r} \to \vec{r}'$ from inside, reduces the vector equation (3-17) to the

---

[1] assuming that the matrix inversion of a matrix of order n requires operations of order n^2.

[2] minimum storage allocation of a matrix of order n is n^2.

following coupled scalar equations:

$$\hat{\phi}(\vec{r}) \cdot \vec{E}^{i}(\vec{r}) = -\tfrac{1}{2}\hat{t}(\vec{r}) \cdot \left[\bar{\bar{Z}}(\vec{r}) \cdot \vec{J}(\vec{r}) \times \hat{n}(\vec{r})\right] - \hat{\phi}(\vec{r}) \cdot \oint_{S_o} \left\{\left[\bar{\bar{Z}}(\vec{r}') \cdot \vec{J}(\vec{r}') \times \hat{n}(\vec{r}')\right] \times \nabla G(\vec{r},\vec{r}') - j\omega\mu_o \vec{J}(\vec{r}') G(\vec{r},\vec{r}') + \frac{1}{j\omega\varepsilon_o}(\nabla_s' \cdot \vec{J}(\vec{r}'))\, \nabla G(\vec{r},\vec{r}')\right\} ds' \tag{3-18}$$

and

$$\hat{t}(\vec{r}) \cdot \vec{E}^{i}(\vec{r}) = \tfrac{1}{2}\hat{\phi}(\vec{r}) \cdot \left[\bar{\bar{Z}}(\vec{r}) \cdot \vec{J}(\vec{r}) \times \hat{n}(\vec{r})\right] - \hat{t}(\vec{r}) \cdot \oint_{S_o} \left\{ \begin{matrix} \text{as in} \\ \text{(3-18)} \end{matrix} \right\} ds' \tag{3-19}$$

where $\hat{t}$ and $\hat{\phi}$ are two orthogonal surface unit vectors such that

$$\hat{\Phi}(\vec{r}) \times \hat{t}(\vec{r}) = \hat{n}(\vec{r}) \tag{3-20}$$

MFIE

Again, the magnetic field integral equation for bodies with impedance boundary conditions is obtained by setting the tangential components of the total magnetic field equal to zero just inside S_o, i.e.

$$\hat{n}(\vec{r}) \times \left[\vec{H}^{i} + \vec{H}^{s}\right] = 0 \tag{3-21}$$

After some algebra, Equ. (3-21) reduces to the following coupled scalar equations:

$$\hat{t}(\vec{r}) \cdot \vec{H}^i(\vec{r}) = -\tfrac{1}{2}\hat{\phi}(\vec{r}) \cdot \vec{J}(\vec{r}) + \hat{t}(\vec{r}) \cdot \int_{S_o} \left\{ \vec{J}(\vec{r}') \times \nabla G(\vec{r},\vec{r}') + j\omega\mu_o \left[\bar{\bar{Z}}(\vec{r}') \cdot \vec{J}(\vec{r}') \times \hat{n}(\vec{r}') \right] G(\vec{r},\vec{r}') - \frac{1}{j\omega\varepsilon_o} \left(\nabla_s' \cdot \left[\bar{\bar{Z}}(\vec{r}') \cdot \vec{J}(\vec{r}') \times \hat{n}(\vec{r}') \right] \right) \nabla G(\vec{r},\vec{r}') \right\} ds' \tag{3-22}$$

and

$$\hat{\phi}(\vec{r}) \cdot \vec{H}^i(\vec{r}) = \tfrac{1}{2}\hat{t}(\vec{r}) \cdot \vec{J}(\vec{r}) + \hat{\phi}(\vec{r}) \cdot \int_{S_o} \left\{ \begin{matrix} \text{as in} \\ \text{(3-22)} \end{matrix} \right\} ds' \tag{3-23}$$

Both of the above sets of integral equations (i.e., ***EFIE*** and ***MFIE***) can be used to determine $\vec{J}$ using the method of moment. However, experience with perfectly conducting scatterers has shown that both formulations suffer from instabilities at the internal renonances. To overcome this difficulty, Mautz and Harrington [64] have developed a combined field integral equation (***CFIE***) for perfectly conducting objects that is free from such internal resonance problems. They also have proved the uniqueness of its solution. Using the same approach, a ***CFIE*** for impedance objects can be developed in the form

$$\hat{n} \times \vec{H}^s + \frac{\alpha}{Z_o} \vec{E}^s_{tan} = -\hat{n} \times \vec{H}^i - \frac{\alpha}{Z_o} \vec{E}^i_{tan} \tag{3-24}$$

to be valid just inside the scattering surface S_o. The parameter α in this equation is a real constant and its value must be selected to give the most stable solution of Equ. (3-24). From a theoretical point of

view, the results should be independent of α but no numerical solution can be expected to assure this property. As a matter of fact, α must not be chosen small otherwise Equ. (3-24) is too close to the ***MFIE***. Similarly, if α is too large Equ. (3-24) is not sufficiently far from the ***EFIE***. Its value in all present computations is selected to be 0.2.

The remaining part of this chapter is devoted to examination of solutions using the obove integral equations, (3-17), (3-21) and (3-24). For the scatterer, rotationally symmetric geometries, i.e., bodies of revolution, are selected. Their respective matrix equations are developed and the accuracy of their solutions is investigated.

3.3 FORMULATION OF MATRIX EQUATIONS:

Consider a scatterer that is rotationally symmetric about the z axis as shown in Fig. 3.1 . A point on its surface can be defined by two orthogonal unit vectors $\hat{t}$ and $\hat{\phi}$ such that $\hat{\phi}(\vec{r}) \times \hat{t}(\vec{r}) = \hat{n}(\vec{r})$. The electric current $\vec{J}$ possesses components along both these vectors and can, therefore, be written as

$$\vec{J}(\vec{r}) = \hat{t}(\vec{r})\ J^{t}(t,\phi) + \hat{\phi}(\vec{r})\ J^{\phi}(t,\phi) \qquad (3\text{-}25)$$

where J^{t} and J^{ϕ} are the $\hat{t}$- and $\hat{\phi}$-directed electric current components, respectively. Similarly, the magnetic current $\vec{M}$ has both tangential components which are related to the components of $\vec{J}$ by

$$\begin{aligned}\vec{M}(\vec{r}) &= \bar{\bar{Z}}(\vec{r}) \cdot \vec{J}(\vec{r}) \times \hat{n}(\vec{r}) \\ &= Z^{t}(t)\ J^{t}(t,\phi)\ \hat{\phi}(\vec{r}) - Z^{\phi}(t)\ J^{\phi}(t,\phi)\ \hat{t}(\vec{r}) \qquad (3\text{-}26)\end{aligned}$$

where, in a general case, both z^t and z^ϕ are curvature dependent. For metallic objects of finite conductivity, they are given by [30]

$$z^t(t) = (1 - q(t))\ z_c \tag{3-27}$$

$$z^\phi(t) = (1 + q(t))\ z_c \tag{3-28}$$

with

$$q(t) = \tfrac{1}{4}\ (1 - j)\ \delta\ (\kappa_t(t) - \kappa_\phi(t)) \tag{3-29}$$

and

$$z_c = \sqrt{\frac{j\omega\mu}{j\omega\varepsilon + \sigma}} \tag{3-30}$$

and κ_t and κ_ϕ are principal curvatures of S_o, and δ is the skin depth. For small signal penetrations and for objects with large radii of curvature, both z^t and z^ϕ on the scattering surface can be assumed to be constant and equal to z_c.

Because of the symmetry of the body, in this case, a Fourier series expansion in terms of the rotation angle (i.e, ϕ) can reduce the problem to the solution of a system of orthogonal modes. The major advantage of introducing these Fourier modes is that one can solve the problem mode by mode, due to the mode orthogonality. Obviously, this will result in a much smaller and manageable matrix equation. A numerical solution of the integral equations may then be obtained by expanding $\vec{J}$ in terms of the azimuthal modes and suitable expansion functions on the generating curve. Equation (3-25) can therefore be written as

$$\vec{J}(t,\phi) = \sum_{m=-M}^{M} \sum_{n=0}^{N} \left(a_{mn} \vec{J}^t_{mn}(t,\phi) + b_{mn} \vec{J}^\phi_{mn}(t,\phi) \right) \tag{3-31}$$

where a_{mn} and b_{mn} are coefficients to be determined, and $\vec{J}^{t}_{mn}$ and $\vec{J}^{\phi}_{mn}$ are expansion functions given by

$$\vec{J}^{t,\phi}_{mn} = (\hat{t},\hat{\phi})\, f_n(t)\exp(jm\phi) \qquad \begin{matrix} n = 1,2,..,N \\ m = 0,\pm1,\pm2,.. \end{matrix} \qquad (3\text{-}32)$$

The basis functions $f_n(t)$ are given by

$$\rho\, f_n(t) = \sum_i T_i(t) \qquad i = 1,2,\ldots \;;\; t \in (t_{n-1}, t_{n+2})$$

$$= 0 \qquad \text{otherwise} \qquad (3\text{-}33)$$

where $T_i(t)$ is the impulse approximation to the triangle function as shown in Fig. (3.2) and ρ is the distance from the axis of the body of revolution to t the center point of the domain of T_i.

$$T_1 = \frac{d_1^2}{2(d_1+d_2)} \qquad T_1^{\bullet} = \frac{d_1}{d_1+d_2}$$

$$T_2 = \frac{(d_1+\tfrac{1}{2}d_2)d_2}{d_1+d_2} \qquad T_2^{\bullet} = \frac{d_2}{d_1+d_2}$$

$$T_3 = \frac{(d_4+\tfrac{1}{2}d_3)d_3}{d_3+d_4} \qquad T_3^{\bullet} = \frac{-d_3}{d_3+d_4}$$

$$T_4 = \frac{d_4^2}{2(d_3+d_4)} \qquad T_4^{\bullet} = \frac{-d_4}{d_3+d_4}$$

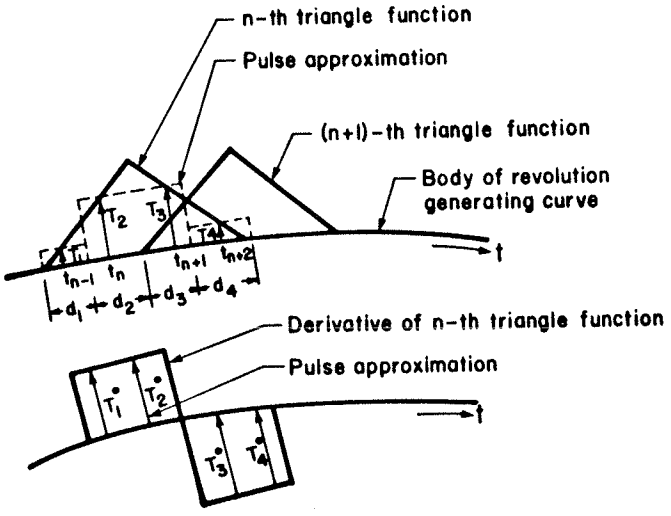

Figure 3.2: Pulse approximation for triangle functions and their derivatives on the surface of the body of revolution.

Several approaches to represent the triangle function $f_j(t)$ and its derivative $f_j^{\bullet}(t)$ have been reported in the literature. The simplest one is to approximate f_j and $f_j^{\bullet}$ by four pulses, denoted by T_i and $T_i^{\bullet}$, respectively, with $i = 1,2,3,4$ where $T_i = \{1/4, 3/4, 3/4, 1/4\}$ and $T_i^{\bullet} = \{1, 1, -1, -1\}$. A more realistic representation of f_j and $f_j^{\bullet}$ is given in [64], where each segment of the generating curve is subdivided into 4 elements and T_i and $T_i^{\bullet}$ vary along the generating curve as shown in Fig. 3.2. The testing functions $\vec{W}_{ln}^{t}$ and $\vec{W}_{ln}^{\phi}$ are defined by

$$\vec{W}_{ln}^{t,\phi} = (\hat{t},\hat{\phi})\, f_n(t)\, \exp(-jl\phi) \qquad n = 1,2,\ldots,N'$$
$$l = 0,\pm 1,\pm 2,.. \qquad (3\text{-}34)$$

to reduce the integral equations to a matrix one. It is common practice to select $N = N'$ (in this case, the general term of the method of moment will be called the Galerkin's method). This is not necessary. However, if $N \neq N'$, the matrix equation will have to be solved by using a generalized inverse of a matrix (i.e., the least square method).

Noticing the sign difference in the exponent between the expansion and testing functions, one can then define the inner product as

$$< \vec{W}, \vec{J} > = \int_{S_o} \vec{W} \cdot \vec{J}\, ds \qquad (3\text{-}35)$$

where $\vec{W}$ and $\vec{J}$ are vectors tangential to S_o. Since $\vec{W}_l$ are orthogonal to $\vec{J}_m$ over 0 to 2π on ϕ for $l \neq m$, all products are zero except those for which $l = m$. This fact allows each mode to be treated completely independent of the other modes. Thus, after testing each side of Equs.

(3-18), (3-19) and (3-22), (3-23) with $\vec{W}_{ln}$, one obtains the generalized matrix equations for each case. The steps leading to the matrix equation are discussed elsewhere, for perfectly conducting surfaces [64], and are omitted here for brevity. Instead, the final form for each matrix equation is given and the coefficient matrices of the impedance objects are related to the corresponding one for perfectly conducting objects.

(a) ***EFIE***

For bodies of revolution with impedance boundary conditions, the ***EFIE*** formulation was developed by Iskander et al. [22]. They have shown that the electric field integral equation can be reduced to a matrix equation of the form

$$\left[Q_m^E \right] \left[I_m \right] = \left[G_m^E \right] \qquad m = 0, \pm 1, \pm 2, \ldots \tag{3-36}$$

where

$$\left[I_m \right] = \begin{bmatrix} a_{mn} \\ \\ b_{mn} \end{bmatrix} \tag{3-37}$$

is the response vector (unknown surface current) of length ***2N***, and

$$\left[G_m^E \right] = \begin{bmatrix} < \vec{W}_{mn}^t, \; 1/Z_o \vec{E}_{tan}^i > \\ \\ < \vec{W}_{mn}^\phi, \; 1/Z_o \vec{E}_{tan}^i > \end{bmatrix} \tag{3-38}$$

is the excitation vector. The moment matrix $[Q_m^E]$ is generally referred to as the impedance matrix. It is an $(2N \times 2N)$ matrix and given by

$$\left[Q_m^E \right] = \begin{bmatrix} [Z_{mn}^{tt,J} + Z_{mn}^{tt,M}] & [Z_{mn}^{t\phi,J} - Z_{mn}^{t\phi,M}] \\ [Z_{mn}^{\phi t,J} - Z_{mn}^{\phi t,M}] & [Z_{mn}^{\phi\phi,J} + Z_{mn}^{\phi\phi,M}] \end{bmatrix} \quad (3-39)$$

In the above equation, the first superscript t refers to the $\hat{t}$-directed current and ϕ to $\hat{\phi}$-directed current, while the second superscript t refers to $\hat{t}$-directed testing function and ϕ to $\hat{\phi}$-directed testing function. Therefore, the elements in the sub-matrix labelled $Z^{t\phi,J}$ relate the $\hat{t}$-directed electric current to the $\hat{\phi}$-directed testing function. The other blocks of the impedance matrix can be interpreted similarly. The sub-matrices $[Z_{mn}^{\alpha\beta,J}]$ for $\alpha,\beta = t$ or ϕ are identical to the respective sub-matrices of the E-field integral equation for perfectly conducting objects [64]. They represent the direct contribution of the equivalent electric current $\vec{J}$. On the other hand, the contribution of the equivalent magnetic current $\vec{M}$ to the coefficient matrix is given by $[Z_{mn}^{\alpha\beta,M}]$ The (i,j)-th elements of the partitioned sub-matrices in Equ. (3-39) are computed from

$$(Z_{mn}^{\alpha\beta,J})_{ij} = jk \int_{S_o} ds \int_{S_o} ds' \left\{ \vec{W}_{mi}^{\alpha}(\vec{r}) \cdot \vec{J}_{nj}^{\beta}(\vec{r}') - \frac{1}{k^2} [\nabla_s \cdot \vec{W}_{mi}^{\alpha}(\vec{r})] \cdot [\nabla_s' \cdot \vec{J}_{nj}^{\beta}(\vec{r}')] \right\} G(\vec{r},\vec{r}') \quad (3-40)$$

$$(Z_{mn}^{tt,M})_{ij} = \pi/Z_o \int_{S_o} d\tau\rho Z^t(t) f_i(t) f_j(t) + k^3/Z_o \int_{S_o} d\tau\rho f_i(t)$$

$$\cdot \int_{S_o} d\tau'\rho' f_j(t') Z^t(t') \left\{ \left((\rho' - \rho)\cos\nu - (z' - z)\sin\nu \right) g_2 \right.$$

$$\left. + g_1 \rho' \cos\nu \right\} \qquad (3\text{-}41)$$

$$(Z_{mn}^{t\phi,M})_{ij} = jk^3/Z_o \int_{S_o} d\tau\rho f_i(t) \int_{S_o} d\tau'\rho' f_j(t') Z^{\phi}(t')$$

$$\cdot \left\{ \rho' \sin\nu \cos\nu' - \rho\cos\nu \sin\nu' - (z'-z)\sin\nu \sin\nu' \right\} g_3$$

$$(3\text{-}42)$$

$$(Z_{mn}^{\phi t,M})_{ij} = jk^3/Z_o \int_{S_o} d\tau\rho f_i(t) \int_{S_o} d\tau'\rho' f_j(t') (z' - z) g_3 \qquad (3\text{-}43)$$

and

$$(Z_{mn}^{\phi\phi,M})_{ij} = \pi/Z_o \int_{S_o} d\tau\rho f_i(t) f_j(t) + k^3/Z_o \int_{S_o} d\tau\rho f_i(t)$$

$$\cdot \int_{S_o} d\tau'\rho' f_j(t') Z^{\phi}(t') \left\{ \left((\rho' - \rho)\cos\nu' - (z' - z) \right.\right.$$

$$\left.\left. \cdot \sin\nu' \right) g_2 - \rho \cos\nu' g_1 \right\} \qquad (3\text{-}44)$$

where z is the rectangular coordinate along the axis of the body of revolution and ν is the angle between $\hat{t}$ and z axis. The values of i and j in Equs. (3-40)-(3-49) are such that the region of integration will cover the generating curve. The quantities $g_1, g_2, \ldots$ result from integration over ϕ and are given in Table 3.1. In the numerical computation of these and similar integrals, a 20-point Gaussian quadrature is used.

Table 3.1

ϕ dependent integrals

$$g_1 = 2\int_0^{\pi} G_1 \sin^2 \frac{\phi'}{2} \cos n\phi' \, d\phi'$$

$$g_2 = \int_0^{\pi} G_1 \cos \phi' \cos n\phi' \, d\phi'$$

$$g_3 = \int_0^{\pi} G_1 \sin \phi' \sin n\phi' \, d\phi'$$

$$g_4 = \int_0^{\pi} G_2 \cos n\phi' \, d\phi'$$

$$g_5 = \int_0^{\pi} G_2 \cos \phi' \cos n\phi' \, d\phi'$$

$$g_6 = \int_0^{\pi} G_2 \sin \phi' \sin n\phi' \, d\phi'$$

$$G_2 = \exp(-jkR)/(kR)$$

$$G_1 = G_2 \cdot (1 + jkR)/(k^2R^2)$$

(b) ***MFIE***

For the magnetic field integral equation, the unknown expansion coefficients in (3-31) are determined by substituting (3-31) into (3-22) and (3-23) and using the Galerkin's formalism of the method of moment. The inner products of the integral operators in (3-22) and (3-23) are formed with tesing functions $\vec{W}_{mn}^{t,\phi}$ yielding a system of algebraic equations that may be written in matrix form as

$$\left[Q_m^H\right]\left[I_m\right] = \left[G_m^H\right] \qquad m = 0, \pm 1, \pm 2, .. \tag{3-45}$$

where

$$\left[G_m^H\right] = \begin{bmatrix} < \vec{W}_{mn}^{t} , \hat{n} \times \vec{H}^{i} > \\ \\ < \vec{W}_{mn}^{\phi} , \hat{n} \times \vec{H}^{i} > \end{bmatrix} \tag{3-46}$$

is the excitation vector of length ***2N***, and

$$\left[Q_m^H\right] = \begin{bmatrix} [\, Y_{mn}^{tt,J} + Y_{mn}^{tt,M} \,] & [\, Y_{mn}^{t\phi,J} - Y_{mn}^{t\phi,M} - \Delta_{mn}^{t\phi} \,] \\ \\ [\, Y_{mn}^{\phi t,J} - Y_{mn}^{\phi t,M} \,] & [\, Y_{mn}^{\phi\phi,J} + Y_{mn}^{\phi\phi,M} + \Delta_{mn}^{\phi\phi} \,] \end{bmatrix} \tag{3-47}$$

is an (***2N*** X ***2N***) moment matrix and known as the admittance matrix.

Again, the sub-matrices $[Y_{mn}^{\alpha\beta,J}]$, $\alpha, \beta = t$ or ϕ are identical to those of the ***MFIE*** for perfectly conducting objects. The superscripts $\vec{J}$ and $\vec{M}$ in Equ. (3-47) correspond respectively, to the contribution of the equivalent electric and magnetic currents to the moment matrix. The

sub-matrices $[\Delta^{t\phi}_{mn}]$ and $[\Delta^{\phi\phi}_{mn}]$ are the contribution of the surface impedance derivatives along the generating curve. The *(i,j)-th* elements of these sub-matrices are computed from

$$(Y^{\alpha\beta,J}_{mn})_{ij} = \tfrac{1}{2}\int_{S_o} ds\ \vec{W}^{\alpha}_{mi}(\vec{r}) \cdot \vec{J}^{\beta}_{nj}(\vec{r}) + \int_{S_o} ds \int_{S_o} ds'\ \vec{W}^{\alpha}_{mi}(\vec{r}) \cdot \cdot\ \hat{n}(\vec{r}') \times \left(\vec{J}^{\beta}_{nj}(\vec{r}') \times \nabla G(\vec{r},\vec{r}') \right) \tag{3-48}$$

$$(Y^{tt,M}_{mn})_{ij} = j/Z_o \int_{S_o} dt\ \rho f_i(t) \int_{S_o} dt'\ \rho' f_j(t') \cdot \left(k^2 g_5 - \frac{m^2}{\rho\rho'}\, g4 \right) Z^t(t') \Big) \tag{3-49}$$

$$(Y^{t\phi,M}_{mn})_{ij} = -1/Z_o \int_{S_o} dt\ \rho f_i(t) \int_{S_o} dt' \left(k^2 \rho' f_j(t')\ sin\ \nu'\ g_6 + \frac{m}{\rho}\ \frac{\partial}{\partial t'} \left(\rho' f_j(t') \right) g_4 \right) Z^{\phi}(t') \tag{3-50}$$

$$(\Delta^{t\phi,M}_{mn})_{ij} = 1/Z_o \int_{S_o} dt\ \rho f_i(t) \int_{S_o} dt'\ \rho' f_j(t')\ \frac{m}{\rho}\ \frac{dZ^{\phi}(t')}{dt'}\ g_4 \tag{3-51}$$

$$(Y^{\phi t,M}_{mn})_{ij} = 1/Z_o \int_{S_o} dt \int_{S_o} dt'\ \rho' f_j(t') \left(k^2 \rho\ f_i(t)\ g_6\ sin\ \nu + \frac{m}{\rho}, \frac{\partial}{\partial t} \left\{ \rho f_i(t) \right\} g_4 \right) Z^t(t') \tag{3-52}$$

$$(Y_{mn}^{\phi\phi,M})_{ij} = j/Z_o \int_{S_o} dt \int_{S_o} dt' \; Z^{\phi}(t') \Bigg(k^2 \rho \, f_i(t) \, \rho' f_j(t') \cdot \Big(g_5 \sin\nu \sin\nu' + g_4 \cos\nu \cos\nu' \Big) - \frac{\partial}{\partial t}\Big\{ \rho f_i(t) \Big\} \frac{\partial}{\partial t'}\Big\{ \rho' \, f_j(t') \Big\} \, g_4 \Bigg) \tag{3-53}$$

and

$$(\Delta_{mn}^{\phi\phi,M})_{ij} = j/Z_o \int_{S_o} dt \int_{S_o} dt' \Bigg(\frac{\partial}{\partial t}\Big\{ \rho \, f_i(t) \Big\} \rho' \, f_j(t') \, \frac{dZ^{\phi}(t')}{dt'} \cdot g_4 \Bigg) \tag{3-54}$$

with g_4, g_5 and g_6 given in Table 3.1.

(c) ***CFIE***

In the present case, utilizing Equ. (3-24), the required moment and excitation matrices can be determined directly from the above results and have the form

$$\left[Q_m^C\right] = \left[Q_m^H\right] + \alpha\left[Q_m^E\right] \tag{3-55}$$

and

$$\left[G_m^C\right] = \left[G_m^H\right] + \alpha\left[G_m^E\right] \tag{3-56}$$

where G_m^E, Q_m^E, G_m^H and Q_m^H are given by Equs. (3-38), (3-39), (3-46) and (3-47), respectively.

3.3.1 *Special cases:*

In all above field integral equations, the surface impedance components are assumed to be variable on the surface. For highly conducting objects and for objects of large radii of curvature, the variation of the surface impedance along the generating curve is negligible. In addition, for reactive coating applications, the surface impedance is a function of the coating thickness and in most cases is assumed to have an average value over the surface. In these cases, the sub-matrices representing the contribution of $\vec{M}$ to the moment matrices are related in a simple form to the corresponding sub-matrices of the perfectly conducting object. For these particular cases, we have

$$[Z_m^{tt,M}] = Z_c/Z_o\ [Y_m^{\phi\phi,J}] \quad ; \quad [Y_m^{tt,M}] = Z_c/Z_o\ [Z_m^{\phi\phi,J}]$$

$$[Z_m^{t\phi,M}] = -Z_c/Z_o\ [Y_m^{\phi t,J}] \quad ; \quad [Y_m^{t\phi,M}] = -Z_c/Z_o\ [Z_m^{\phi t,J}]$$

$$[Z_m^{\phi t,M}] = -Z_c/Z_o\ [Y_m^{t\phi,J}] \quad ; \quad [Y_m^{\phi t,M}] = -Z_c/Z_o\ [Z_m^{t\phi,J}]$$

$$[Z_m^{\phi\phi,M}] = Z_c/Z_o\ [Y_m^{tt,J}] \quad ; \quad [Y_m^{\phi\phi,M}] = Z_c/Z_o\ [Z_m^{tt,J}]$$

with $[Z_m^{\alpha\beta,J}]$ and $[Y_m^{\alpha\beta,J}]$ for $\alpha,\beta = t$ or ϕ given by Equs. (3-40) and (3-48), respectively.

3.3.2 *Far Scattered Fields:*

Once the surface current $\vec{J}$ is determined, the scattered field at a far field point can be determined from the following equation [73],

$$\vec{E}^s = \frac{exp(-jkr)}{r} \left(F_1(\theta,\phi)\ \hat{\theta} + F_2(\theta,\phi)\ \hat{\phi} \right) \qquad (3\text{-}57)$$

where

$$F_1(\theta,\phi) = -\frac{j\omega\mu_o}{4\pi} \int_{S_o} \left(\vec{J} \cdot \hat{\theta} + 1/Z_o \left\{ \bar{\bar{Z}} \cdot \vec{J} \times \hat{n} \right\} \cdot \hat{\phi} \right) \cdot exp(jk\hat{r} \cdot \vec{r}')\ ds' \qquad (3\text{-}58)$$

and

$$F_2(\theta,\phi) = -\frac{j\omega\mu_o}{4\pi} \int_{S_o} \left(\vec{J} \cdot \hat{\phi} - 1/Z_o \left\{ \bar{\bar{Z}} \cdot \vec{J} \times \hat{n} \right\} \cdot \hat{\theta} \right) \cdot exp(jk\hat{r} \cdot \vec{r}')\ ds' \qquad (3\text{-}59)$$

with

$$\hat{\theta} = cos\ \theta\ cos\ \phi\ \hat{x} + cos\ \theta\ sin\ \phi\ \hat{y} - sin\ \theta\ \hat{z} \qquad (3\text{-}60)$$

and

$$\hat{\phi} = -sin\ \phi\ \hat{x} + cos\ \phi\ \hat{y} \qquad (3\text{-}61)$$

Equations (3-57) to (3-61) can also be used to determine the bistatic cross section of the scatterer, which is defined as

$$S(\theta,\phi) = 4\pi r^2 \left| \frac{\vec{E}^s(r,\theta,\phi)}{E_o} \right|^2 \qquad (3\text{-}62)$$

where E_o is the intensity of the incident field.

To evaluate numerically the far scattered fields, the measurement matrix defined by Mautz and Harrington [64], for a conducting body of revolution is generalized to include the magnetic current contribution through the impedance boundary conditions. The final form for the *m-th* mode is given by

$$\vec{E}^{s}_{m} \cdot \hat{u} = (-j\omega\mu_{o}/4\pi r)\, exp(-jkr)\, [R_{m}]\, [K_{m}]$$

where $\hat{u}$ is a unit vector specifying the polarization (i.e., $\hat{\theta}$ or $\hat{\phi}$) and

$$[R_{m}] = [\, \langle \vec{P}_{E}, \vec{J}^{t}_{m} \rangle \quad \langle \vec{P}_{E}, \vec{J}^{\phi}_{m} \rangle \quad \langle \vec{P}_{H}, Z^{\phi}\vec{J}^{\phi}_{m} \rangle \quad - \langle \vec{P}_{H}, Z^{t}\vec{J}^{t}_{m} \rangle \,] \tag{3-64}$$

and

$$[K_{m}] = [\, a_{mn} \quad b_{mn} \quad -Z^{\phi}_{n} b_{mn} \quad Z^{t}_{n} a_{mn} \,]^{T} \tag{3-65}$$

with

$$\vec{P}_{E} = \hat{u}\, exp(-j\vec{k} \cdot \vec{r}_{i}) \tag{3-66}$$

and

$$\vec{P}_{H} = (\hat{k} \times \hat{u})/Z_{o}\, exp(-j\vec{k} \cdot \vec{r}_{i}) \tag{3-67}$$

where $\vec{k} = k\hat{k}$ is a wave vector pointing in the direction of propagation of the scattered field and $\vec{r}_{i}$ is the coordinate vector to a point on S_{o}.

3.4 NUMERICAL RESULTS:

3.4.1 Validity of IBC:

Since the concept of the impedance boundary conditions is approximate, it is necessary to examine its validity. As a penetrable object, a lossy dielectric sphere is selected, for which analytic solutions can be obtained by two separate methods (see *Appendix A*). An exact solution in terms of spherical functions is well-known. It can be obtained by allowing the permittivity ε to have a complex value. A similar boundary value solution can also be obtained by enforcing the impedance boundary conditions. In the present work, both of these solutions are used to compute the scattered fields. Numerical solutions using *EFIE*, *MFIE* and *CFIE* formulations are also generated and the results are compared to determine the accuracy of the solution.

It should be noted that, although the surface impedance generally varies over the scattering surfaces, all results presented in this chapter are computed by asssuming constant surface impedance values over each segment of the generating curve and neglecting their derivatives in the *MFIE* and *CFIE*. The excellent agreement of the numerical and analytic solutions indicates that the effect of the impedance variation due to the curvature on the results is negligible. For the special case of imperfectly conducting objects the computed scattering data for both constant and variable impedances are compared later in this section. It is found that the most significant difference between the results of the two cases is near the forward scattering region, but it is small and within a few percent range.

Figures 3.3 and 3.4 show the computed results. In all cases, the excitation is due to an x-polarized plane wave propagating along the z axis, i.e., $\theta^i = 180°$ (only $m = +1$ and -1 modes are excited for the axial incidence). The sphere radius is selected to be 1 m and its physical constants are assumed to be $\sigma = 5$ S/m, $\mu_r = 1$, and $\varepsilon_r = 1$. Figure 3.3 shows the computed results for an incident wave of wavelength $\lambda = 5$ m. It is evident that the solutions using IBC are in good agreement with the exact ones. The *EFIE* solutions, on the other hand, are satisfactory only in the backscattered region. Towards the forward scattering direction the accuracy of the *EFIE* solution deteriorates progressively and perdicts somewhat larger forward scattering data. This poor performance of the *EFIE* was also reported for perfectly conducting objects.

Figure 3.4 shows the above results at a higher frequency with $\lambda = 2.5$ m. Since the frequency is twice as large, the penetration depth is reduced by a factor of $\sqrt{2}$ and the computed results show better agreement. It should be noted that increasing the frequency also increases the surface impedance and consequently the significance of the magnetic current. The computed data also indicate that the backscattering cross section decreases with increasing the surface impedance. This effect of a conducting coating can be used to reduce the backscattering, by coating the scattering surface with a highly lossy material.

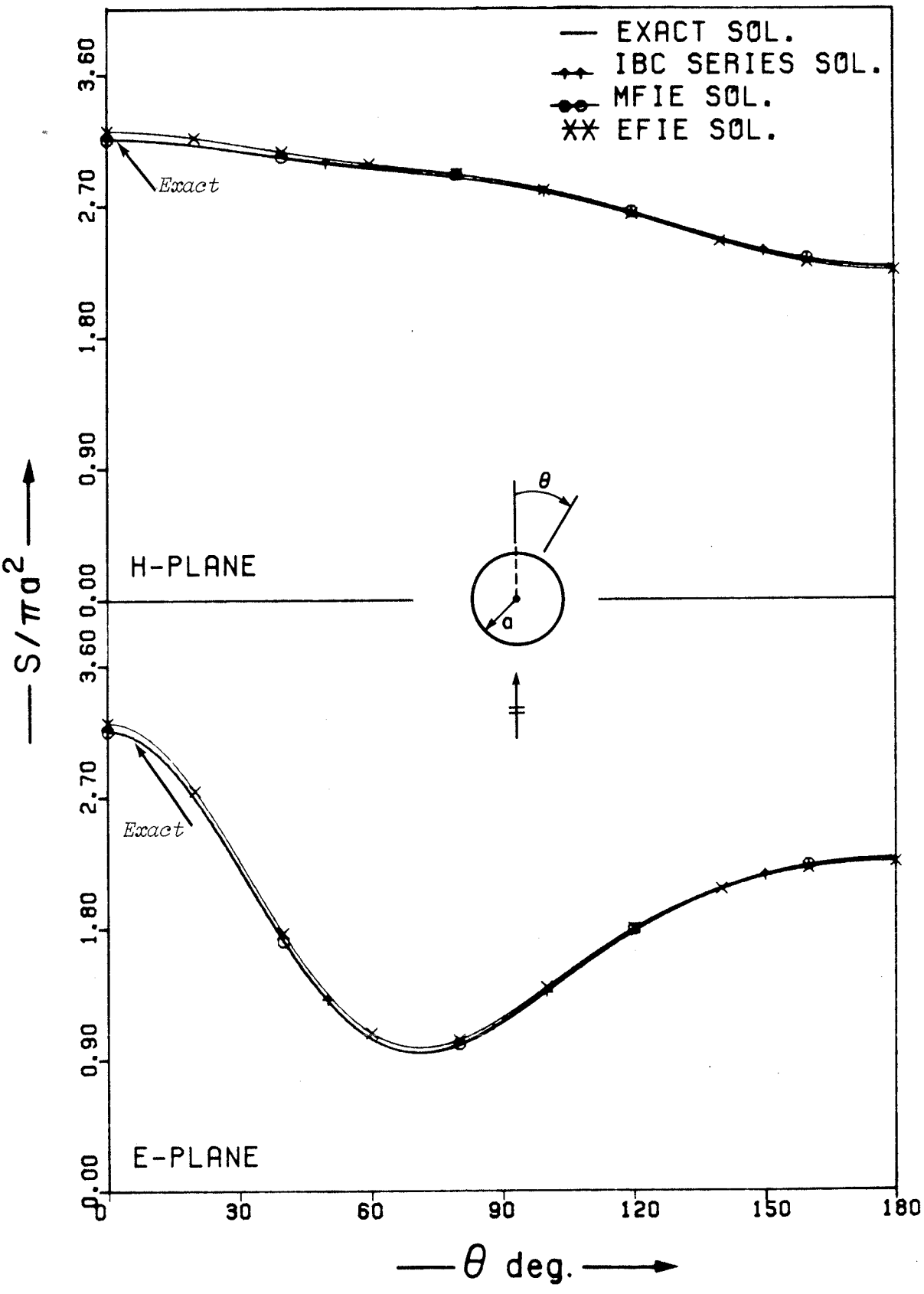

Figure 3.3: Normalized bistatic cross section $S/\pi a^2$ as a function of θ for an imperfectly conducting sphere of radius a = 1 m, for λ = 5 m.

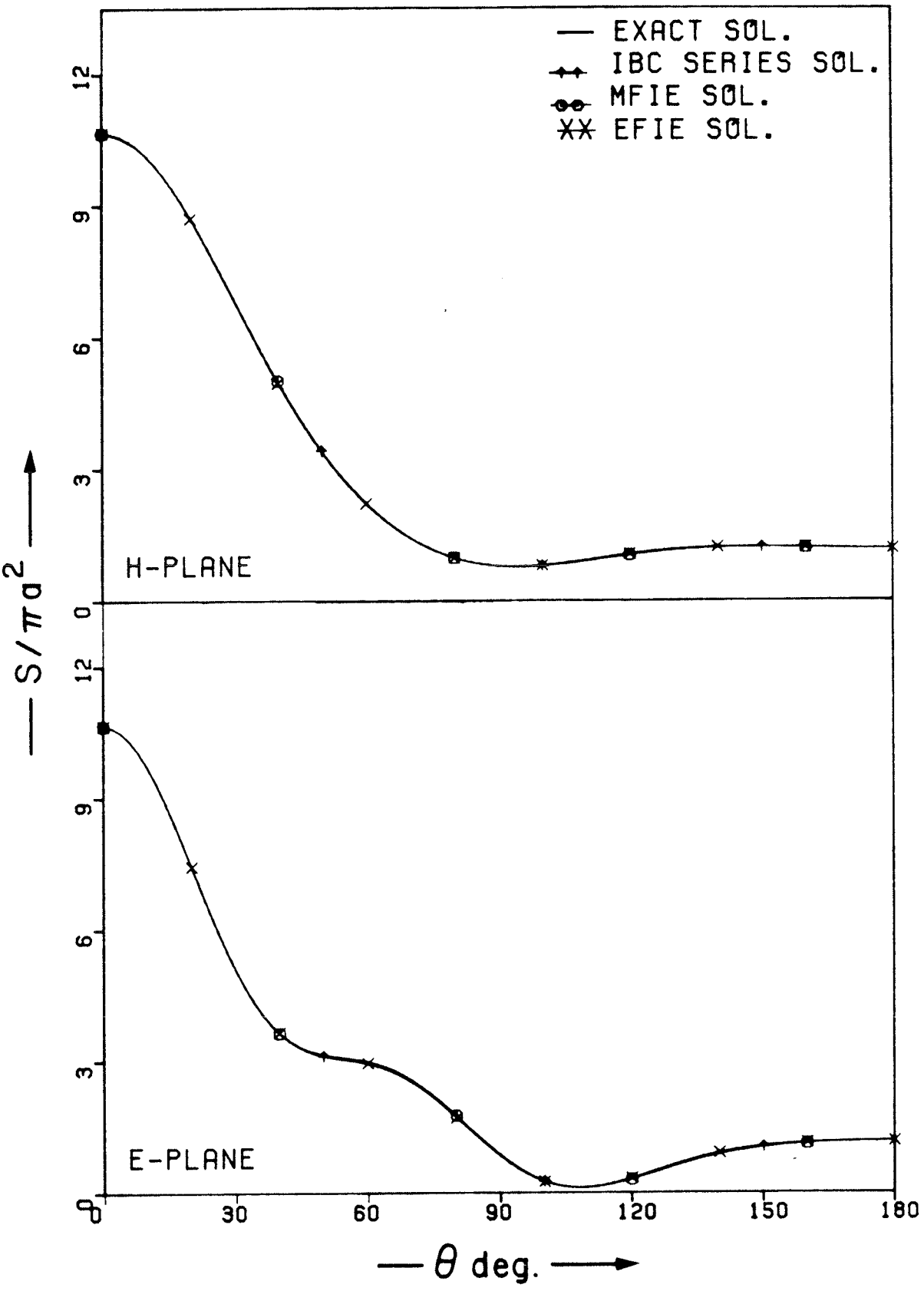

Figure 3.4: Same as Fig. 3.3 except λ = 2.5 m.

To examine the accuracy of the solutions using different integral equation formulations, Fig. 3.5 is included. It compares the results for an imperfectly conducting sphere and spheres with both inductive and capacitive surface impedances. The radius of the sphere is $0.5\ \lambda$ and the incident field is a plane wave propagating along the negative z axis, i.e, $\theta^i = 180°$. Both *CFIE* and *MFIE* give results that agree well with those of series solutions using the impedance boundary conditions. However, the *EFIE* again predicts larger scattering data towards the forward scattering direction. To obtain comparable results with the *CFIE* or *MFIE*, it is found (not shown here) that using *EFIE* requires about 30% more sampling points than the other two field integral equations.

3.4.2 Other Geometries:

To demonstrate the versatility of the numerical code, three basic shapes including a prolate spheroid, base-to-base bicone and hemisphere-cylinder-hemisphere are considered. Of particular interest in radar applications is the backscattering cross section. Without loss of generality, two cases in which the incident wave is either θ or ϕ polarized travelling in the xz plane are considered. Therefore, for the backscattering the respective angles are $\theta = \theta^i$ and $\phi = 0°$. The various backscattering patterns for different surface impedances are given in Figs. 3.6-3.8 . The generating curves' lengths as well as the maximum cross sectional areas normal to the axis of symmetry of these geometries are selected to be equal.

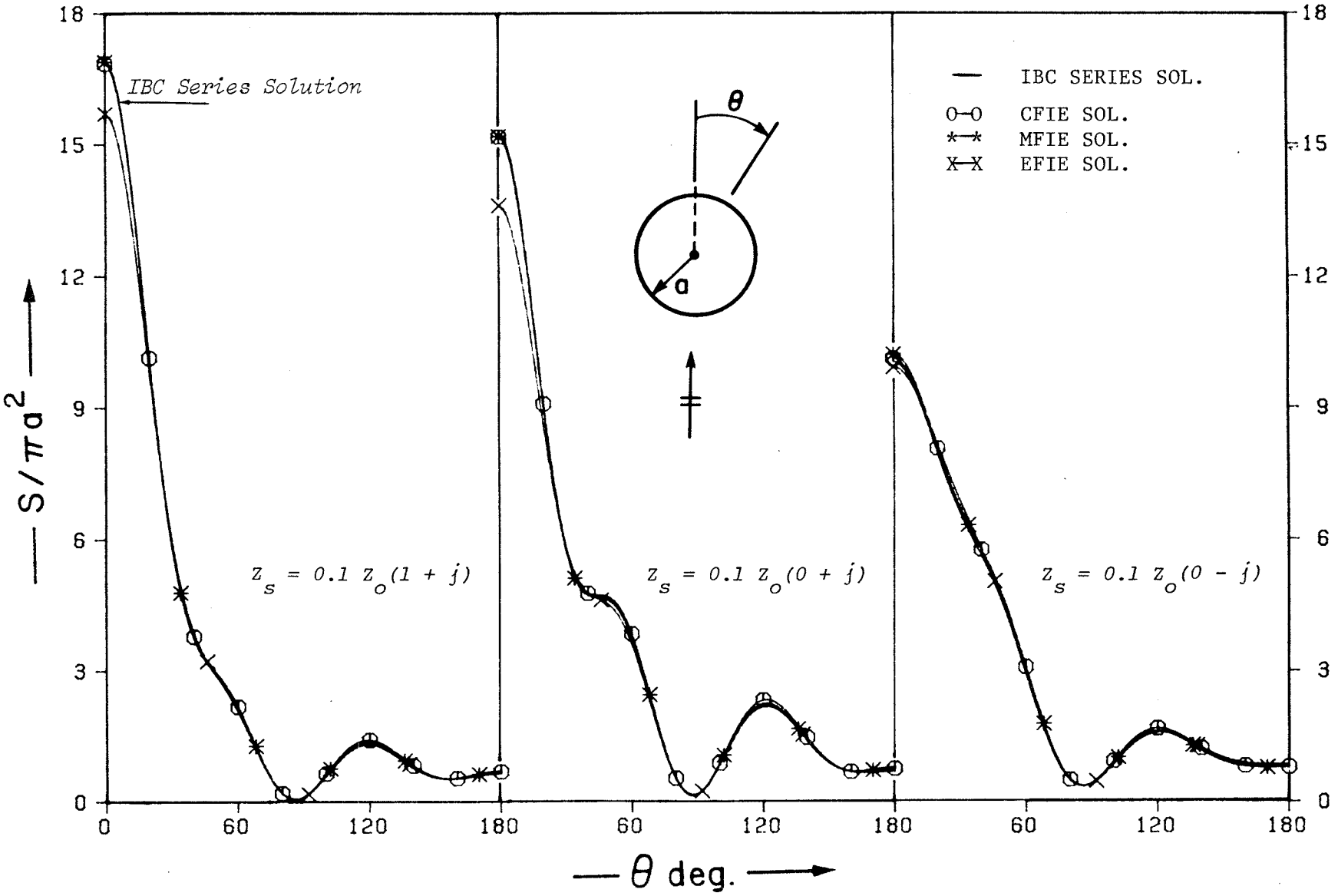

Figure 3.5: Normalized bistatic cross section $S/\pi a^2$ as a function of θ for three impedance spheres of radius $a=0.5\ \lambda$, for $\lambda=2m$.

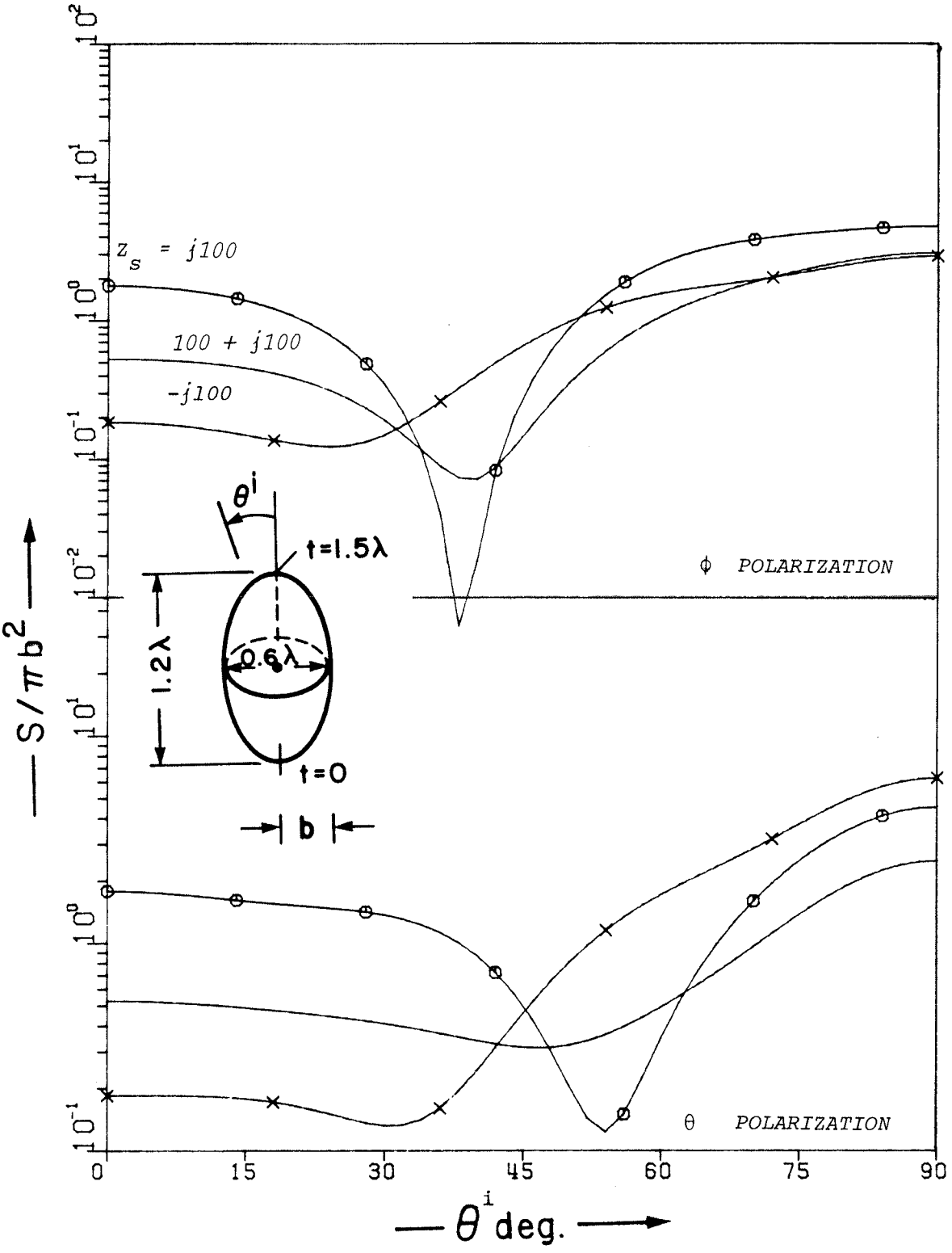

Figure 3.6: Normalized backscattering cross section S/(maximum cross section area) as a function of θ^i for three impedance spheroids.

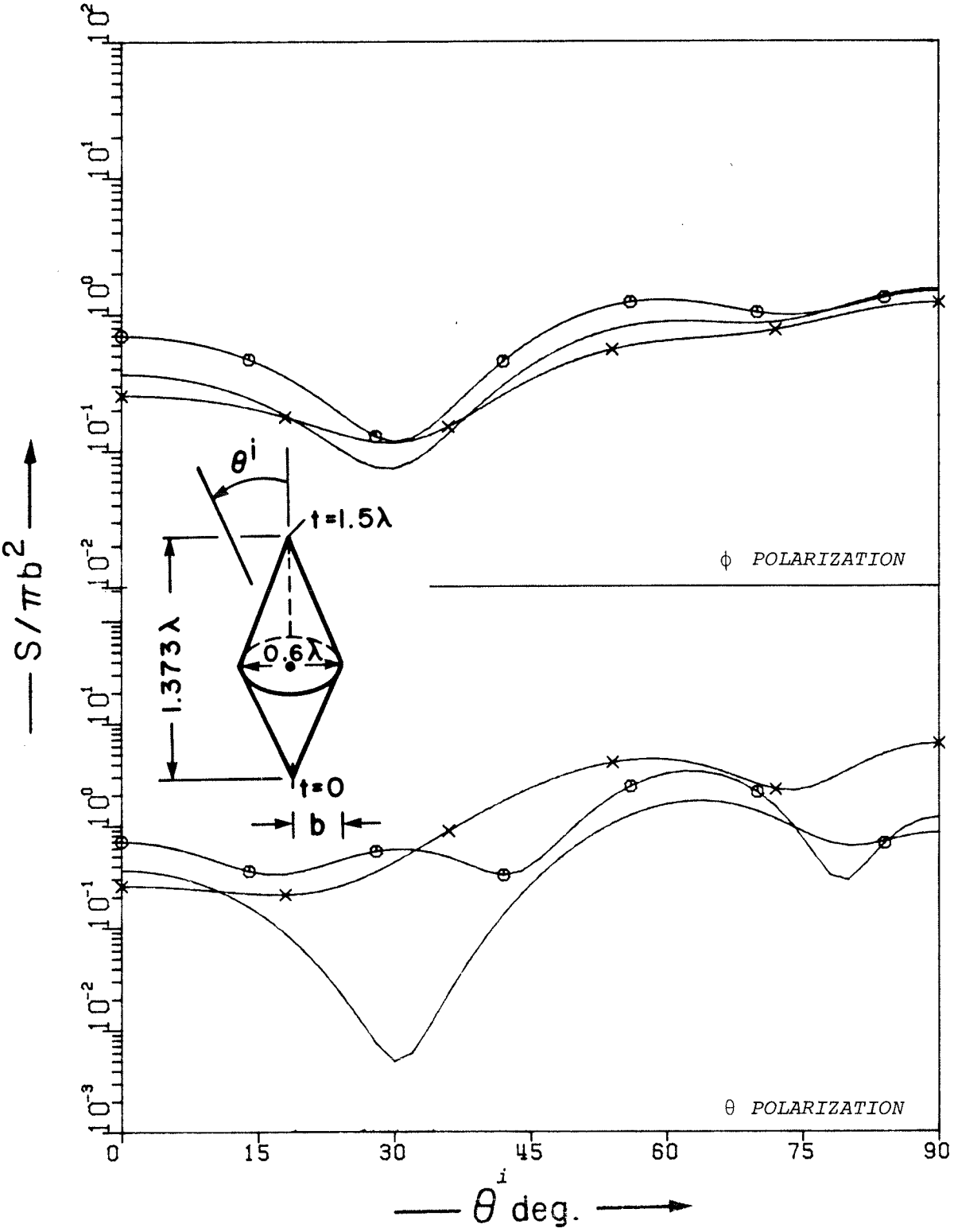

Figure 3.7: Same as Fig. 3.6 except the scatterer is base-to-base bicone.

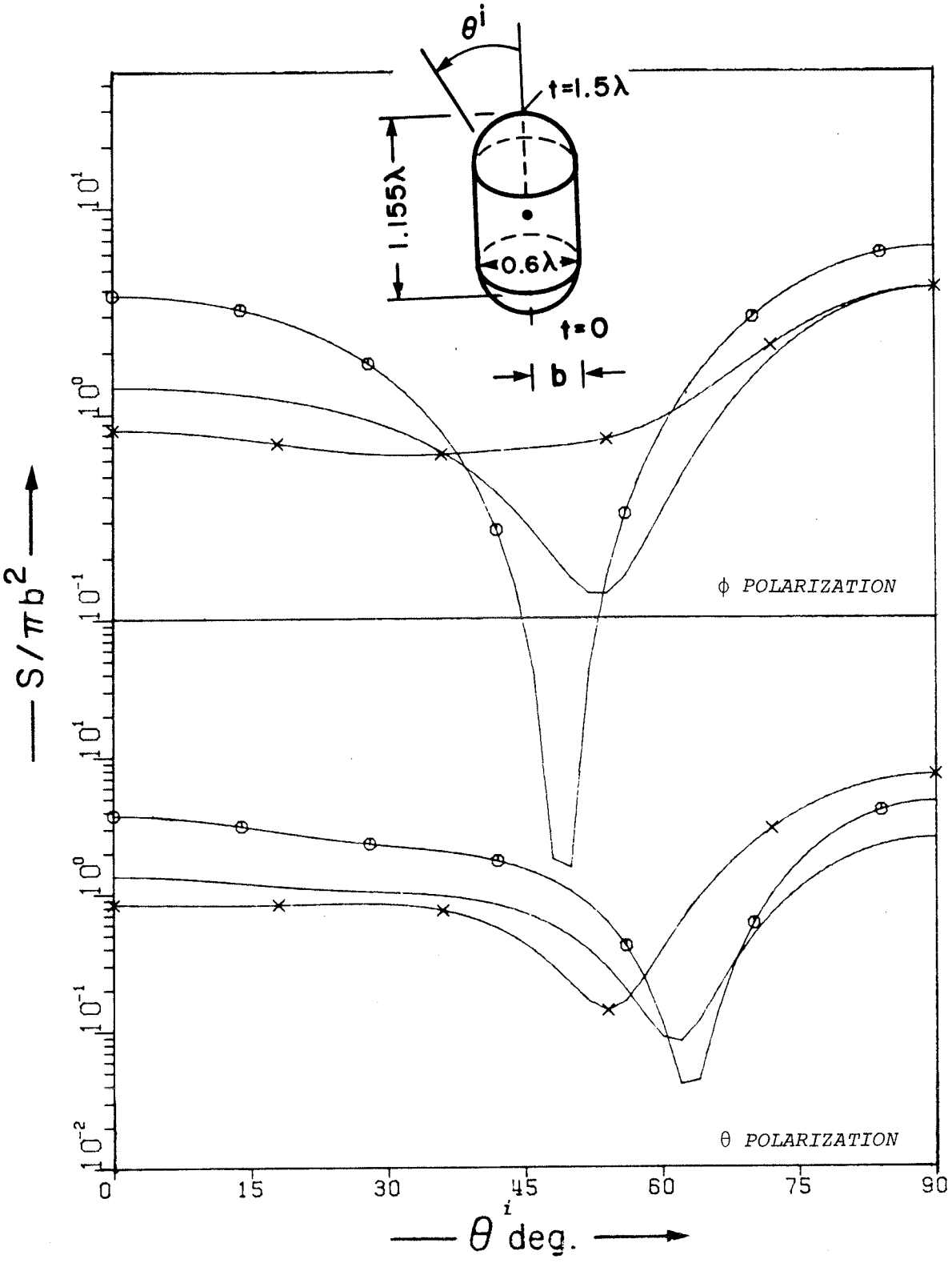

Figure 3.8: Same as Fig. 3.6 except the scatterer is hemisphere-cylinder-hemisphere.

In all cases, the propagation constant k and the generating curve length of the object are *3.7947* and *1.5* λ, respectively. The series in Equ. (3-31) are truncated at $M = 10$ and $N = 29$, which correspond to *21* modes and *61* sampling points along the generating curve. Due to the symmetry of the problem, the numerical code involves *11* matrix inversions each of order *58*. The *CFIE* has been used in the numerical solution.

The shape effect on the backscattering data is obvious from Figs. 3.6-3.8, which also show that the capacitive coating (i.e, Z_s is -ve and pure imaginary) reduces the backscattering for a wide range of incident angles compared with the imperfectly conducting case. On the other hand, an inductive coating results in increased backscattering for both θ and ϕ polarizations.

Finally, Fig. 3.9 shows the effect of the surface impedance phase on the scattered field. The scatterer is a prolate spheroid with an axial ratio of 2 and a semi-major axis of *1 m*. The excitation is due to an x-polarized plane wave prpopagating along the z axis (i.e., θ^i = 180°). It is clear that increasing the phase factor results in increasing the backscattered field. However, the effect on the forward scattered field is not noticable in this case. Note that this increase in the phase factor corresponds to a decrease in the real part of Z_s. As can be seen from Equ. (3-30), the phase of Z_s is material and frequency dependent. For a highly conducting object and at moderate frequencies, the phase factor is about 45°. On the other hand, for a coated object, Z_s is pure imaginary with its sign dependent on the electrical size of the outer layer.

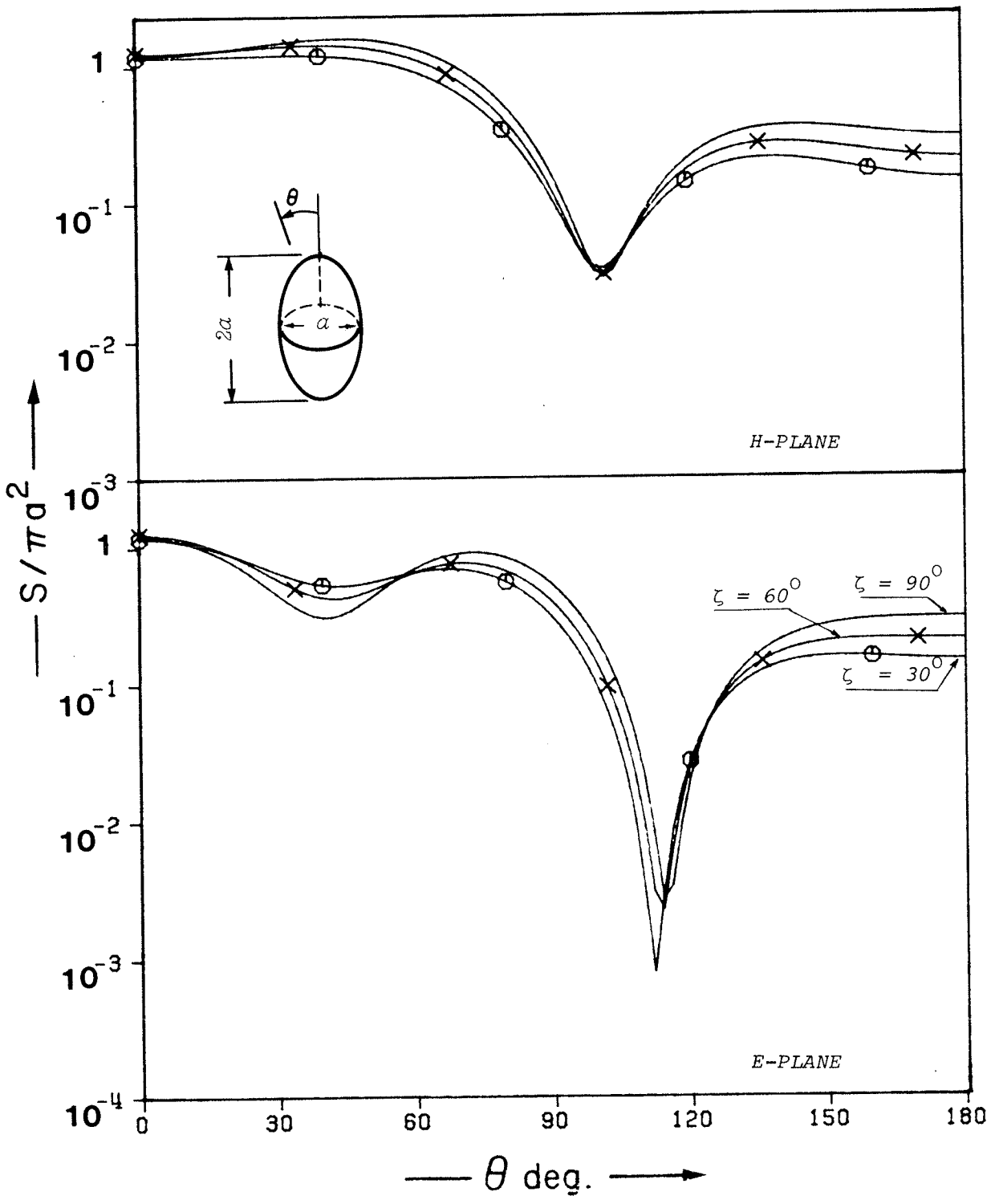

Figure 3.9: Normalized bistatic cross section $S/\pi a^2$ as a function of θ for three impedance spheroids, $Z_s = 0.1\ Z_o\ exp(j\zeta)$.

3.4.3 *Effect of Internal Resonances:*

For perfectly conducting scatterers, the problem of internal resonances is relatively well understood and stable solutions may be obtained by combining the electric and magnetic field integral equations [64]. For objects with surface impedance boundary conditions, a similar procedure can also be used. Recently [74], it has been shown that, similar to a perfectly conducting sphere, both electric and magnetic integral equations suffer from internal resonance effects and fail to give accurate results for impedance spheres. However, solutions by the combined formulation overcome this problem and are free of internal resonance problems.

For further examination of the effect of the internal resonance on the various solutions, the scattering by a solid impedance right circular cylinder of radius a and height $3a$ is also investigated. The cylinder is illuminated by an x-polarized plane wave axially incident on the flat end of the cylinder. In general, the resonance frequency for this structure is mode and height dependent. For a $\cos\phi$ mode and for the above height, the resonance frequency is given by [75],

$$f = \frac{1}{2\pi a \sqrt{\mu\varepsilon}} \sqrt{x_{11}^2 + \left(\frac{\pi a}{d}\right)^2} \qquad (3\text{-}68)$$

where a and d are the cylinder radius and height respectively and $x_{11} = 1.841$ is the smallest positive root of $J_1(x) = 0$, where $J_1(x)$ is the Bessel function of the 1st order and argument x. The normalized backscattered fields in the vicinity of this resonance frequency are

shown in Fig. 3.10 for different surface impedances. Again, both *EFIE* and *MFIE* indicate divergent solutions. In addition, for the capacitive coating case, the *EFIE* solution is affected by a false resonance, which is not related to the internal resonance of the above cylinder. It is important to note that physically the phenomenon of resonance does not exist for the external scattering problem. The occurrence of resonance phenomenon in the numerical computation is a mathematical problem. In fact this occurrence is sometimes an advantage. For some applications such as classification of objects by their natural frequencies, the location of these natural (resonance) frequencies depends on the object shape and material constitution. They represent a basic tool, in the singularity expansion method [76], whereby the natural frequencies of an object are represented by simple poles in the complex frequency plane. These natural frequencies for complicated geometries, can be found via numerical methods such as integral equation techniques. The main advantage in using those natural frequencies is that they are independent of the angle of incidence and polarization of the incident wave.

The main concern here is to obtain a stable solution for the external field. Therefore, for objects of arbritrary shape, the *CFIE* formulation must be preferred. The price to be paid in this case, is an increase in the computation time.

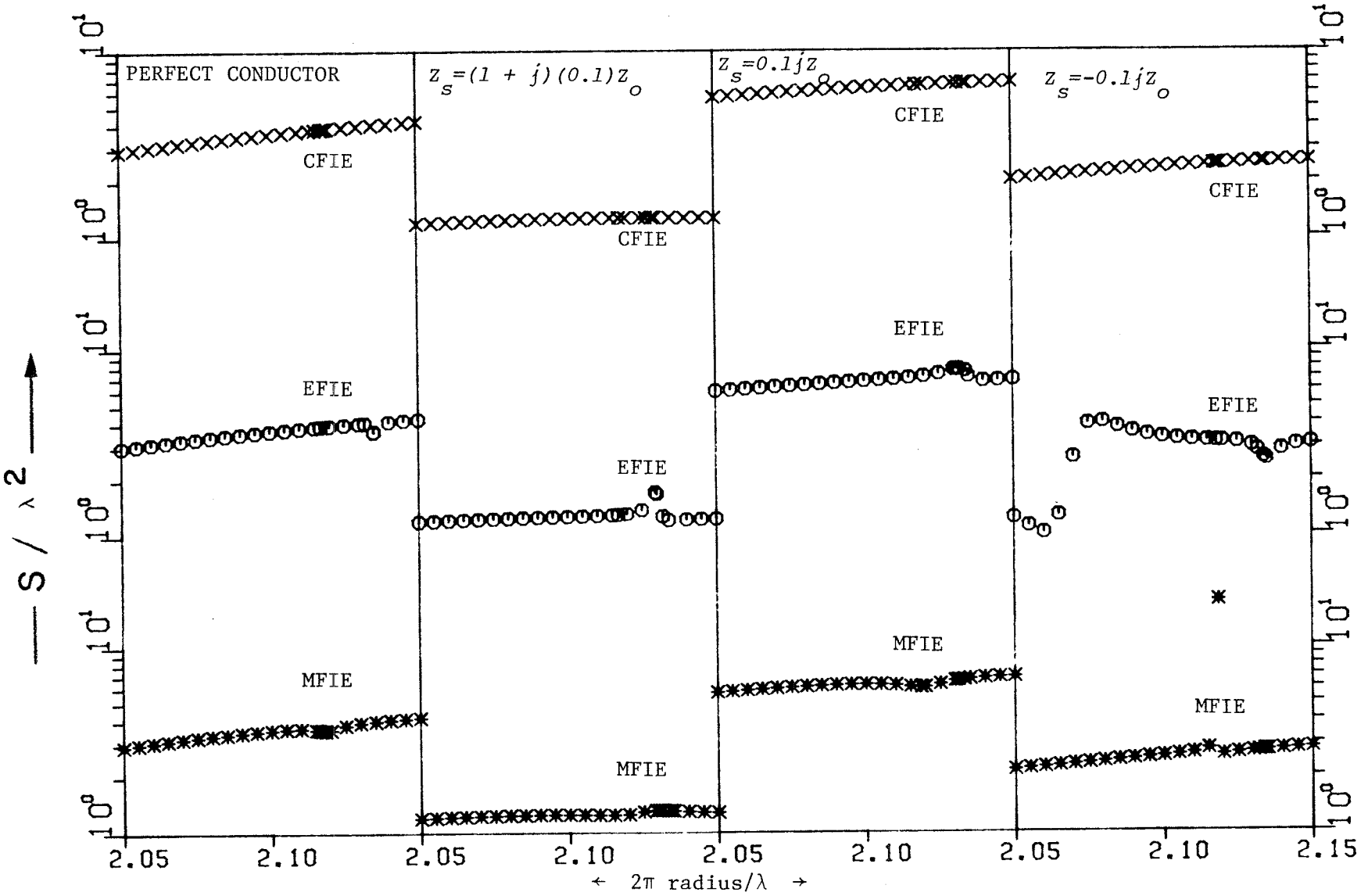

Figure 3.10: Normalized backscattering cross section S/λ^2 as a function of the electrical size (2π radius/λ) for three impedance cylinders (length = 3 m. and radius = 1 m.).

3.4.4 *Effect of Surface Impedance Variation:*

For imperfectly conducting objects, Mitzner [30] has indicated that when the radii of curvature are small, a correction factor q which is dependent on the principal curvatures, and given by Equ. (3-29), must be included in the impedance boundary conditions. In such a case and for bodies of revolution, both Z^t and Z^ϕ and their derivatives become dependent on the variable t. One therefore expects the computed results for both surface currents and scattered fields to be dependent on the variation of the surface impedance over each segment of the generating curve. To examine this possibility, scattering by imperfectly conducting spheres and cone-spheres is investigated using both constant and variable surface impedance. In the first case, the surface impedances over each segment are assumed to be constant and their derivatives are neglected. In the latter case, on the other hand, the surface impedances and their derivatives are calculated at each sample point of each segment on the generating curve. The computed results for the forward and back scattering data are shown in Table 3.2 for two different values of surface impedance Z_c. These results indicate that the maximum deviations between the results of the two cases is less than 5 percent. It should be noted that the maximum deviation in the results was found to be in the forward scattering data, but its range was generally dependent on the direction of the incident field. From these results it can be concluded that, for imperfectly conducting objects assuming constant surface impedance values over each segment of the generating curve (i.e., neglecting curvature) does not affect the accuracy of the results to a great extent, and can be used to simplify

the formulation if desired. Unfortunately, the effect of impedance variation on the accuracy of the results for objects with a reactive surface impedance could not be studied. A reactive surface impedance may be obtained by utilizing a thin coating on a conducting surface. Since the dependence of the surface impedance on the coating and object parameters can not be generalized, an investigation of its variation effect will not provide a conclusive result. However, the above investigation for imperfectly conducting objects indicates that accurate results can usually be obtained by assuming a constant surface impedance over each segment, and the accuracy improves with increasing conductivity.

TABLE 3.2

Normalized bistatic cross section in forward and backward directions for constant and variable surface impedances.

geometry	$Z_c(\Omega)$	S/λ^2 backward direction		S/λ^2 forward direction		surface impedance
		$\theta^i = 0.$	$\theta^i = 180.$	$\theta^i = 0.$	$\theta^i = 180.$	
sphere	37.67(1+j)	0.2479		0.4573		constant
(a=0.2λ)		0.2466		0.4554		variable
	113.1(1+j)	0.1215		0.6506		constant
		0.1193		0.6431		variable
cone-sphere	37.67(1+j)	0.1561	0.1218	0.5554	0.5636	constant
		0.1543	0.1217	0.5540	0.5508	variable
	113.1(1+j)	0.1208	0.0602	1.5729	1.5882	constant
		0.1157	0.0599	1.5565	1.5242	variable

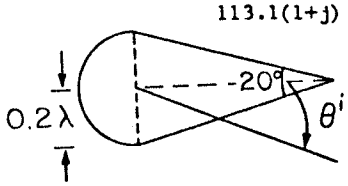

3.5 *SUMMARY:*

Numerical solutions of scattering by objects with impedance boundary conditions were investigated using the electric, magnetic, and combined integral equation formulations. For a spherical object, comparison of the analytic and numerical solutions indicates that representation of an imperfectly conducting scatterer by an impedance one is valid, provided the signal penetration into the body is small. Furthermore, the combined field integral equation always gives results in good agreement with analytic solutions. The electric field integral equation, on the other hand, always predicted larger forward scattering data.

The effect of internal resonances on the accuracy of numerical solutions was also investigated. Both *EFIE* and *MFIE* solutions were divergent near internal resonance frequencies, similar to the case of a perfectly conducting scatterer. However, the resonant frequencies depend on the surface impedance. By increasing the surface impedance, the *EFIE* resonance points moved towards higher frequencies and those of the *MFIE* shifted towards lower frequencies. It was also found that the degree of solution divergence increased by increasing the surface impedances. The solutions by the combined formulation, however, were always stable. This combined formulation was then used to compute the scattered field of other geometrical shapes. The results indicated that increasing the loss factor in the surface impedance always reduces the backscattered field. However, reactive coatings affected the scattering data in a more complex manner, and the results depend on the wave polarization as well as the geometric shape of the scatterer.

Chapter Four

SCATTERING FROM IMPERFECTLY CONDUCTING AND IMPEDANCE OBJECTS: BODIES OF ARBITRARY SHAPE

4.1 INTRODUCTION:

The purpose of this chapter is to describe an approximate method to solve the problem of scattering by imperfectly conducting objects of arbitrary shape. The method of solution used here, has three main features:

1) It uses available numerical codes for perfectly conducting objects to generate the solution for imperfectly conducting ones,

2) It simplifies the required matrix equation in the numerical solution of the problem, and

3) it uses a single matrix equation solution to generate the scattering data for objects of different surface impedances.

It is generally known that the most effective approach for solving such a problem is to use an integral equation formulation in conjuction with the method of moment, using a proper surface modeling of the scatterer. Two approaches to the surface modeling have been reported in the literature: the surface patch and the wire-grid models [8].

The surface patch model has been remarkably successful in treating three-dimensional problems [8],[77]-[79]. For perfectly conducting bodies, the magnetic field integral equation (*MFIE*) is simpler than the electric field integral equation (*EFIE*). The difficulty with the *EFIE*

is primarily due to the presence of various tangential derivatives in the integral equation for the unknown surface currents. However, for thin or open objects, one must use the *EFIE* because the *MFIE* is not applicable for such a class of geometries [60]. In this case, the wire-grid model [8] is more attractive. One advantage of using a wire-grid model is that all integrals are one dimensional along the center-line of the wire. On the other hand, if a wire-grid model has been used to model a conducting surface, the computed near field and surface currents should be approached with caution. This was reported by Miller and Deadrick [80], wherein arose ill-conditionel moment matrices, incorrect currents at the cavity resonance frequencies and existence of certain loop currents, all when a wire-grid was utilized to model a closed conducting surface.

For imperfectly conducting objects, both *EFIE* and *MFIE* contain tangential derivatives which complicate the resulting matrix equation and force one to select smooth base functions. Both problems can be overcome for highly conducting objects, for which the surface impedance is small. In this chapter, a general numerical method to generate the scattered fields by imperfectly conducting objects is presented. It is based on computing the electric current distribution on the surface of perfectly conducting object of the same shape as that under consideration. The concept of the impedance boundary conditions is then used to generate the equivalent magnetic current distribution which is then used together with the electric current to calculate the scattered field.

4.2 FORMULATION:

Consider a scattering object bounded by a closed smooth surface S_o and characterized by a conductivity σ, permittivity ε and permeability μ, as shown in Fig. 4.1. The object is illuminated by an electromagnetic wave with $\vec{E}^i$ and $\vec{H}^i$ being the incident electric and magnetic fields, respectively. As discussed earlier in *Chapter Three*, this general scattering problem may be solved by the integral equation approach. Introduction of the impedance boundary condition to the resulting matrix equation reduces the number of unknown surface currents by one half, which simplifies the solution of the obtained matrix equation, increases its efficiency and gives reasonably acceptable accuracies for most applications.

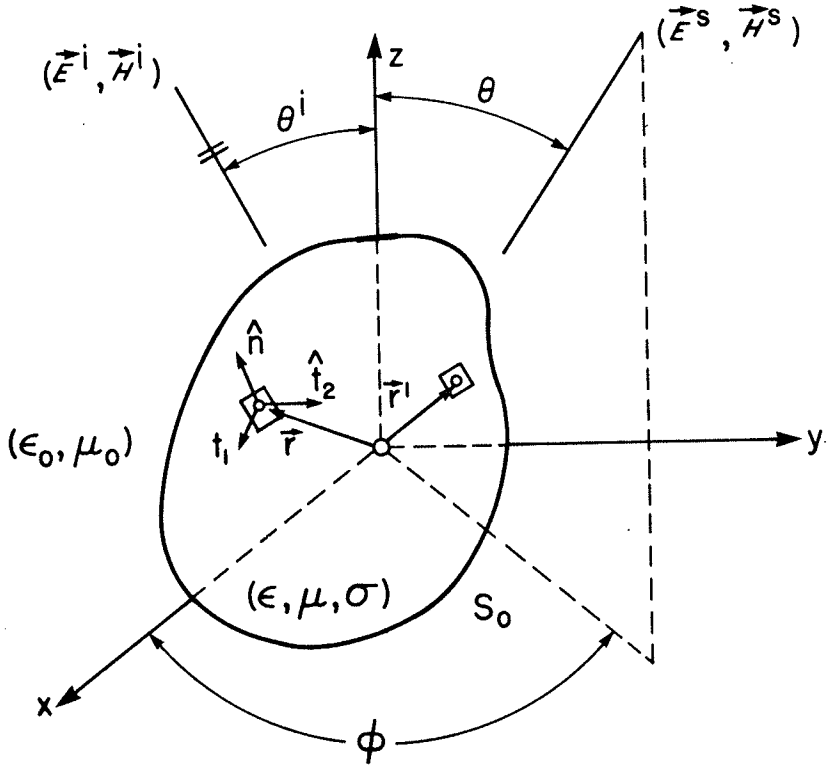

Figure 4.1: Geometrical configuration of an arbitrary scatterer.

For an object with impedance boundary conditions the ***EFIE*** and ***MFIE*** have been derived in ***Chapter Three*** and rewritten here for convenience.

EFIE

$$\hat{t}_1(\vec{r}).\vec{E}^i(\vec{r}) = -\tfrac{1}{2}\hat{t}_2(\vec{r}) \cdot [\bar{\bar{Z}}(\vec{r}) \cdot \vec{J}(\vec{r}) \times \hat{n}(\vec{r})]$$

$$-\hat{t}_1(\vec{r}) \cdot \int_{S_o} \Big([\bar{\bar{Z}}(\vec{r}').\vec{J}(\vec{r}') \times \hat{n}(\vec{r}')] \times \nabla G(\vec{r},\vec{r}')$$

$$-j\omega\mu_o \vec{J}(\vec{r}')G(\vec{r},\vec{r}') + \frac{1}{j\omega\mu_o}[\nabla'_s.\vec{J}(\vec{r}')] \nabla G(\vec{r},\vec{r}') \Big) ds' \qquad (4\text{-}1)$$

and

$$\hat{t}_2(\vec{r}).\vec{E}^i(\vec{r}) = \tfrac{1}{2}\hat{t}_1(\vec{r}) \cdot [\bar{\bar{Z}}(\vec{r}) \cdot \vec{J}(\vec{r}) \times \hat{n}(\vec{r})]$$

$$-\hat{t}_2(\vec{r}) \cdot \int_{S_o} \Big(\begin{matrix} \text{as in} \\ (4\text{-}1) \end{matrix} \Big) ds' \qquad (4\text{-}2)$$

MFIE

$$\hat{t}_2(\vec{r}).\vec{H}^i(\vec{r}) = -\tfrac{1}{2}\hat{t}_1(\vec{r}).\vec{J}(\vec{r}) + \hat{t}_2(\vec{r}) \cdot \int_{S_o} \Big(\vec{J}(\vec{r}') \times \nabla G(\vec{r},\vec{r}')$$

$$+j\omega\mu_o \Big(Z(\vec{r}') \cdot \vec{J}(\vec{r}') \times \hat{n}(\vec{r}') \Big) G(\vec{r},\vec{r}')$$

$$-\frac{1}{j\omega\varepsilon_o} \Big[\nabla'_s \cdot \Big(Z(\vec{r}') \cdot \vec{J}(\vec{r}') \times \hat{n}(\vec{r}') \Big) \Big] \nabla G(\vec{r},\vec{r}') \Big) ds' \qquad (4\text{-}3)$$

and

$$\hat{t}_1(\vec{r}).\vec{H}^i(\vec{r}) = \tfrac{1}{2}\hat{t}_2(\vec{r}) \cdot \vec{J}(\vec{r}) + \hat{t}_1(\vec{r}) \cdot \int_{S_o} \Big(\begin{matrix} \text{as in} \\ (4\text{-}3) \end{matrix} \Big) ds' \qquad (4\text{-}4)$$

with

$$\hat{t}_1 \times \hat{t}_2 = \hat{n} \qquad (4\text{-}5)$$

where $\hat{t}_1$ and $\hat{t}_2$ are two orthogonal surface unit vectors.

$$\hat{t}_1(\vec{r}) \cdot \vec{H}^i(\vec{r}) = \sum_{n=1}^{N} \left[a_n \left(\hat{t}_1(\vec{r}) \cdot \int_{S_o} \left\{ \begin{matrix} \text{as in} \\ \cdots\cdots\cdots \\ (4\text{-}7) \end{matrix} \right\} ds' \right) \right.$$

$$\left. + b_n \left(\tfrac{1}{2} f_n(\vec{r}) + \hat{t}_1(\vec{r}) \cdot \int_{So} \left\{ \begin{matrix} \text{as in} \\ \cdots\cdots\cdots \\ (4\text{-}7) \end{matrix} \right\} ds' \right) \right] \qquad (4\text{-}8)$$

Because of the three-dimensional nature of the problem, the exact evaluation of the integrals in Equs. (4-7) and (4-8) becomes very involved even for a simple form of the base functions.

For the application of the method of moment, the three-dimensional Dirac delta functions $W_m = \delta(\vec{r}-\vec{r}_m')$, $m = 1,2,..,N$ are chosen as the test functions, and Equs. (4-7) and (4-8) are enforced at the center $\vec{r}_m$ of each surface S_m, $m = 1,2,..,N$, provided that the patches S_m are sufficiently small, so that the surface currents over them can be considered constant. One then operates with the integral operators given by (4-3) and (4-4) on the expansion function term by term, and tests the resulting equations using W_m as the testing functions. The unknown constants a_n and b_n are then determined by the solution of the resulting set of simultaneous equations derived from (4-7) and (4-8) which may be represented in a matrix form as

$$[A]\ [J] = [J^i] \qquad (4\text{-}9)$$

In this general case, one can represent the surface S_o by N small flat patches and select a finite set of N base functions $f_n(\vec{r})$ in terms of which the unknown currents are expanded. In terms of the orthogonal surface unit vectors $\hat{t}_1$ and $\hat{t}_2$, the electric surface current may be written in the form

$$\vec{J}(\vec{r}) = \sum_{n=1}^{N} \left(a_n \hat{t}_1(\vec{r}_n) + b_n \hat{t}_2(\vec{r}_n) \right) f_n(\vec{r}) \qquad (4.6)$$

where $\vec{r}_n$ is a coordinate vector terminating at the n-th patch center and $f_n(\vec{r})$ are base functions. The coefficients a_n and b_n are to be determined.

Substituting Equ. (4-6) into Equs. (4-3), (4-4), and after some algebra the following expressions can be obtained,

$$\begin{aligned}
\hat{t}_2(\vec{r}) \cdot \vec{H}^i(\vec{r}) = \sum_{n=1}^{N} \Bigg[& a_n \Bigg(-\tfrac{1}{2} f_n(\vec{r}) + \hat{t}_2(\vec{r}) \cdot \int_{S_o} \Big\{ f_n(\vec{r}') \\
& \cdot \left[\hat{t}_1(\vec{r}') \times \nabla G(\vec{r},\vec{r}') + j\omega\mu_o \left(-\hat{t}_2(\vec{r}') Z_1(\vec{r}') G(\vec{r},\vec{r}') \right) \right] \\
& - \frac{1}{j\omega\varepsilon_o} \nabla G(\vec{r},\vec{r}') \nabla'_s \cdot \left[-\hat{t}_2(\vec{r}') Z_1(\vec{r}') f_n(\vec{r}') \right] \Big\} ds' \Bigg) \\
& + b_n \Bigg(\hat{t}_2(\vec{r}) \cdot \int_{S_o} \Big\{ f_n(\vec{r}') \Big[\hat{t}_2(\vec{r}') \times \nabla G(\vec{r},\vec{r}') \\
& + j\omega\mu_o \, \hat{t}_1(\vec{r}') \, Z_2(\vec{r}') \, G(\vec{r},\vec{r}') \Big] \\
& - \frac{1}{j\omega\varepsilon_o} \nabla G(\vec{r},\vec{r}') \nabla'_s \cdot \left(\hat{t}_1(\vec{r}') \, Z_2(\vec{r}') \, f_n(\vec{r}') \right) \Big\} ds' \Bigg) \Bigg]
\end{aligned} \qquad (4-7)$$

where [J] is a column vector of the unknown constants, $[J^i]$ is a column vector with its elements being the left hand side of (4-7) and (4-8) evaluated at patch centers and [A] is the moment matrix. Solving the system matrix in (4-9), one obtains

$$[J] = [B]\ [J^i] \tag{4-10}$$

where [B] is merely $[A]^{-1}$ and is a characteristic of the scattering body and is independent of the incident field.

Many difficulties and questions arise when one tries to evaluate [B]. Besides numerical stablity of the matrix equation, surface divergence terms in (4-1) to (4-4) force one to select smooth basis functions to represent the surface currents. The basis functions can be selected as triangle functions to solve the problem of scattering by bodies of revolution, where the currents need to be expanded along the generating curve. For complex geometries, pulse expansion functions have been used in solutions of problems involving perfectly conducting objects where only Equs. (4-3),(4-4) with the absence of $\vec{M}$ including the surface divergence term [8],[77]-[79] need to be solved. This type of expansion functions can not be used to solve the general scattering problem due to the presence of the divergence operator. If a further simplification of the formulation is feasible, it is generally desirable, so that the complexity of the matrix equation can be removed.

For highly conducting objects, the surface electric current $\vec{J}$ is closely related to that of the perfectly conducting one. In addition, the contribution of the magnetic surface current $\vec{M}$ to the scattered

fields calculated at the body surface is small. Therefore a possible approximation to either *EFIE* or *MFIE*, by initially neglecting the terms involving $\vec{M}$, has been studied. The solution of the remaining part of *EFIE* or *MFIE* gives $\vec{J}$ on the surface of the perfectly conducting object of the same shape. This is equivalent to the replacement of the actual components of $\vec{H}$, at the boundary under consideration, with the values corresponding to a perfectly conducting surface, without much error, since the signal penetration is very small compared to the wavelength. The computed electric surface current $\vec{J}$ is then used together with the *IBC* to determine $\vec{M}$, both of which are then used to compute the scattered fields. However, with this type of approximation, *EFIE* still contains a surface divergence term which will restrict the general solution desired. Therefore, *MFIE* is more suitable for this case to compute the surface electric current $\vec{J}$.

Aside from overcoming the surface divergence difficulty in *MFIE*, the reason for selecting this approach is the fact that numerical codes for perfectly conducting objects are readily available and can be expanded to objects with *IBC*. Additional benefits arising from this method are the simplicity of the matrix equation, reduction of the computation time required to fill the moment matrix and the fact that scattered fields from the same object with different surface impedances can readily be generated from the same surface current $\vec{J}$ after the solution of a single matrix equation.

4.3 EVALUATION OF MOMENT AND EXCITATION MATRICES:

After taking the dot products of Equs. (4-7) and (4-8) with the testing functions and setting Z_1, Z_2 equal to zero, integration of the results over S_o yields the following matrix equation

$$\begin{bmatrix} A_{ij}^{(1)} & A_{ij}^{(2)} \\ A_{ij}^{(3)} & A_{ij}^{(4)} \end{bmatrix} \begin{bmatrix} a_i \\ b_i \end{bmatrix} = \begin{bmatrix} V_j^{(1)} \\ V_j^{(2)} \end{bmatrix} \qquad (4\text{-}11)$$

The matrix of A_{ij}'s on the L.H.S. of Equ. (4-11) is the moment matrix and that of V_j's on the R.H.S. is the excitation column matrix. The *(i,j)-th* elements of these sub-matrices are given by

$$A_{ij}^{(1)} = Q(R_{ij})\ \hat{t}_2(\vec{r}_i) \cdot \left(\vec{R}_{ij} \times \hat{t}_1(\vec{r}_i)\right) \qquad i \neq j$$

$$= -\tfrac{1}{2} \qquad i = j \qquad (4\text{-}12)$$

$$A_{ij}^{(2)} = Q(R_{ij})\ \hat{t}_2(\vec{r}_i) \cdot \left(\vec{R}_{ij} \times \hat{t}_2(\vec{r}_i)\right) \qquad (4\text{-}13)$$

$$A_{ij}^{(3)} = Q(R_{ij})\ \hat{t}_1(\vec{r}_i) \cdot \left(\vec{R}_{ij} \times \hat{t}_1(\vec{r}_i)\right) \qquad (4\text{-}14)$$

$$A_{ij}^{(4)} = Q(R_{ij})\ \hat{t}_1(\vec{r}_i) \cdot \left(\vec{R}_{ij} \times \hat{t}_2(\vec{r}_i)\right) \qquad i \neq j$$

$$= \tfrac{1}{2} \qquad i = j \qquad (4\text{-}15)$$

and

$$V_j^{(1)} = \hat{t}_2(\vec{r}_j) \cdot \vec{H}^i(\vec{r}_j) \tag{4-16}$$

$$V_j^{(2)} = \hat{t}_1(\vec{r}_j) \cdot \vec{H}^i(\vec{r}_j) \tag{4-17}$$

where

$$Q(R_{ij}) = \frac{1 + jkR_{ij}}{R_{ij}^3} \exp(-jkR_{ij}) \, S_i \tag{4-18}$$

and

$$\vec{R}_{ij} = \vec{r}_j - \vec{r}_i \tag{4-19}$$

Once the elements of the moment and excitation matrices are computed, the matrix equation (4-9) is then solved for $\vec{J}$. The magnetic current $\vec{M}$ over S_o is now computed from

$$\vec{M}(\vec{r}) = \bar{\bar{Z}}(\vec{r}) \cdot \vec{J}(\vec{r}) \times \hat{n}(\vec{r})$$

Both $\vec{J}$ and $\vec{M}$ are then used in the computation of the scattered field outside the object surface.

4.4 FAR SCATTERED FIELD:

At a far field point (r,θ,ϕ) the scattered electric field is given by,

$$\vec{E}^s = \vec{E}_J^s + \vec{E}_M^s \tag{4-20}$$

where the subscripts J and M refer respectively to the contribution of the electric and magnetic surface currents. In the far field zone

$$\vec{E}_J^s = -j\omega\mu_o \frac{exp(-jkr)}{4\pi r} \left(\hat{\theta} \int_{S_o} [\hat{\theta} \cdot \vec{J}] \, exp(jk\hat{r} \cdot \vec{r}') \, ds' \right.$$

$$\left. + \hat{\phi} \int_{S_o} [\hat{\phi} \cdot \vec{J}] \, exp(jk\hat{r} \cdot \vec{r}') \, ds' \right) \tag{4-21}$$

and

$$\vec{E}_M^s = \frac{-j\omega\mu_o}{Z_o} \frac{exp(-jkr)}{4\pi r} \left(\hat{\theta} \int_{S_o} [\hat{\phi} \cdot \vec{M}] \, exp(jk\hat{r} \cdot \vec{r}') \, ds' \right.$$

$$\left. - \hat{\phi} \int_{S_o} [\hat{\theta} \cdot \vec{M}] \, exp(jk\hat{r} \cdot \vec{r}') \, ds' \right) \tag{4-22}$$

The bistatic radar cross section is then computed from

$$S(\theta, \phi) = 4\pi r^2 \left| \frac{\vec{E}_J^s + \vec{E}_M^s}{E_o} \right|^2 \tag{4-23}$$

where E_o is the intensity of the incident field.

4.5 NUMERICAL RESULTS:

In any program, to develop techniques for solving scattering problems, it is necessary to verify the technique. One way to do this is to apply the newly developed technique to problem classes, where accepted solutions already exist. To examine the accuracy of the surface current $\vec{J}$ and the scattering fields, computed by the above method, Figs. 4.2-4.5 are included. The scatterers are chosen to be axisymmetric geometries for which direct solutions of the integral equations are available for comparison, as discussed earlier in *Chapter Three*. For spherical and spheroidal objects the validity and limits of the method were previously established [81]-[83]. It was shown that this method gives the scattering fields accurately, particularly the backscattering data, for either imperfectly conducting bodies or for objects with capacitive or inductive coating, for a wide range of impedance variations.

For other geometries, consider a cone-sphere body. The electric currents on a highly lossy dielectric cone-sphere, excited by a plane wave axially incident on the cone tip are plotted in Fig. 4.2 (a) and for an axially incident wave on the sphere end in Fig. 4.3 (a), using the direct and approximate solutions of *MFIE*. Figs. 4.2 (b) and 4.3 (b) plot the scattering patterns of the same body in the E and H planes. As can be seen the overall agreement is good. However, as the conductivity decreases, Figs. 4.4 (a) to 4.5 (b), the divergence of the data near the forward directions, focuses attention on the limitation of the method. Again, as in the case for the spherical and spheroidal objects, this method predicts the backscattering data accurately.

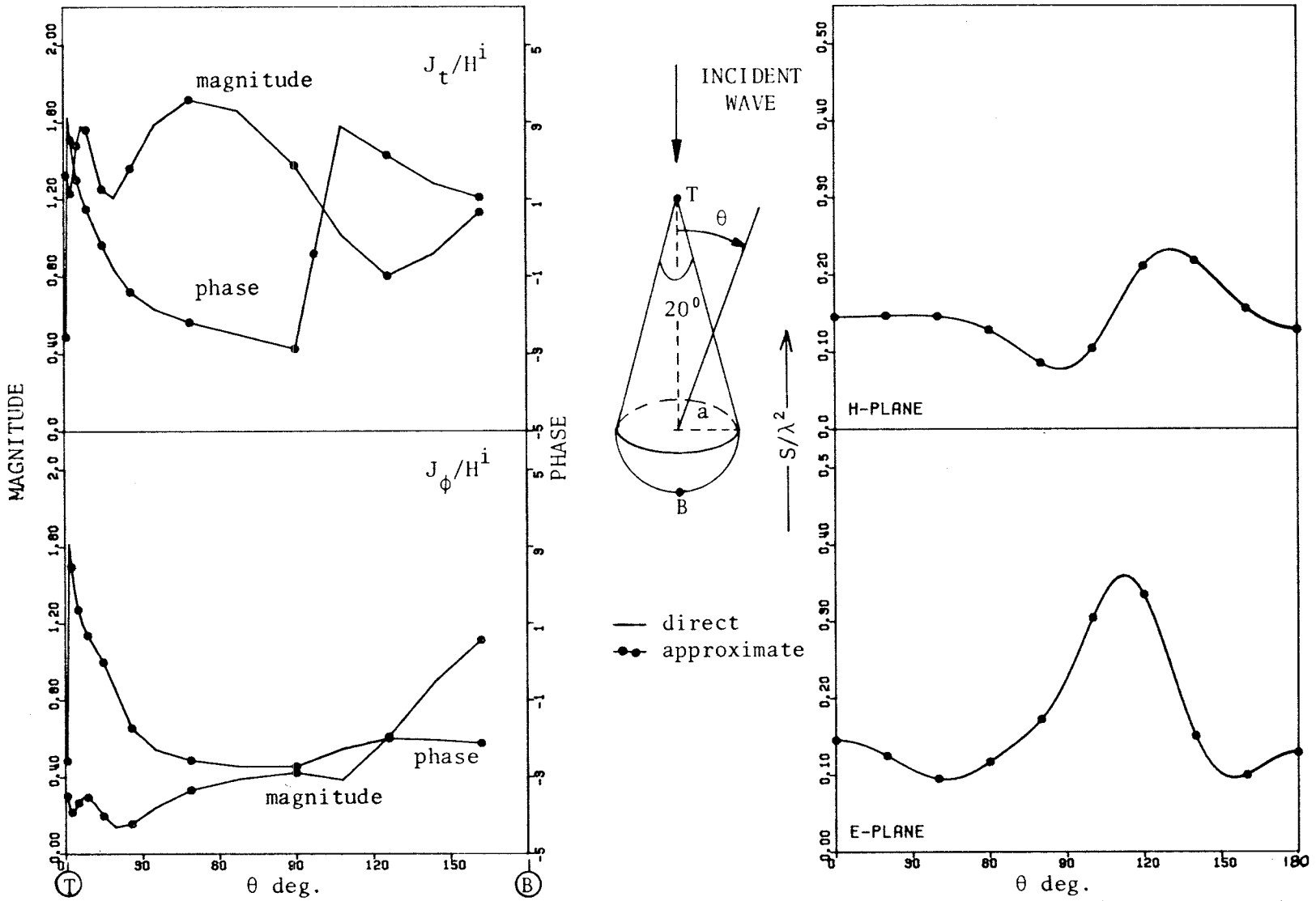

Figure 4.2: Current and field distributions for an imperfectly conducting cone-sphere ($a = 0.2\lambda = 1m$), $\sigma = 10^3$ S/m. and $\theta^i = 0^o$.

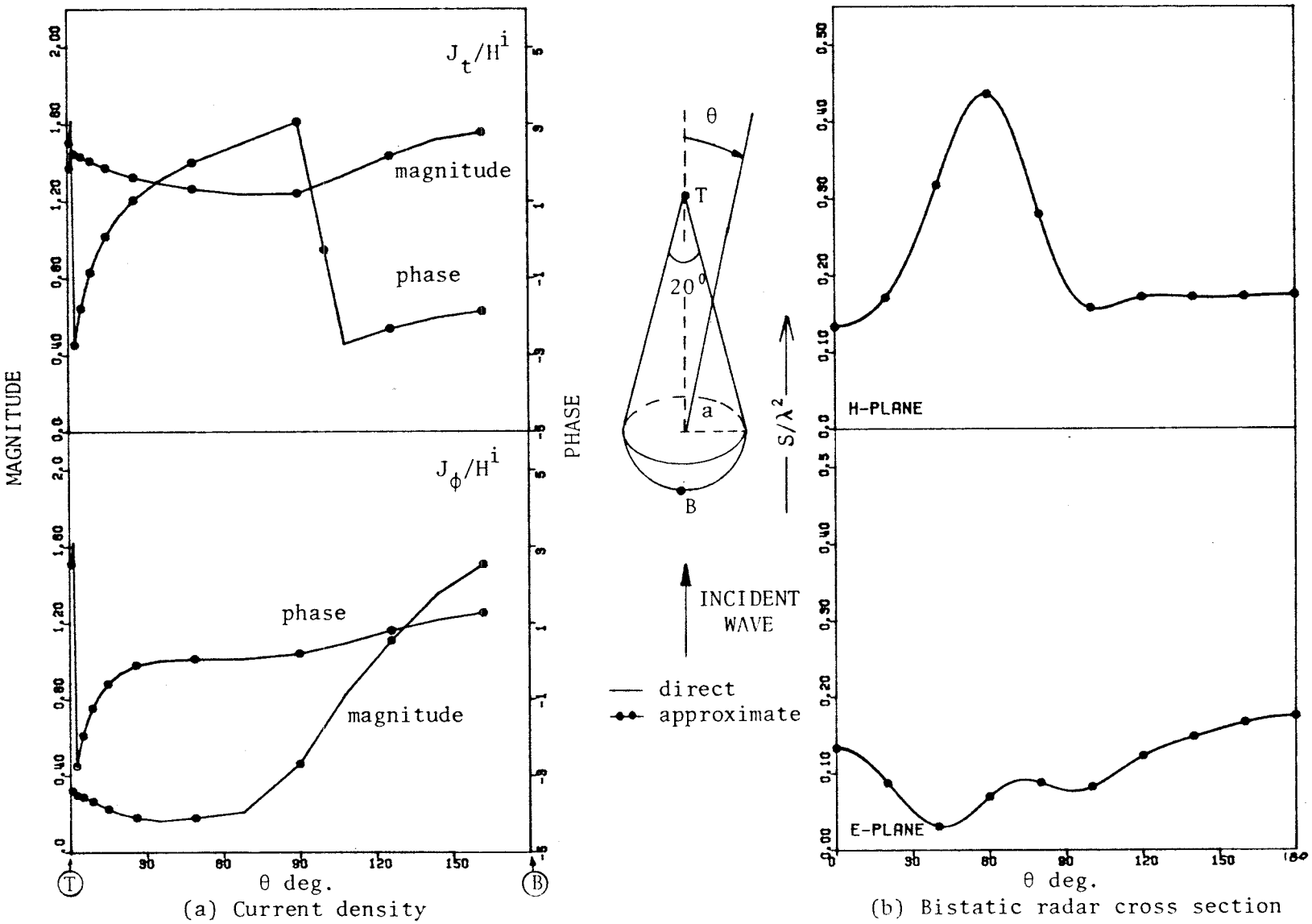

Figure 4.3: Current and field distributions for an imperfectly conducting cone-sphere (a = 0.2 λ = 1 m), σ = 10^3 S/m. and θ^i = 180°.

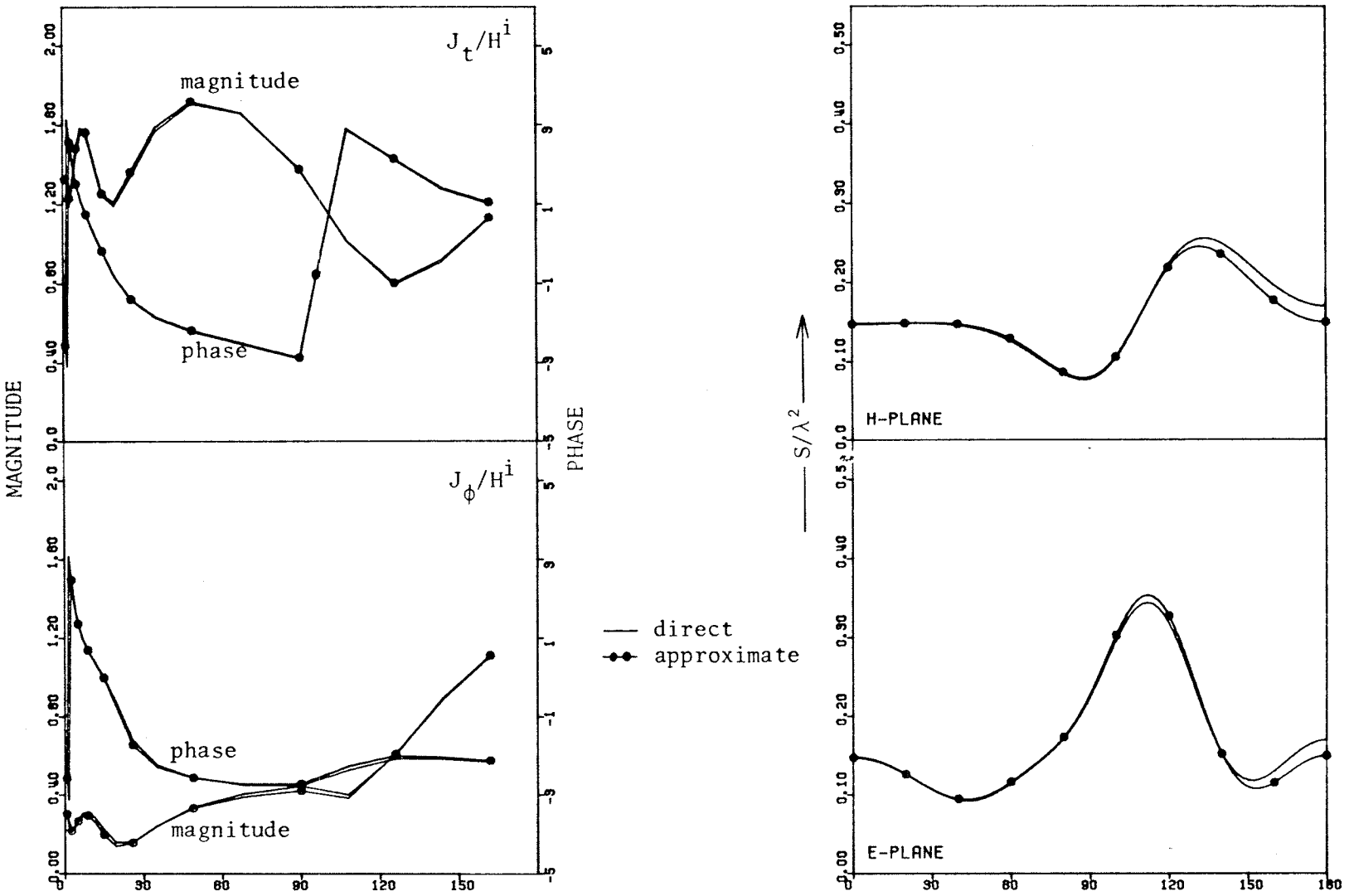

Figure 4.4: Same as Fig. 4.2 except σ = 10 S/m.

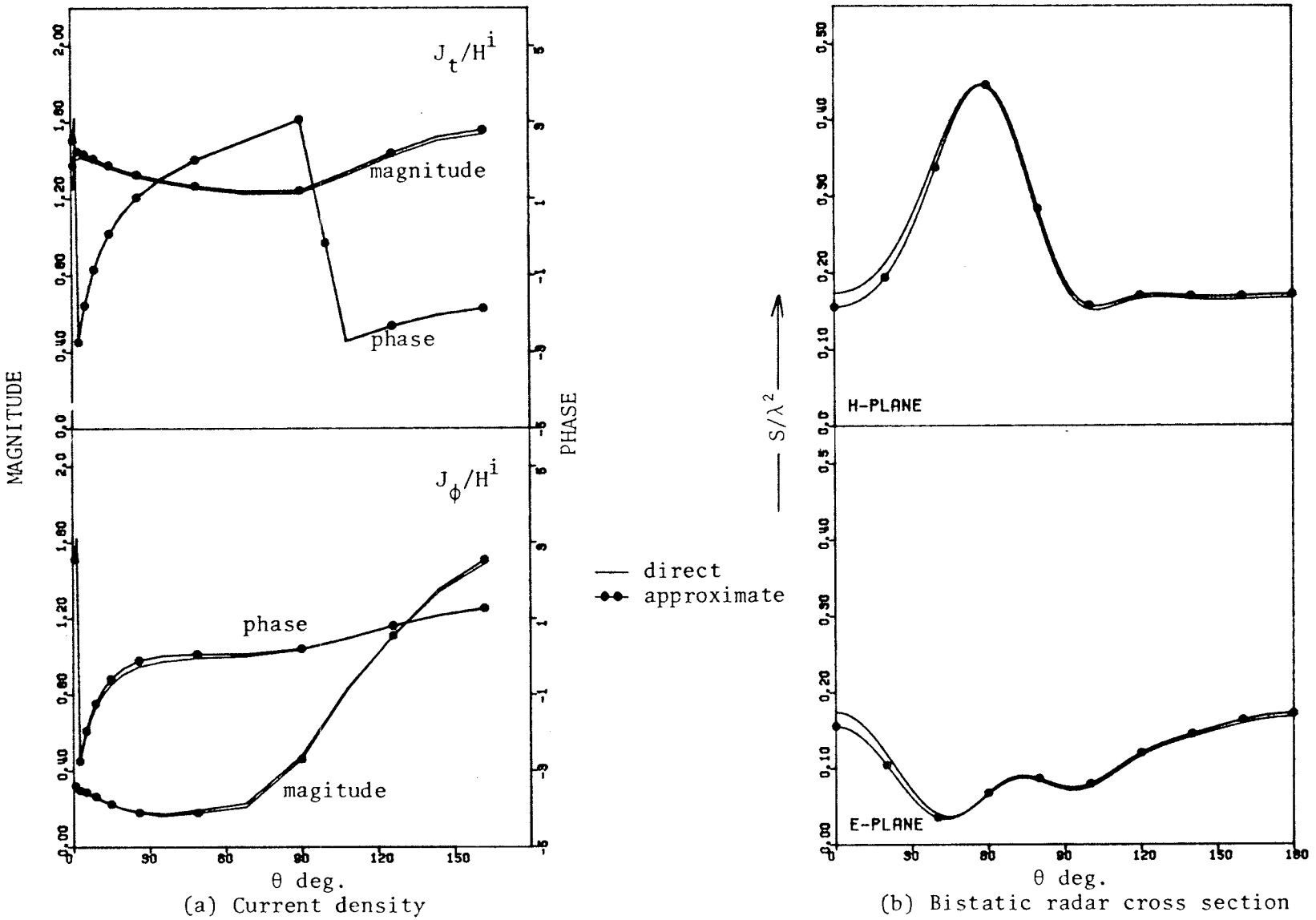

Figure 4.5: Same as Fig. 4.3 except σ = 10 S/m.

According to the reciprocity theorem[3], the forward scattering cross section must be the same for the directions of incidence in Figs. 4.2 and 4.3. This provides a useful check on the accuracy of the obtained numerical solutions. Although the induced current distributions for the two cases are entirely different, the computed values of the forward scattering cross sections were found to agree within 2.6 %.

Finally, the currents and scattering patterns for a cone-cylinder body are given in Figs. 4.6 (a) to 4.7 (b). The agreements between the two solutions are very clear, particularly, in the backscattering direction. To facilitate the comparison, Table 4.1 is included. It compares the bistatic radar cross section in the forward ($\theta = 180°$ for $\theta^i = 0°$ and $\theta = 0°$ for $\theta^i = 180°$) and backward ($\theta = 0°$ for $\theta^i = 0°$ and $\theta = 180°$ for $\theta^i = 180°$) directions for the two objects. It can be seen from this table that the approximate solutions for $\sigma = 10$ S/m in the backward direction agree quite satisfactorily with the direct solutions. Also, the concept of reciprocity is satisfied with an error ranging from 2.7 to 7 %. The maximum error between the two solutions occurs in the forward direction as mentioned before and can be 12 % in these particular cases.

---

[3] the reciprocity theorem states that the phase and strength of the scattered field are unchanged when the angles of incidence and scattering are interchanged.

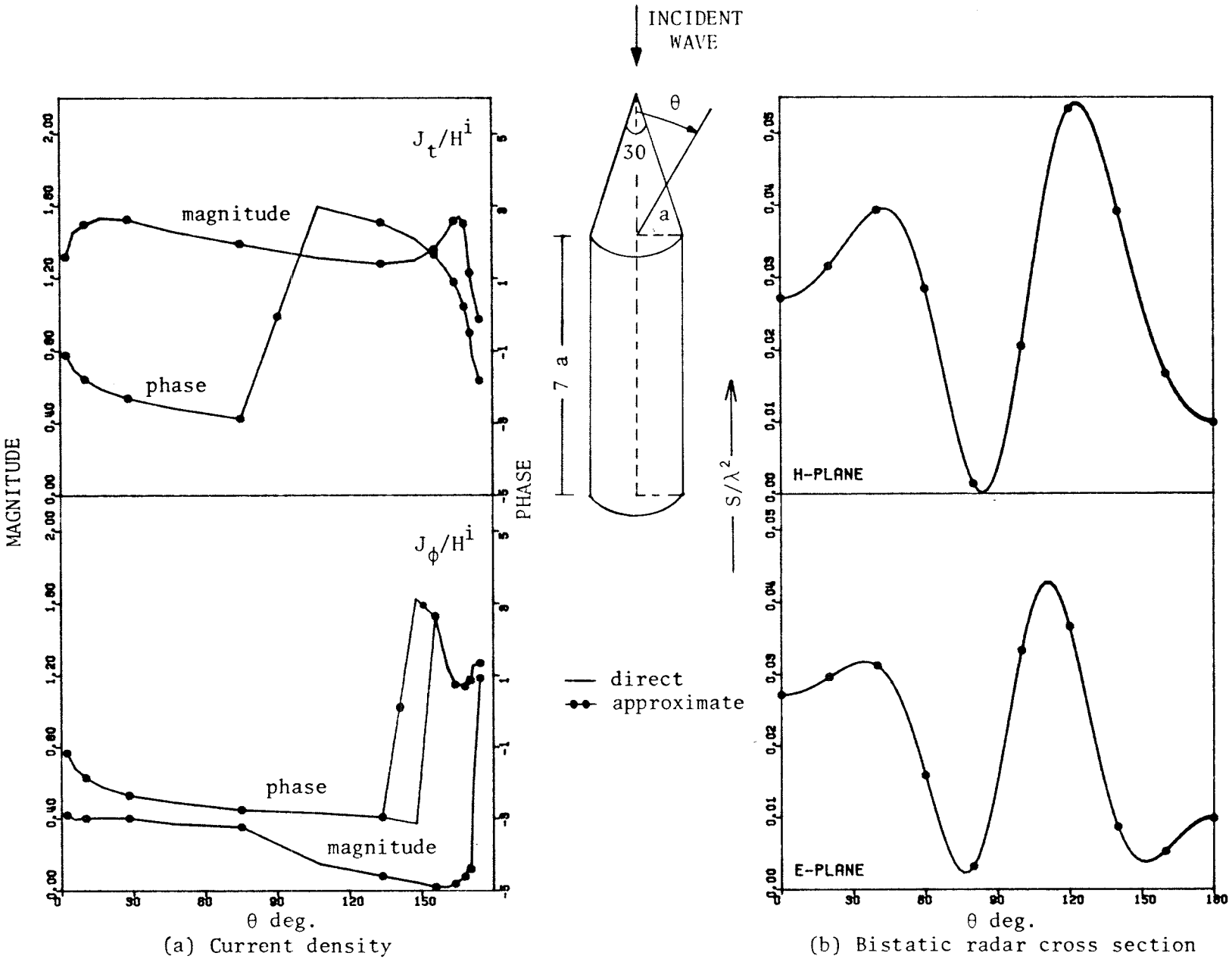

Figure 4.6: Current and field distributions for an imperfectly conducting cone-cylinder ($a = 0.2\lambda = 1m$), $\sigma = 10^3$ S/m. and $\theta^i = 0^o$.

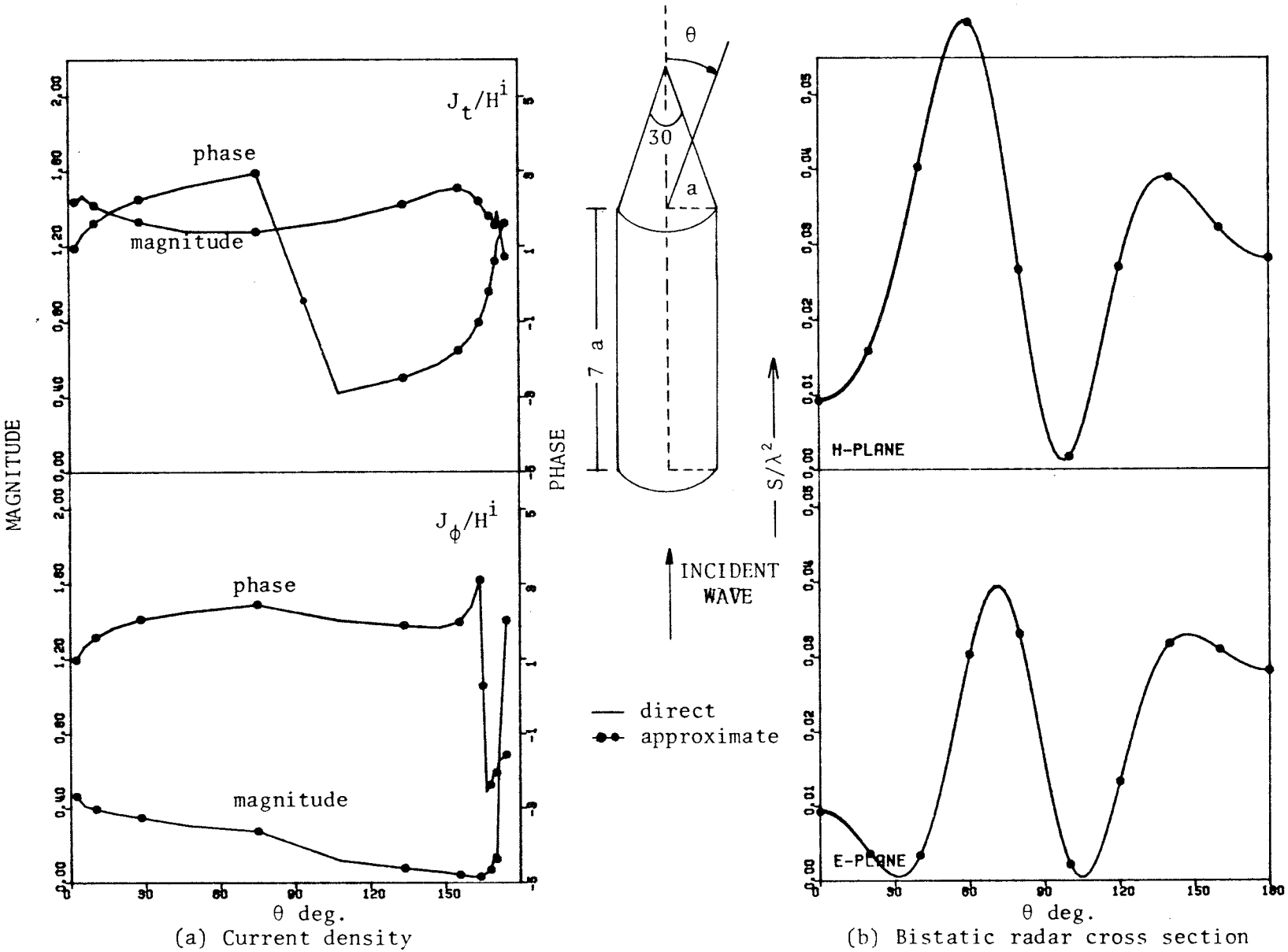

(a) Current density

(b) Bistatic radar cross section

Figure 4.7: Same as in Fig. 4.6 except $\theta^i = 180°$.

TABLE 4.1

Normalized bistatic cross section in forward and backward directions using direct and approximate solutions of the *MFIE*.

OBJECT GEOMETRY	σ (S/m)	S/λ^2 backward direction $\theta^i = 0.$	S/λ^2 backward direction $\theta^i = 180.$	S/λ^2 forward direction $\theta^i = 0.$	S/λ^2 forward direction $\theta^i = 180.$	MFIE SOLUTION
cone-cylinder	1000.0	0.027150	0.028134	0.010188	0.009556	direct
		0.027141	0.028153	0.009847	0.009244	approximate
cone-sphere	1000.0	0.145776	0.174890	0.131243	0.134843	direct
		0.145656	0.175335	0.129360	0.133115	approximate
cone-sphere	10.0	0.148063	0.167666	0.169870	0.174040	direct
		0.147020	0.172005	0.149612	0.155465	approximate

4.6 LOW-FREQUENCY BEHAVIOUR OF NUMERICAL SOLUTIONS:

The scattering of electromagnetic waves at extremely low-frequencies (frequency range 1.0 Hz to 3000 Hz) has received considerable attention [84]-[87]. A general approach to low-frequency scattering problems has been proposed by Stevenson [14]. He has provided a general solution for the coefficients in a power series expansion in the wavenumber k of the scattering field and applied it successfully to solve the problem of scattering by a perfectly conducting prolate spheroid [84].

For arbitrary objects, a more general approach to solve a scattering problem is the numerical approach. It is well-known that numerical techniques are reasonably accurate in the resonance region corresponding to the range of frequencies for which the maximum dimension of the body is of the order of the wavelength. The purpose of this section is to examine the accuracy of the numerical solutions presented in the previous sections at low-frequencies.

It is found that the solutions based on *EFIE* begin to loose accuracy when the object dimension is about 0.01 λ and become worse as the frequency decreases. The same behaviour occurs with the *CFIE* solutions. Recently, Mautz and Harrington [88] have presented a new *EFIE* formulation for the electric current and charge on a perfectly conducting surface. The main feature of their numerical solutions is the proper selection of the expansion functions which are suitable for expanding the magnetostatic current and the electrostatic charge. Solutions of this new equation are reasonably accurate for object dimension as small as $2 \times 10^{-15} \lambda$.

To examine the lower limits of the numerical solution of *MFIE* for an arbitrary object, Fig. 4.8 is included. The solution is based on representing the object surface by small flat patches. The problem of scattering of electromagnetic plane wave by a sphere, for which an analytic solution exists, has been selected to test the accuracy of the numerical solution of *MFIE* at low-frequencies. Both perfectly and imperfectly conducting spheres are considered. For perfectly conducting objects, it is found that the lower limit of the object dimension is obout $10^{-7}\lambda$, to obtain accurate scattered fields in both back and forward directions with less than 0.1 % error. As can be seen from Fig. 4.8 (a), the main error in the numerical solutions occurs near the null and this, in general, is a characteristic of the numerical solutions.

For imperfectly conducting case, the approximate method which has been described earlier, is used to generate the numerical solution. At very low frequencies, the penetration level of the electromagnetic wave is high, this results in the inaccuracy in Fig. 4.8 (b). The maximum error in this case does not exceed 6.5 % in either the back or forward directions. When the frequency increases, the electrical dimension of the body increases. In this case, the percentage penetration of the signal decreases, which improves the accuracy of the numerical solution.

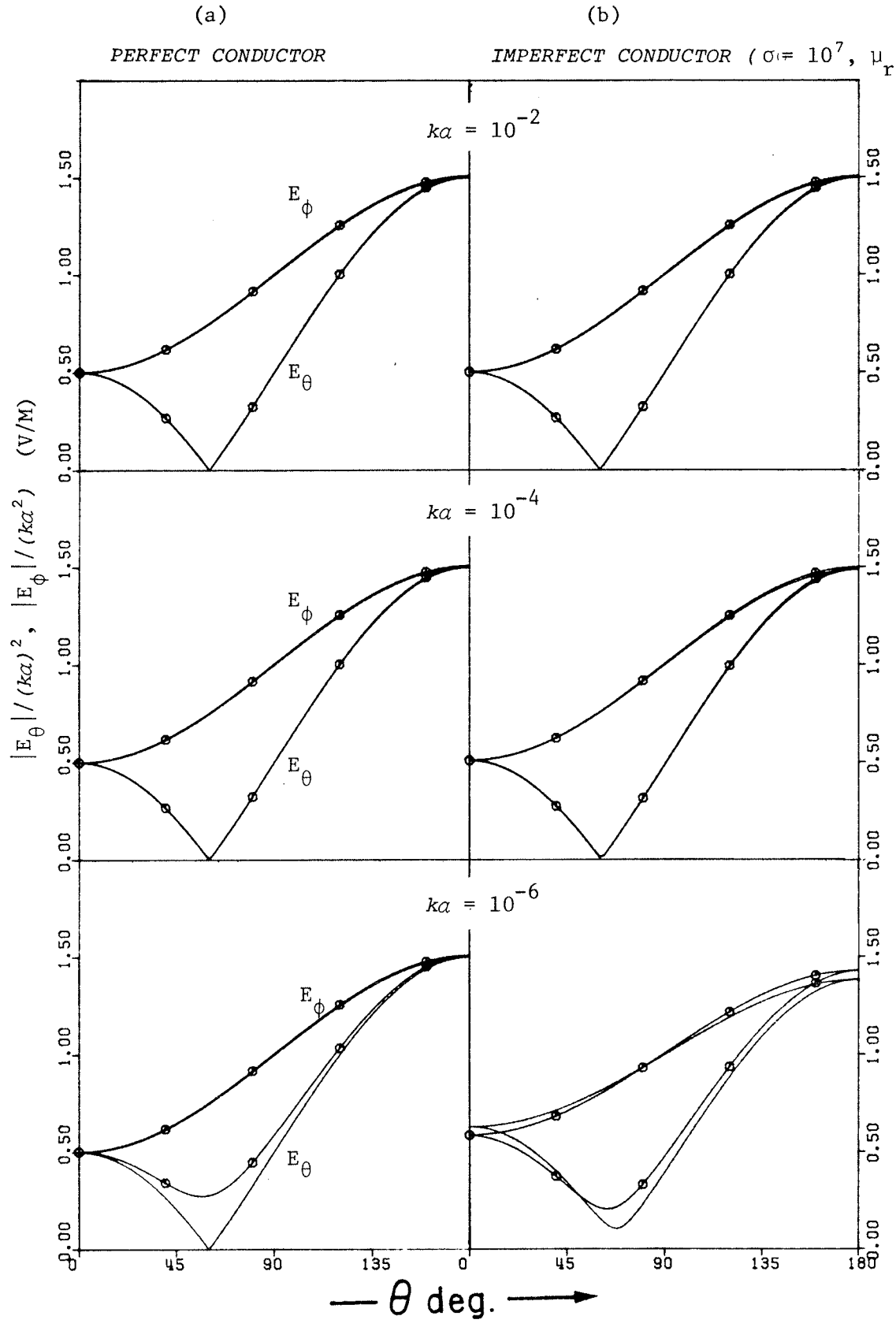

Figure 4.8: Comparison of the numerical (curves with circles) and analytic (solid curves) solutions of low-frequeny scattering by a sphere of radius a for selected small values of ka, $\theta^1 = 180°$.

4.7 SURFACE MODELING EFFECT:

In order to illustrate the effect of patch modeling on the numerical results, Fig. 4.9 is included which shows the computed normalized bistatic scattering cross sections and field phases in the principal plane (ϕ = 0°) for different angle of incidence. The scatterer is a permeable sphere of radius $a=(\lambda/2\pi)$, whose surface is divided into 18 patches per octant. A very good agreement with the exact solution is obtained for all angles of incidence. It is found that, in general, a patch model of the surface is suitable for a wide band of frequencies, as well as any arbitrary angle of incidence.

For bodies of revolution there are two factors which may have effects on the accuracy of the numerical solution presented in *Chapter Three*. One of them is the number of segments along the generating curve and the other is the number of modes to be selected. It was found there that, solutions based on the *EFIE*, in general, required more segments than the other two cases to yield certain accuracy. On the other hand, for an oblique incidence of the wave, all solutions need at least 10 modes to obtain reasonable accuracy. However, for axial incidence, only two modes ($m = +1$ and -1) in Equ. (3-31) are excited.

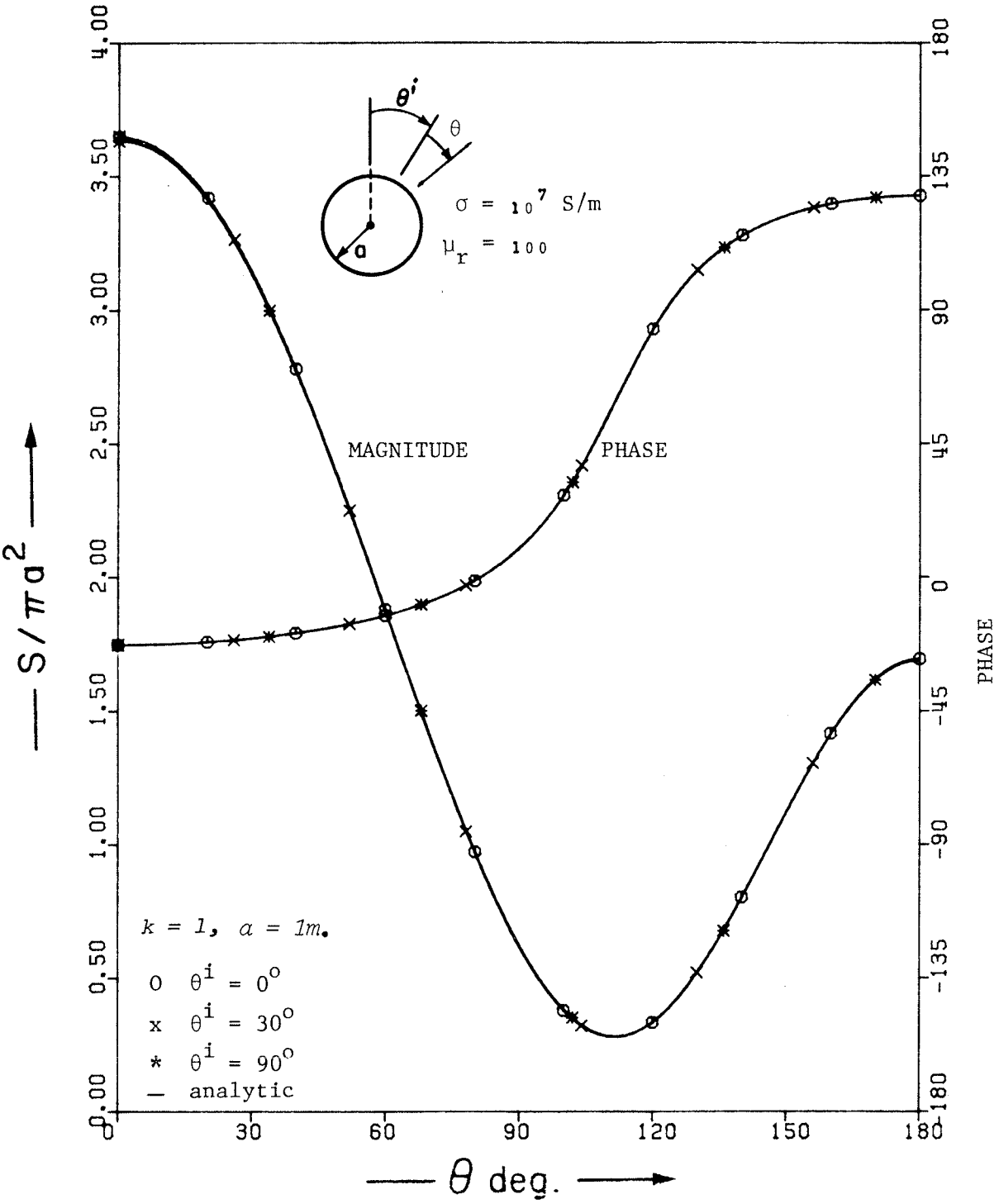

Figure 4.9: Effect of the surface modeling scheme on the numerical solution.

4.8 SUMMARY:

An approximate numerical method to determine the scattered field of arbitrarily shaped objects with impedance boundary conditions has been presented. It utilizes the well-known integral equation formulation of perfectly conducting objects to determine the surface electric current distributions. The surface magnetic currents are generated, from the computed electric currents, using the impedance boundary conditions. Comparing the results with the analytic or the direct integral equation solutions, it was found that, although the method gives approximate electric and magnetic currents, the accuracy of the backscattering data is always reasonable. Its main advantages are in the use of available numerical codes for perfectly conducting objects, the simplicity of the required matrix equation and finally, in the use of a single matrix equation solution to generate the scattering data for the same object with different surface impedances.

Chapter Five

TRANSIENT RESPONSE

5.1 INTRODUCTION:

In the previous chapter, steady state solutions of scattering by imperfectly conducting objects were discussed. The method which has been used is based on applying the concept of the impedance boundary conditions to simplify the numerical solutions of this problem and to increase its efficiency. In this chapter, solutions of this problem are considered in the time domain, where the transient response of an object to a particular incident field is related to its geometry and its material parameters.

The time response of a scatterer under the influence of a short electromagnetic pulse has been studied previously [41]-[47]. It may be obtained either by a transformation of the frequency domain data using the transform technique, or a direct solution of the space-time integral equation using the direct technique [10]. In the transform technique, the transient response is obtained from a Fourier transform of its corresponding data in the frequency domain. In this case, all the frequency domain solutions, up to an effective frequency, must be obtained and the entire results must be transformed. For arbitrarily shaped objects, the solution for the scattered field is usually obtained by the method of moment, which reduces the initial integral equation to a matrix equation. Most of the computation time is therefore used to

generate the matrix elements and to solve the resulting matrix equation. Because this matrix is independent of the incident wave in the frequency domain formulation, considerable saving in computation can be achieved if the solution for a large number of incident waves arriving from different directions is required. In contrast, the direct technique obtains solutions by "marching on in time" procedure, along the direction of propagation, using the space-time integral equation. Thus, the solution is clearly valid for the incident wave arriving from a particular direction. On the other hand, this technique is more efficient than the transform technique for a given incident wave, and is generally preferred when the number of the incident waves is moderate.

The scattering of plane electromagnetic waves by perfectly conducting objects in the time domain has been considered by many investigators. The backscattering by a perfectly conducting sphere was studied by Weston [89], Kennaugh [90],[91] and Rheinstein [92],[93]. Using impulse response approximations, Kennaugh and Moffatt have calculated the axial echo area of perfectly conducting cone-spheres [94] and prolate spheroids [95]. Using the physical optics approximation and the time domain interpretation of the creeping wave mechanism, Chaudhuri [96] has presented a time domain synthesis approach to solve a 3-dimensional scattering problem involving perfectly conducting ellipsoids.

This chapter considers a procedure for efficient computations of the electromagnetic transient response of imperfectly conducting permeable objects. Since a solution to the interior field of arbitrarily shaped objects is difficult to obtain, the impedance

boundary conditions are used to formulate the problem. However, the impedance boundary conditions are not known in the time domain and hence the transform technique is used in which the frequency domain scattered fields are computed numerically. Since only highly conducting objects are considered, the use of the impedance boundary conditions is valid and conveniently relates the solutions to the physical parameters of the object.

The excitation is assumed to be due to a periodic pulse train and generated by a circular loop. Noting that the tangential components of the electric field on a highly conducting object are small, a simplified numerical method is used to compute the frequency domain scattered fields. The method initially neglects the magnetic surface currents and determines them from the electric surface currents using the impedance boundary conditions. The method therefore computes the scattered fields of imperfectly conducting objects using the numerical codes of the perfectly conducting objects, which are readily available. The validity of such an approximation was previously established [81]-[83] and was shown to give the backscattering data accurately. The general theory and method of computation were given in detail in *Chapter Four.*

In the computation of the transient[4] respone, only very low fundamental frequencies are selected, which can be used in detection of buried objects. At sufficiently low-frequencies, the signal penetration into the ground is high and the air-earth interface has a negligible effect on the returned responses [97]. The use of the exciting loop

[4] Although, the term "transient" in a general sense is normally used to describe the time domain response due to a step or single pulse function, it has been used here to represent the response due to a periodic pulse train.

also minimizes the ground conductivity effect. For the computational purposes, a conducting permeable spheroid is selected and the transient responses are computed for different spheroid parameters and orientations.

5.2 FORMULATION:

The geometry of the scatterer, the source and the receiver are illustrated in Fig. 5.1. A prolate spheroid is considered to be a reasonable geometrical model to study the transient response of finite or bounded objects. Thus, a spheroid of semi-major axis A, semi-minor axis B and having a semi-focal distance F is assumed to be located centrally at the origin of the coordinate system. Its physical parameters are represented by a conductivity σ, a permeability μ and a permittivity ε. A small current loop of radius RT is located at (x_o, y_o, DT) and carries a current I, which is a periodic pulse train with 50 percent duty cycle and having the fundamental frequency f_o. For a small loop radius, this source therefore is equivalent to a magnetic dipole, oriented in the direction of the outward normal to the loop surface. *Appendix B* provides the derivations of the field components radiated by the loop.

Using the Fourier series of the pulse train, the time-dependent part of the incident field may be represented by

$$H^i(t) = \sum_{n = 1,3,5,..} A_n \cos(n\omega_o t) + A_o \qquad (5\text{-}1)$$

where

$$A_o = 1$$
$$A_n = 2/n\pi \ (-1)^{\left(\frac{n+3}{2}\right)} \qquad (5\text{-}2)$$

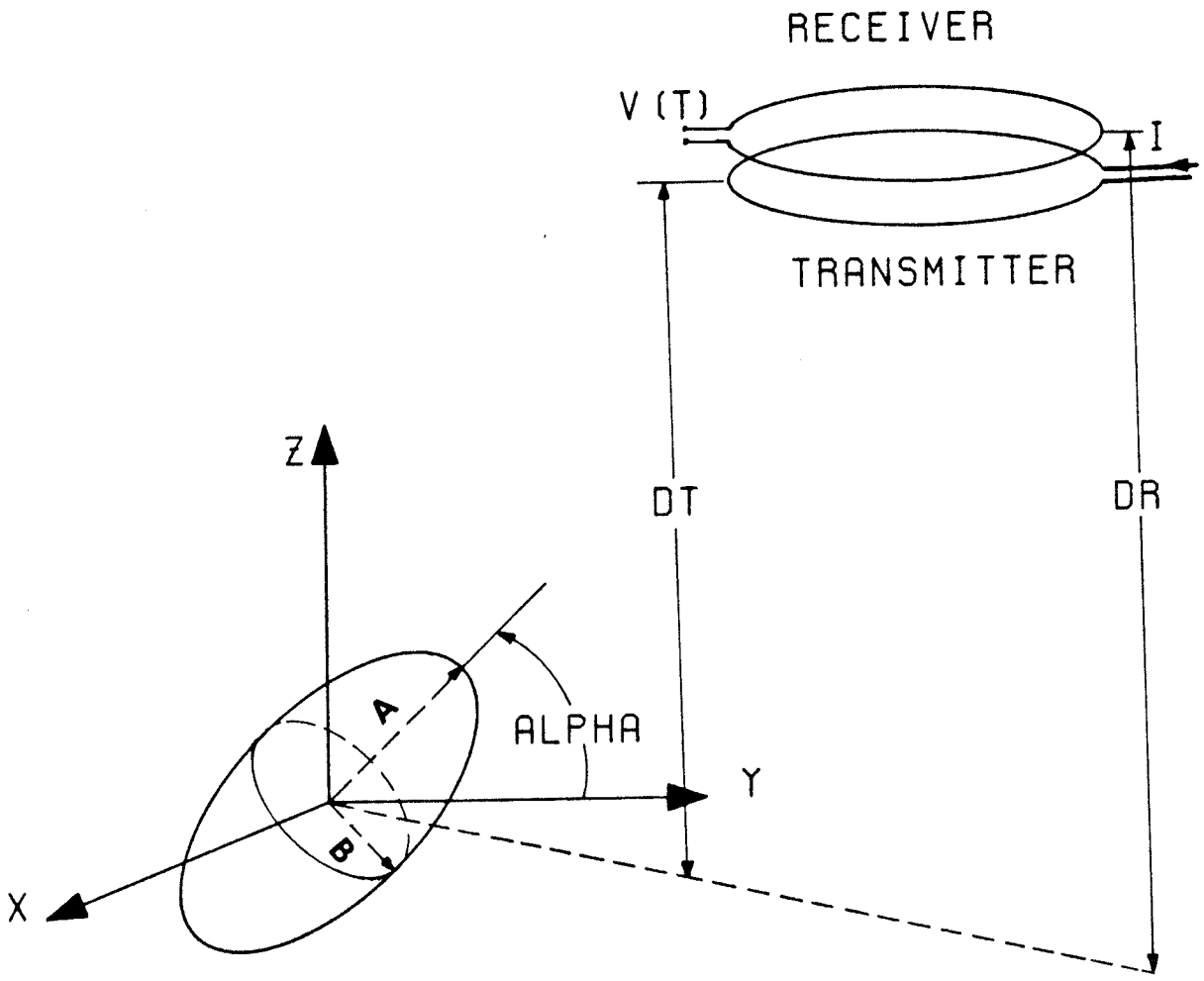

Figure 5.1: Geometry of spheroid, transmitter and receiver loops.

To compute the transient response of an object, it is assumed that the object and its surrounding medium constitute a linear system, the medium being the free space. Since the concept of the impedance boundary conditions is not known in the time domain, the transient response is obtained using the frequency domain data. The transient response of the body at a point (x,y,z) can therefore be written in the form

$$\mathcal{G}(x,y,z,t) = Re \sum_{n = 1,3,5,..} A_n \; F(x,y,z,jn\omega_0) \; exp(jn\omega_0 t) \qquad (5-3)$$

where $F(x,y,z,jn\omega_0)$ is the scattered field at frequency $(n\omega_0)$, calculated at the space point (x,y,z). The scattered field components in the frequency domain are obtained by solving the *MFIE* at the fundamental frequency of the incident field and its harmonics using the method of moment, and are discussed later. The return signal in the time domain $\mathcal{G}(x,y,z,t)$ may be measured using a receiving circular loop of radius RR with its center located at (x_1, y_1, DR). In such a case, the measured signal is the induced voltage due to the scattered field. This induced voltage may be calculated either by a line integral of the electric field along the loop, or by a surface integral of the time derivative of the magnetic field. That is

$$v(t) = \oint_{\text{loop length}} \vec{E}^s(t) \cdot d\vec{l} \qquad (5-4)$$

or,

$$v(t) = -\mu_o \int_{\text{loop surface}} \frac{\partial \vec{H}^s(t)}{\partial t} \cdot d\vec{s} \qquad (5\text{-}5)$$

where $\vec{E}^s(t)$ or $\vec{H}^s(t)$ are given by Equ. (5-3) with $F(x, y, z, jn\omega_o)$ representing the scattered electric or magnetic fields, respectively.

Equation (5-4) seems easier to handle numerically, since it requires only a line integration. In contrast, Equ. (5-5) involves a surface integration and is thus more difficult to handle. In addition, a time derivative of $\vec{H}^s$ in Equ. (5-5) deteriorates the convergence of the series, due to the introduction of an additional factor $(jn\omega_o)$ in each term of the series. Thus, an evaluation of the return signal using Equ. (5-4) should be preferred. However, in evaluation of the transient response $v(t)$ at very low-frequencies and at locations adjacent to the object, it was found that the computed data for $\vec{H}^s(jn\omega_o)$ were more accurate than the results for $\vec{E}^s(jn\omega_o)$. The difficulty with accurate computation of the scattered electric field was related to round off errors at very low-frequencies, and did not cause inaccuracy of computation at higher frequencies. Since we were interested in generating data at very low-frequencies, we used Equ. (5-5) for all our computation by a surface integration of the magnetic field.

Since the convergence of the series in Equ. (5-5) deteriorates due to an additional time derivative, an alternative approach was used to calculate $v(t)$. That is, in Equ. (5-5) the order of integration and differentiation was changed. Initially, the computed data for $\vec{H}^s(jn\omega_o)$

were used to compute the total flux linkage in the receiver loop. The results were then used to calculate the time derivatives of the total flux by using a numerical differentiation. An examination of the results of this approach indicated that they were accurate and required less computer time than a summation of the series for the magnetic field time derivatives.

5.3 COMPUTATION OF THE FREQUENCY DOMAIN DATA:

In this section, a brief review of the method that was used previously to compute the scattered field of imperfectly conducting objects [81]-[83], is given. The method was described in some detail in *Chapter Four*. It is based on the numerical solution of the *MFIE* on the surface of the scatterer. Usually, the surface is divided into sub-areas or patches and the surface integral expressed as a sum of integrals over each patch. The method of moment is then used to reduce the integral equation to a matrix one of the form

$$\begin{bmatrix} A_{ij}^{(1)} & A_{ij}^{(2)} \\ A_{ij}^{(3)} & A_{ij}^{(4)} \end{bmatrix} \begin{bmatrix} a_i \\ b_i \end{bmatrix} = \begin{bmatrix} V_j^{(1)} \\ V_j^{(2)} \end{bmatrix} \tag{5-6}$$

where A_{ij}'s are the elements of the moment matrix and were given explicitly by Equs. (4-12)-(4-15) of *Chapter Four* and a_i, b_i are the unknown electric surface currents and V_j's are the elements of the excitation vector.

5.3.1 *Evaluation of the Circular loop Excitation Vector:*

A loop of radius c is defined by the position vector of its center $\vec{R}_o$ and the normal $\hat{p}$ to its plane, as shown in Fig. 5.2. For a given loop orientation, the magnetic field components in terms of the loop coordinates are given by (see *Appendix B*)

$$H_\theta = \frac{jI}{2R_i}\sum_{n=1}^{\infty}\left[\frac{2n+1}{n(n+1)}\hat{J}_n(kc)\,\hat{H}_n^{(2)\prime}(kR_i)\,P_n^1(0)\,P_n^1(\cos\theta_i)\right] \quad (5\text{-}7)$$

$$H_R = -\frac{jI}{2kR_i^2}\sum_{n=1}^{\infty}\left[\frac{2n+1}{n(n+1)}\hat{J}_n(kc)\,\hat{H}_n^{(2)}(kR_i)\,P_n^1(0)\cdot\left(\frac{dP_n^1(\cos\theta_i)}{d\theta}+\cos\theta_i\frac{P_n^1(\cos\theta_i)}{\sin\theta_i}\right)\right] \quad (5\text{-}8)$$

for $R_i > c$.

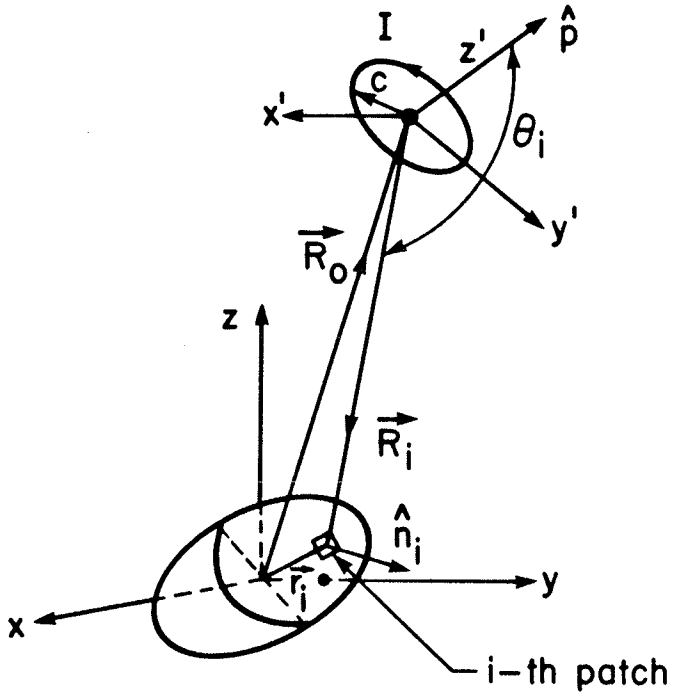

Figure 5.2: Coordinate parameters for spheroid and circular loop.

The elements of the excitation vector are computed from

$$V_i^{1,2} = \hat{t}_{2,1} \cdot \vec{H}^i$$

$$= \hat{t}_{2,1} \cdot \left[H_p \hat{p} + H_{\rho'} \hat{\rho}' \right]$$

$$= \hat{t}_{2,1} \cdot \left[\left\{ H_R \cos\theta_i - H_\theta \sin\theta_i \right\} \hat{p} + \left\{ H_R \sin\theta_i + H_\theta \cos\theta_i \right\} \hat{\rho}' \right] \qquad (5\text{-}9)$$

where

$$\vec{\rho}' = \left\{ \hat{R}_i - (\hat{p} \cdot \hat{R}_i)\, \hat{p} \right\} \qquad (5\text{-}10)$$

$$\hat{\rho}' = \vec{\rho}' / |\vec{\rho}'| \qquad (5\text{-}11)$$

$$\vec{R}_i = \vec{r}_i - \vec{R}_o \qquad (5\text{-}12)$$

$$\cos\theta_i = \hat{R}_i \cdot \hat{p} \qquad (5\text{-}13)$$

5.4 NEAR FIELD COMPUTATION:

The scattered magnetic field $\vec{H}^s$ is computed at $\vec{r}=(x,y,z)$ due to the electric current $\vec{J}_i$ and the magnetic current $\vec{M}_i$ on the patch i centered at $\vec{r}_i=(x_i,y_i,z_i)$. The magnetic current $\vec{M}_i$ is given by

$$\vec{M}_i(\vec{r}_i) = \bar{\bar{Z}}_i(\vec{r}_i) \cdot \vec{J}_i(\vec{r}_i) \times \hat{n}_i(\vec{r}_i) \qquad (5\text{-}14)$$

where $\overline{\overline{Z}}_i$ and $\hat{n}_i$ are respectively the dyadic surface impedance matrix and the normal to the patch at $\vec{r}_i$.

The magnetic field due to patch i, is approximated by

$$\vec{H}^s_i = \vec{H}^s_{J_i} + \vec{H}^s_{M_i} \tag{5-15}$$

where

$$\vec{H}^s_{J_i} = -\frac{1}{4\pi}\left[\left\{1 + jkR_i\right\}\frac{\exp(-jkR_i)}{R_i^3}\right]\vec{R}_i \times \vec{J}_i S_i \tag{5-16}$$

$$\vec{H}^s_{M_i} = \frac{\lambda}{18\pi^2 Z_o}\left[\frac{-(1 + jkR_i - k^2R_i^2)}{R_i^3}\vec{M}_i + \frac{3 + j3kR_i - k^2R_i^2}{R_i^5}\left\{\vec{M}_i \cdot \vec{R}_i\right\}\vec{R}_i\right]\exp(-jkR_i)S_i \tag{5-17}$$

with $\vec{R}_i = \vec{r} - \vec{r}_i$ and S_i is the area of patch i. The $\vec{H}^s$ field due to N patches is then computed by

$$\vec{H}^s = \sum_{i=1}^{N} \vec{H}^s_i \tag{5-18}$$

5.5 NUMERICAL RESULTS:

In evaluation of the transient response using Equs. (5-3) and (5-5), about 400 harmonics of the fundamental frequency were utilized. The fundamental frequency of the pulse train was selected to be 500 Hz. The convergence of the series depends on the object surface impedance, namely, the ratio of μ_r/σ. Generally a reduction of this ratio deteriorates the convergence and additional harmonics are needed to achieve satisfactory convergence. In all cases, however, an adequate number of harmonics were retained to ensure convergence. In all graphs, the geometrical parameters are represented by the following notations:

ST: steel ($\sigma = 10^7$ S/m)

AL: aluminum ($\sigma = 3.5 \times 10^7$ S/m)

DT: vertical distance between transmitter loop and spheroid center

DR: vertical distance between receiver loop and spheroid center

MUR: relative permeability of spheroid

ALPHA: angle between spheroid major axis and the y axis, in degrees

A and B: semi-major and semi-minor axes of spheroid

RT and RR: transmitter and receiver loop radii

V(T): transient response $v(t)$.

To examine the accuracy of the computed results, Fig. 5.3 is included, which compares the results for a steel sphere. Three different approaches are selected: the present method, an analytic solution by replacing the loop by its equivalent magnetic dipole, and a

solution based on quasi-static transient analysis [98]. The agreement between the results is satisfactory , even though the excitation fields in the magnetic dipole and quasi-static analysis cases are somewhat different. The results of this numerical method fall between the other two cases. This is an expected result, since the magnetic dipole represents a point source and the quasi-static method assumes uniform field over the sphere. The main differences between the three results occur at the initial and final values of the response. Apart from the effect of the exciting source, these differences are partly due to the Gibb's phenomena which is an inherent characteristic of the frequency domain analysis (see ***Appendix C***).

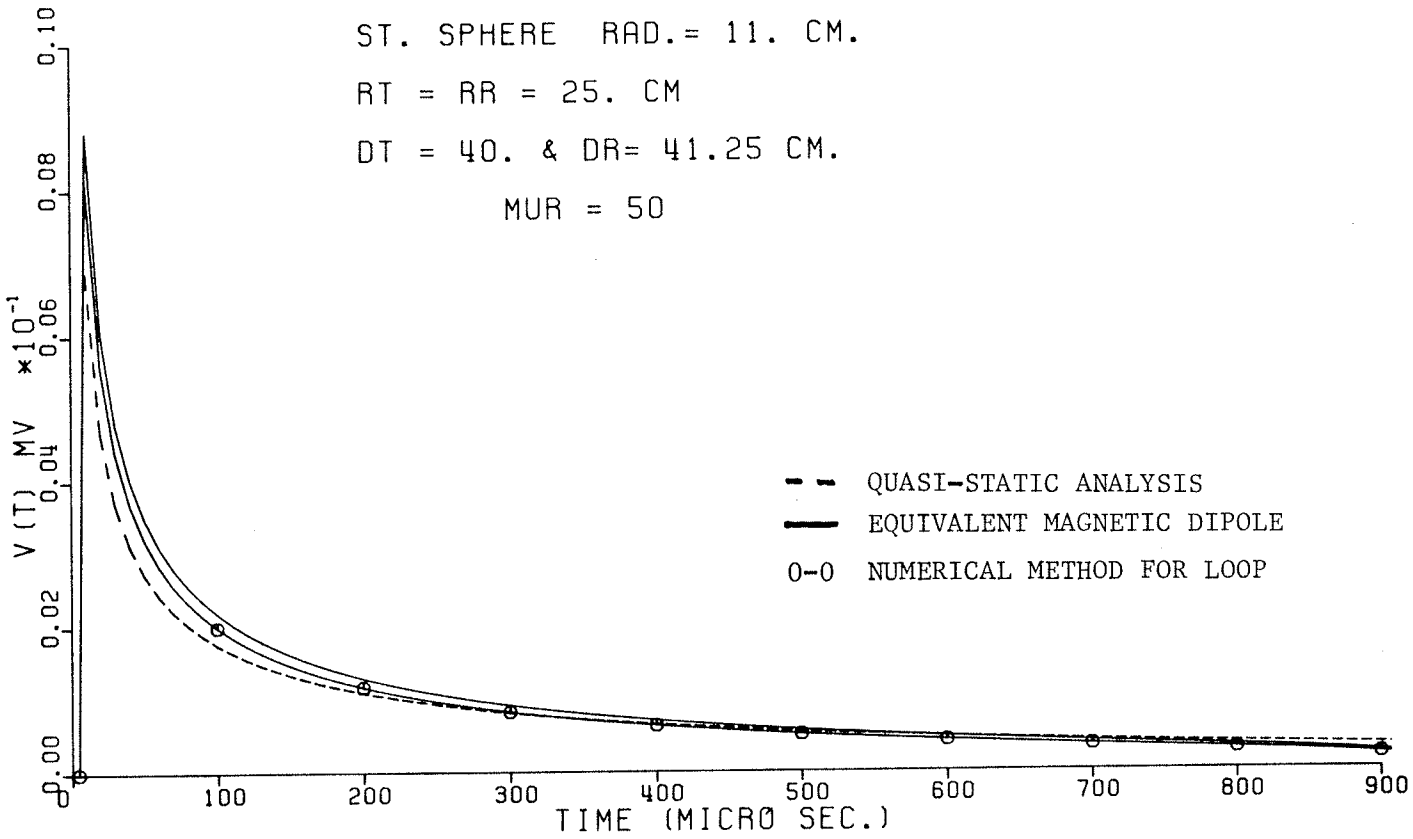

Figure 5.3: Comparison of calculated time responses of a steel sphere.

5.5.1 *Two-Dimensional Field Map:*

On a plane normal to the z axis (shown in Fig. 5.1), the time response of a spheroid depends on its location and orientation with respect to the transmitter and receiver loops. To indicate this dependence, Figs. 5.4-5.6 are presented, which show the variations of the time response in the x-y plane at a distance DT = DR = 0.4 meters above the spheroid center. In all cases the transmitter and receiver loops are coaxial, and the vertical axes show $v(t)$ in Micro Volt. Note that different scales have been used in Figs. 5.3-5.5 to facilitate the comparisons. Since the spheroid geometry is symmetrical about the y-z plane, only the results for positive x axis are shown. From these figures, it is evident that the return signal is maximum when the object is just under the loops (the z axis is co-incident with the axes of loops). The signals decay rapidly as the loops move away from the spheroid axis. This information is a significant one, which helps in locating a buried spheroid.

5.5.2 *Orientation Effect:*

The two-dimensional field maps of Figs. 5.4-5.6 indicate also the effect of orientation of the spheroid. In Fig. 5.4, the object is symmetric about the z axis. The time responses are therefore the same for equal displacements of the loops from the z axis along + y or $\pm$ x axes. In Figs. 5.5 and 5.6, the spheroid geometry is not symmetric about the z axis. Thus, the signals are not equal for equal displacements along x or y axis. However, in Fig. 5.6,

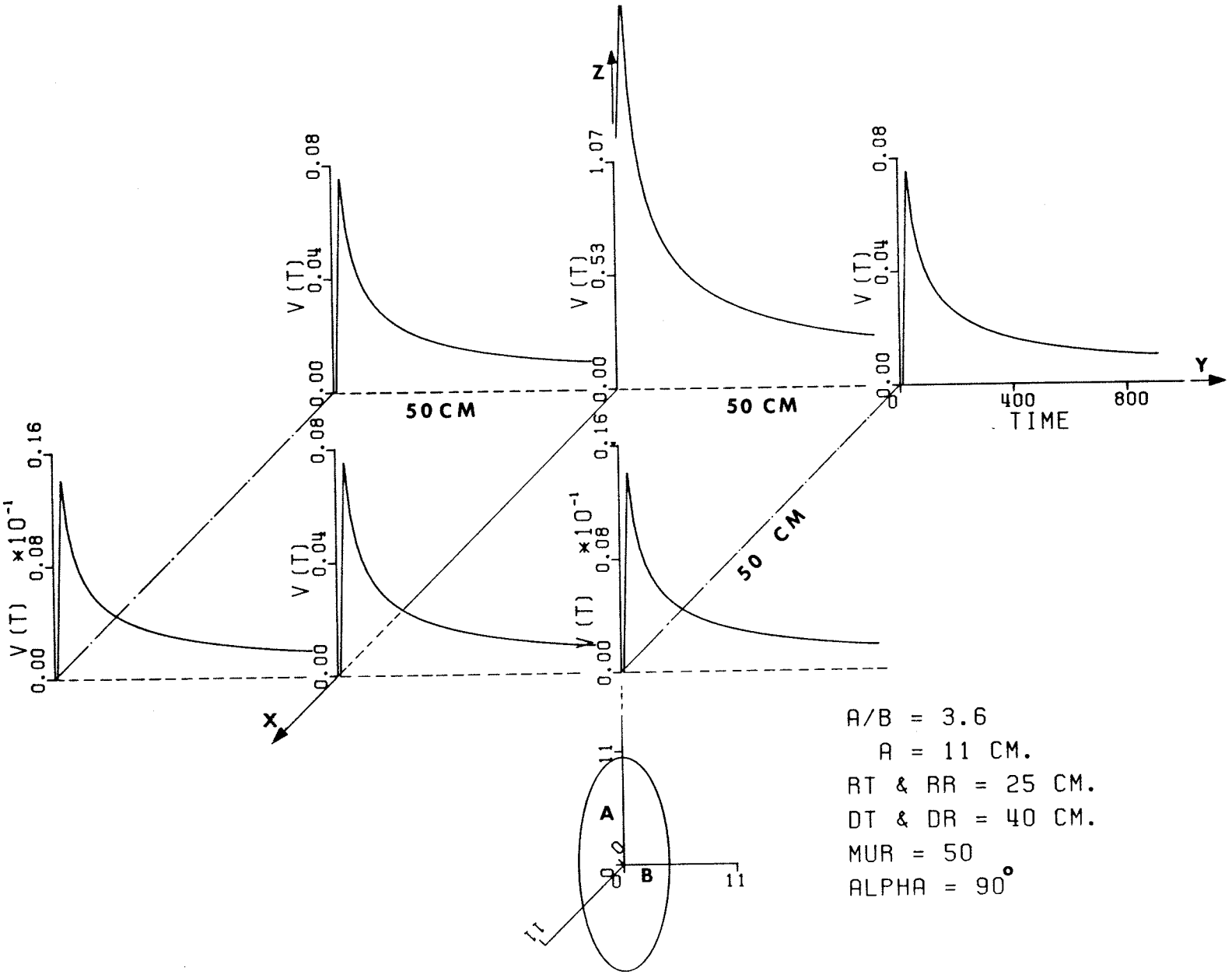

Figure 5.4: Two dimensional field map of the time response of a vertical steel spheroid (ALPHA = 90) in a horizontal plane at a distance DR = 40 cm. above the spheroid center, vertical axes in μv.

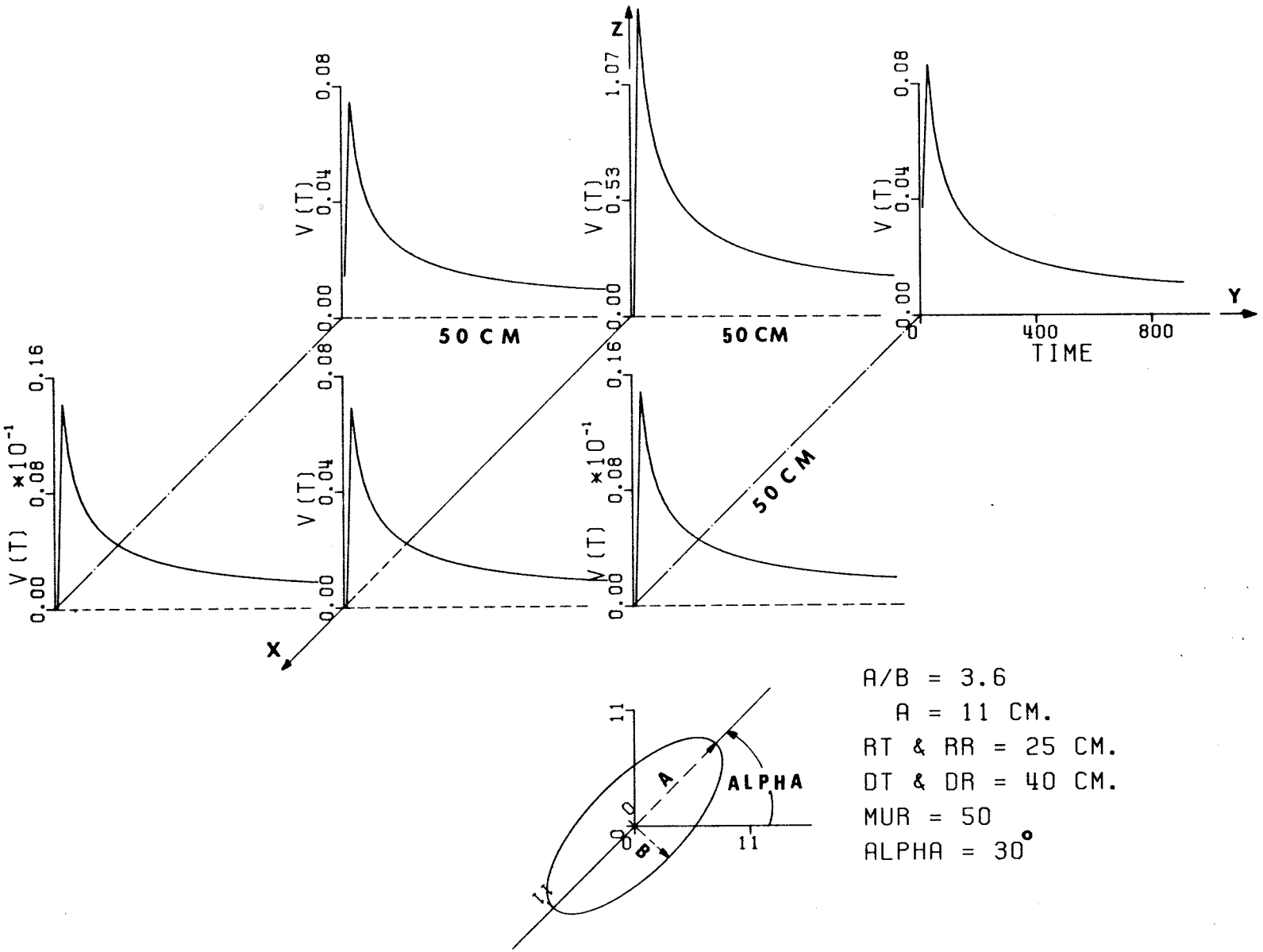

Figure 5.5: Same as Fig. 5.4 except ALPHA = 30.

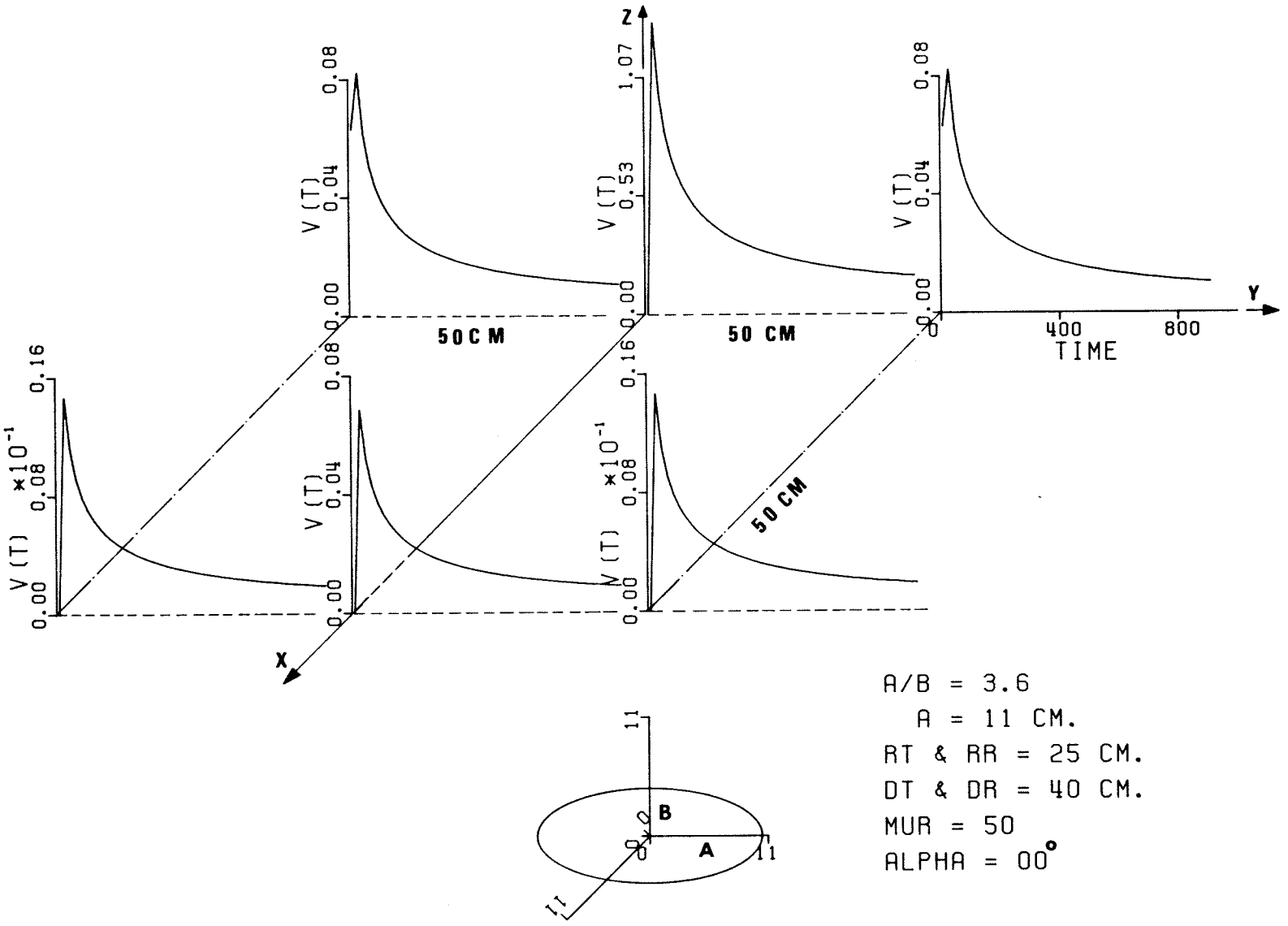

Figure 5.6: Same as Fig. 5.4 except ALPHA = 0.

the symmetry of the object about the x-z plane gives identical results for + ve or - ve displacement along y axis. In Figs. 5.4-5.6, by comparing the return signal levels, calculated along the z axis, one can note that a vertical spheroid (ALPHA = 90°) gives the highest signal level, while the horizontal one (ALPHA = 0°) gives the lowest signal. However, the return signal levels along the y axis have different behaviours. For example, while ALPHA = 30° gives the lowest relative level on the negative y axis and the highest relative level on the positive y axis, ALPHA = 0° gives the highest relative level on the negative y axis and a level between ALPHA = 30° and ALPHA = 90° on the positive y axis. The relative signal levels along both x and y axes are of great interest in determining the orientation of a buried object.

5.5.3 Material Effect:

The effect of object conductivity and permeability on the transient response is illustrated in Fig. 5.7 by showing the results for an aluminum spheroid (AL: $\sigma = 3.5 \times 10^7$ S/m, $\mu_r = 1$) and two steel spheroids (ST: $\sigma = 10^7$ S/m, $\mu_r = 25$ and 50). It is clear that the signal returns from steel spheroids are significantly larger than that from the aluminum one. Similarly, for the steel spheroid of $\mu_r = 50$, the return response is larger than that of the spheroid with $\mu_r = 25$. This behaviour is true at all space points shown in Figs. 5.4-5.6 and for values of ALPHA = 0° , 30° , 60° and 90° . If these return signals are normalized with respect to their corresponding final values, one finds that the rate of decay for steel is normally higher than that of the aluminum.

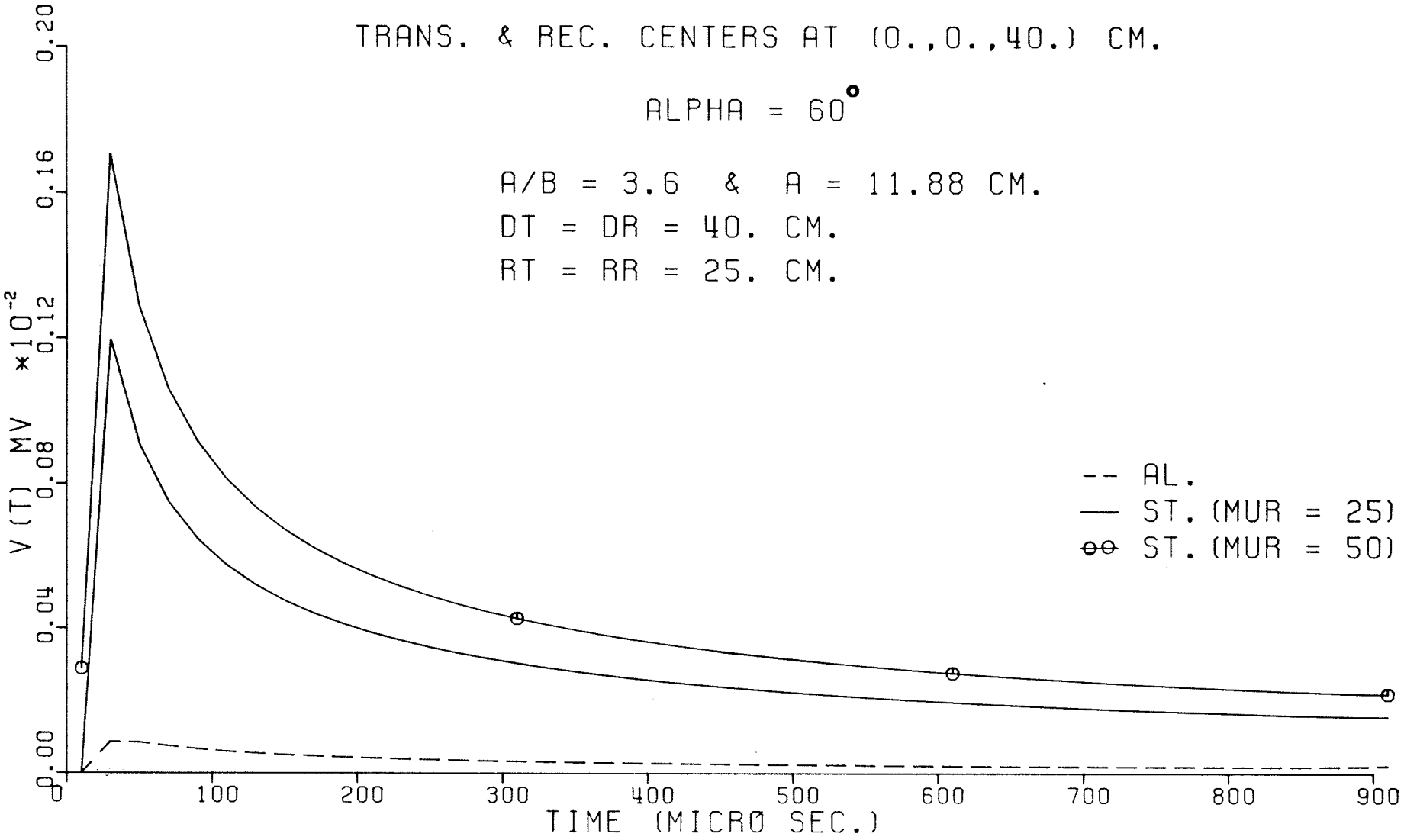

Figure 5.7: Comparison of time responses of spheroids for different material.

5.5.4 *Size and Shape Effect:*

Figure 5.8 shows the results for two different sizes of the spheroid. For the large object the return signal is, of course, larger. However, the rate of signal decay for different objects are not the same. For small objects the signal decay, due to the horizontal loop displacements, is small. On the other hand, for a larger object, the calculated signal along the z axis increases by a larger factor than at other points. This means that the ratios of the signals for two different sizes of a spheroid decrease as the loops move horizontally from the z axis.

Figure 5.9 shows the effect of spheroid axial ratios on the transient response. The spheroid major axis is retained constant which means a smaller axial ratio represents a larger object. However, the computed data shows that the ratio of the signals at every point is almost constant and is nearly equal to the increase in the axial ratio.

5.5.5 *RMS Variations:*

5.5.5.1 *Horizontal Displacement Of Receiver:*

In the previous sub-sections, the variations of the return signal as a function of time for different object parameters and at different space positions were discussed. In general, the return signal depended on the characteristics of the waveform corresponding to each of these parameters. A universal method to compare the variation of the return signal at different space position is therefore useful. One such method is the use of *rms* (root-mean-square) values for periodic voltages.

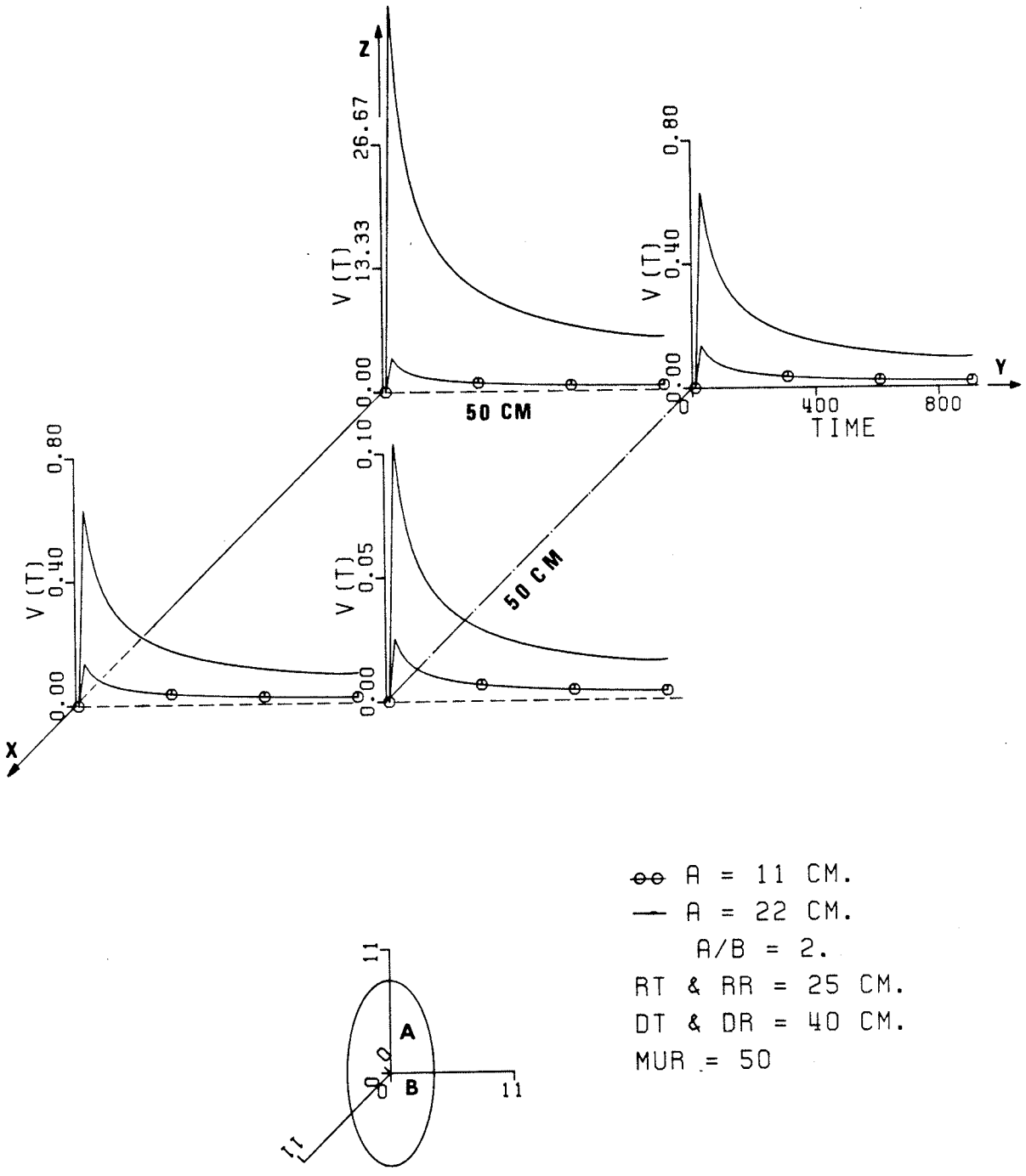

Figure 5.8: Two dimensional field map of the time response of a vertical steel spheroid in a horizontal plane for two different spheroid semi-major axes, plane distance from spheroid center DR = 40 cm and vertical axes in μv.

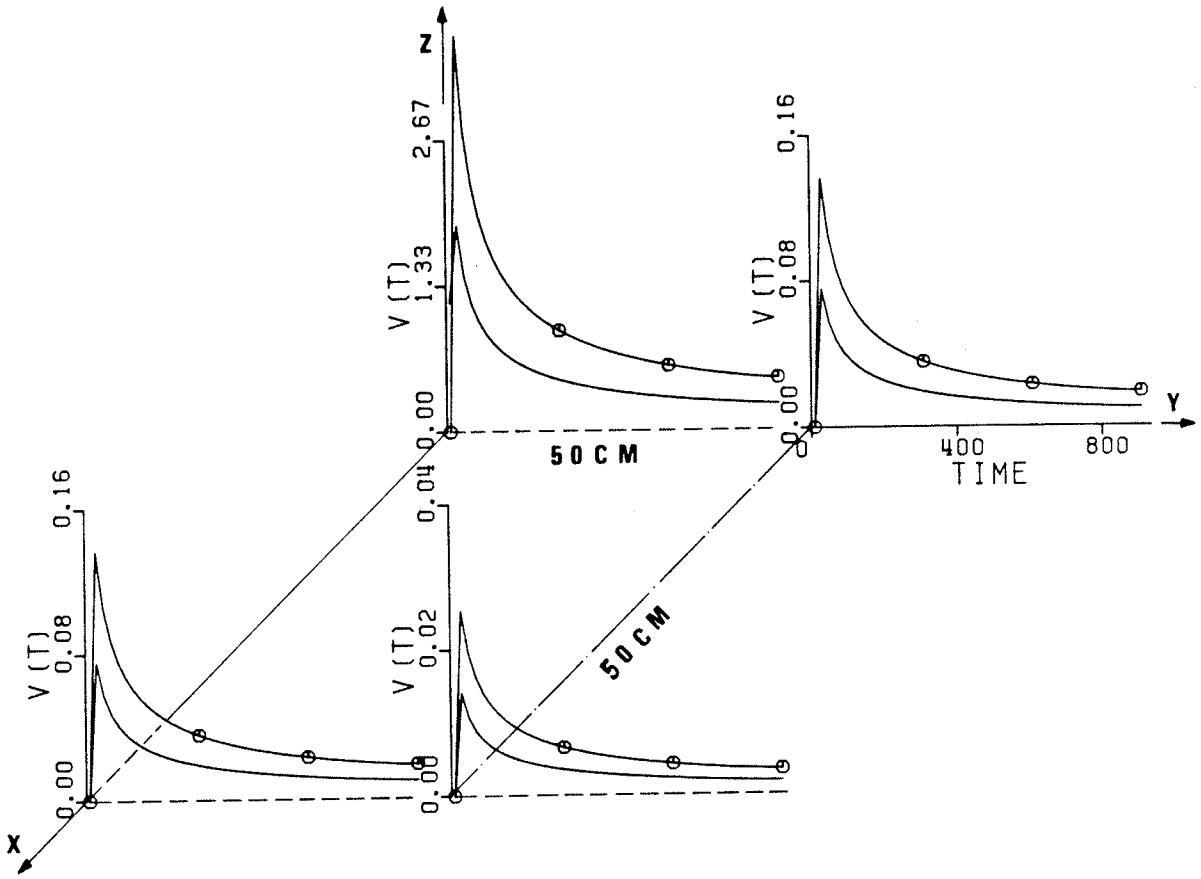

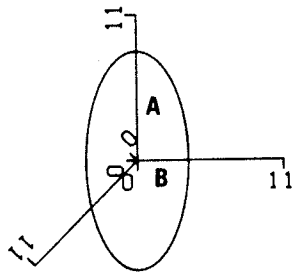

A/B = 2.
A/B = 3.6
A = 11 CM.
RT & RR = 25 CM.
DT & DR = 40 CM.
MUR = 50

Figure 5.9: Same as Fig. 5.8, but for two different axial ratios.

The *rms* value of a periodic voltage $v(t)$, V_{rms} is given by

$$V_{rms} = \sqrt{\frac{1}{T}\int_0^T v^2(t)\, dt}$$

where T is the fundamental period.

To examine the variation of V_{rms} as a function of the spheroid orientation, the receiver loop is displaced along the y axis. Fig. 5.10 shows the computed induced voltages V_{rms}, for two steel spheroids of relative permeabilities 50 and 100. For both spheroids, the peak signal levels move towards the positive y values by changing the spheroid angle ALPHA. The rise in the signal level, from its value on the z axis (Y = 0), is however small and within about 0.5 percent. Also, for each spheroid orientation the rate of the signal variation with y is larger for μ_r = 100. These results confirm the expectation that the peak signal level must move towards the closer end of the spheroid.

To amplify the rates of signal variation with y, the above results are normalized with their respective values on the z axis and are shown in Fig. 5.11. The rates of change, for μ_r = 100, are higher for all spheroid orientations. For a given spheroid, however, the rate of *rms* voltage drop increases with the angle ALPHA. These results can be explained using the magnetostatic approach. A permeable spheroid concentrates the magnetic flux lines along its major axis as shown in Fig. 5.12. Thus, when a receiver loop, which is normal to the flux lines, moves in a plane normal to the spheroid axis (ALPHA = 90°), it gives a signal level that decreases most rapidly with displacement. The rate of signal variation becomes minimum, when the loop is parallel to the spheroid axis and moves along it (ALPHA = 0° case).

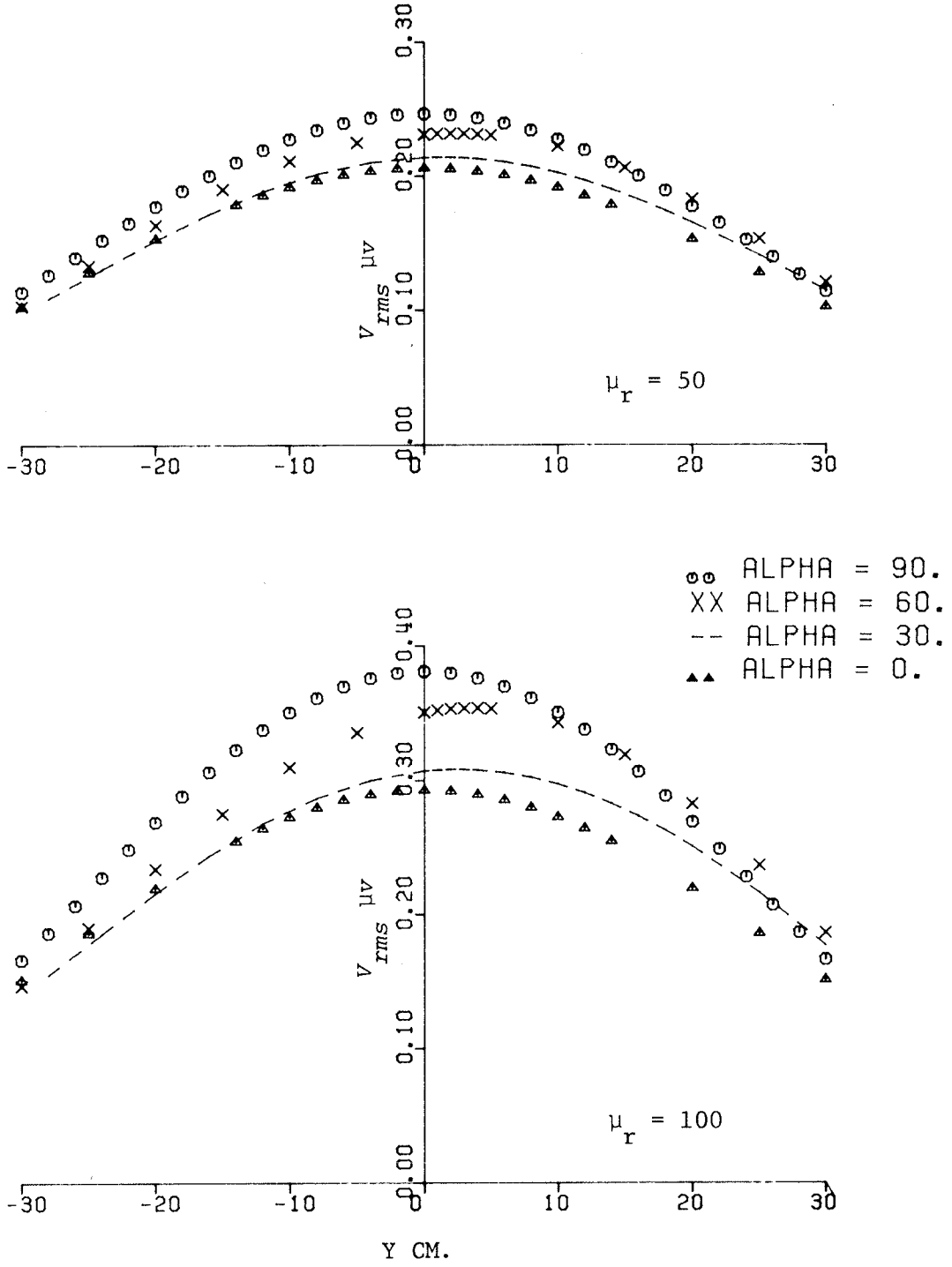

A/B = 3.6 & A = 11.88 CM
RT = 29.2 & RR = 24. CM
TRANS. & REC. CENTER AT (0.,Y,40.) CM.

Figure 5.10: Induced voltages as a function of lateral displacement along the y axis for two steel spheroids.

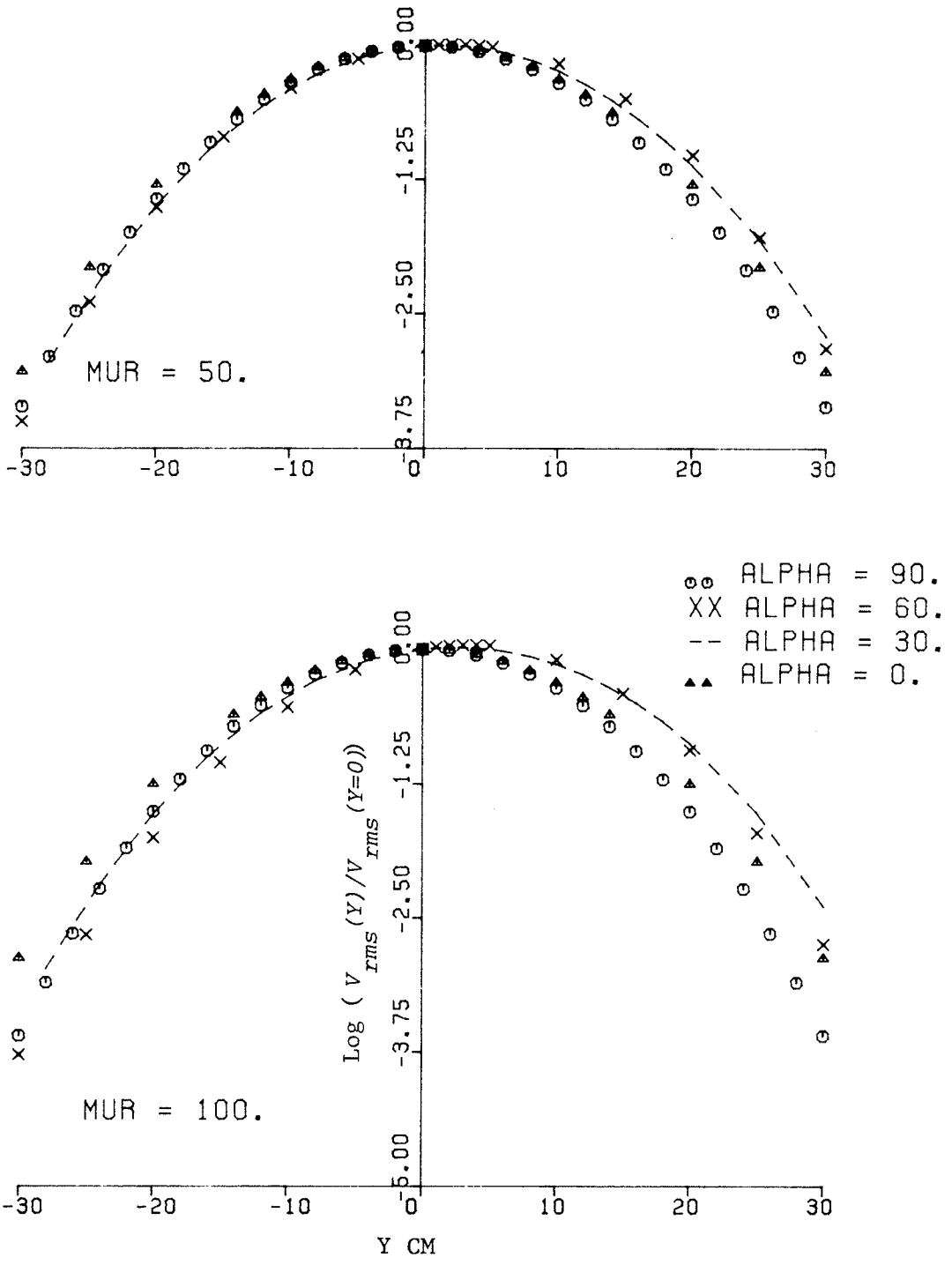

Figure 5.11: Ratio of the induced voltages (rms) relative to their values on the z axis (y = 0).

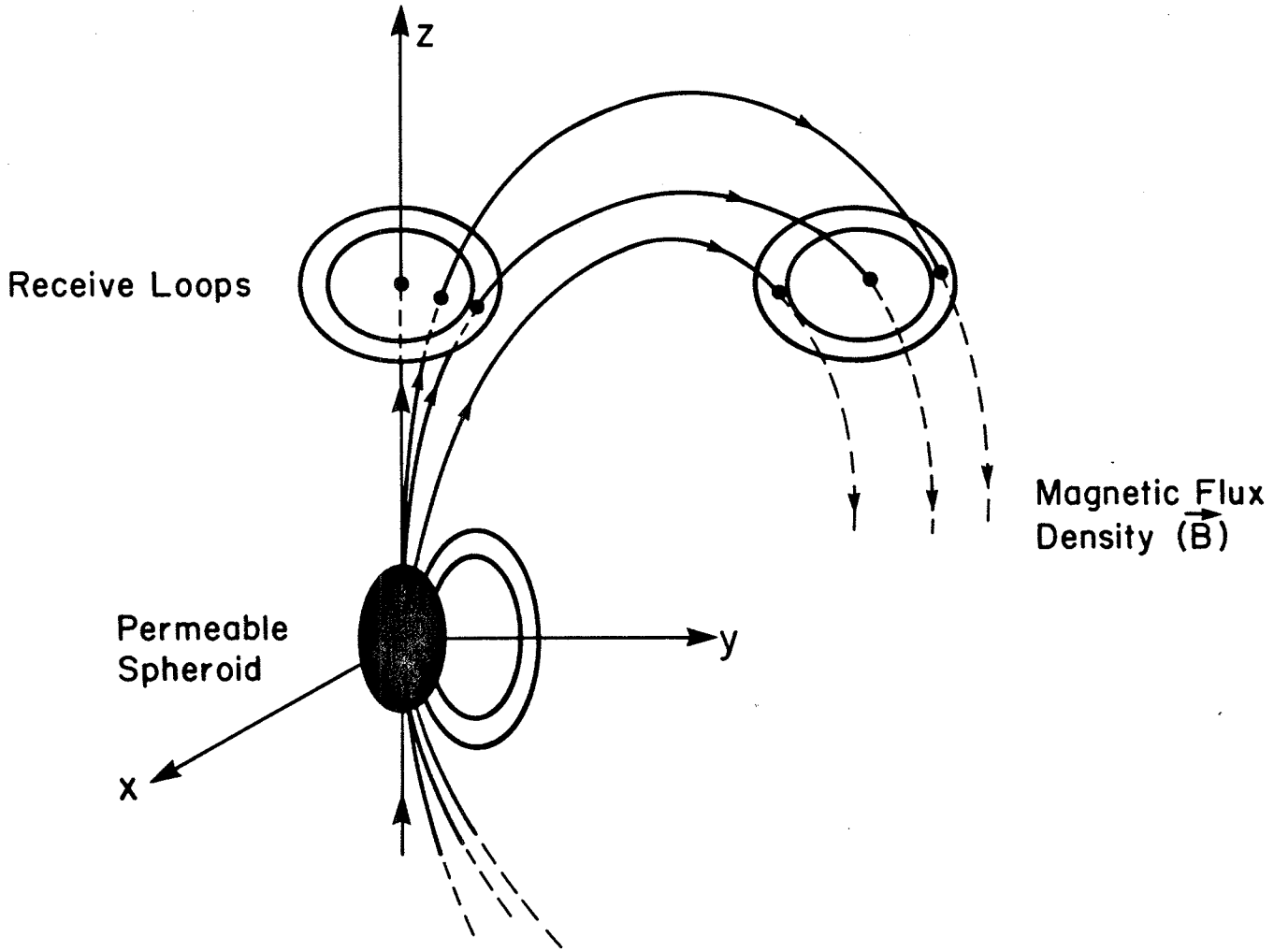

Figure 5.12: Lines of the magnetic induction $\vec{B} = \mu\vec{H}$ for a permeable spheroid in the presence of a primary field.

5.5.5.2 Vertical Displacement Of Receiver:

In this sub-section, the above computations are repeated for vertical displacement of receivers. Fig. 5.13 shows the variation of the *rms* received voltages for two spheroids with μ_r = 50 and 100. The receiver is centered on the z axis and the results are nearly the same for any spheroid orientation. Comparing these results with those of lateral displacement of the loop in Fig. 5.10, it is clear that the rate of signal decay along the vertical axis is much higher. In addition, the rate of decay reduces with increasing z, which is opposite to that in Fig. 5.10, where the rate of decay increases with y.

5.5.5.3 Two Receivers:

In this case, two receivers of radii 17. and 24. cm are used. The ratio of their radii is therefore 1.411. For a co-planar arrangement of these loops, the ratios of their respective *rms* induced voltages as a function of loop displacements along the y axis are shown in Fig. 5.14. It is expected that the variation of this ratio is a function of the object geometry and may be used effectively in inverse scattering applications. It is interesting to note that the results are almost independent of the spheroid permeability. Also, the variation of the signal ratios is opposite to the variation of the signal received by a single receiver loop. That is, the ratio of the signal received by two loops increases with the lateral displacement y, and is symmetrical about the xz plane for ALPHA = 0° and 90° cases.

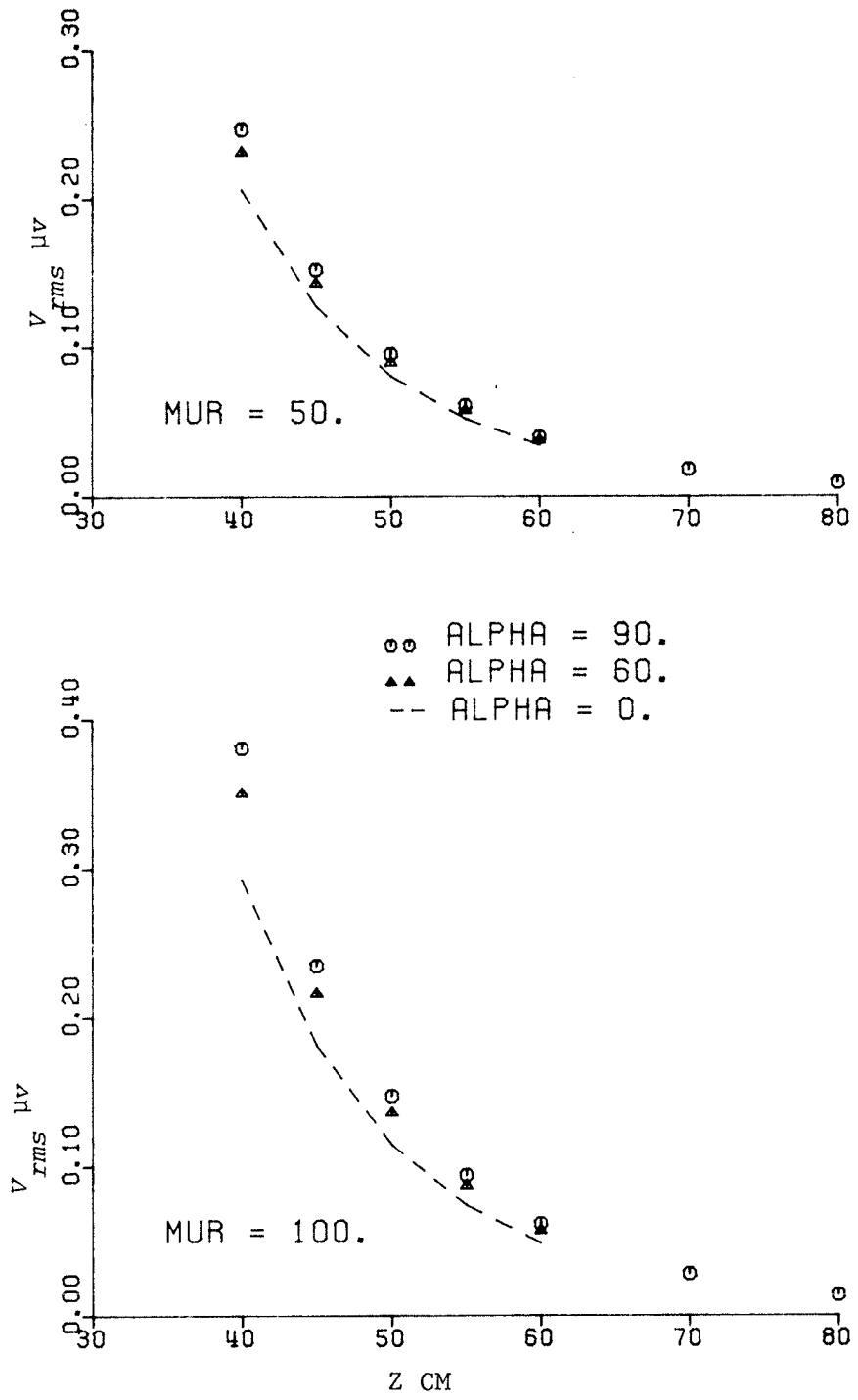

Figure 5.13: Same as Fig. 5.10, but for displacement along the z axis.

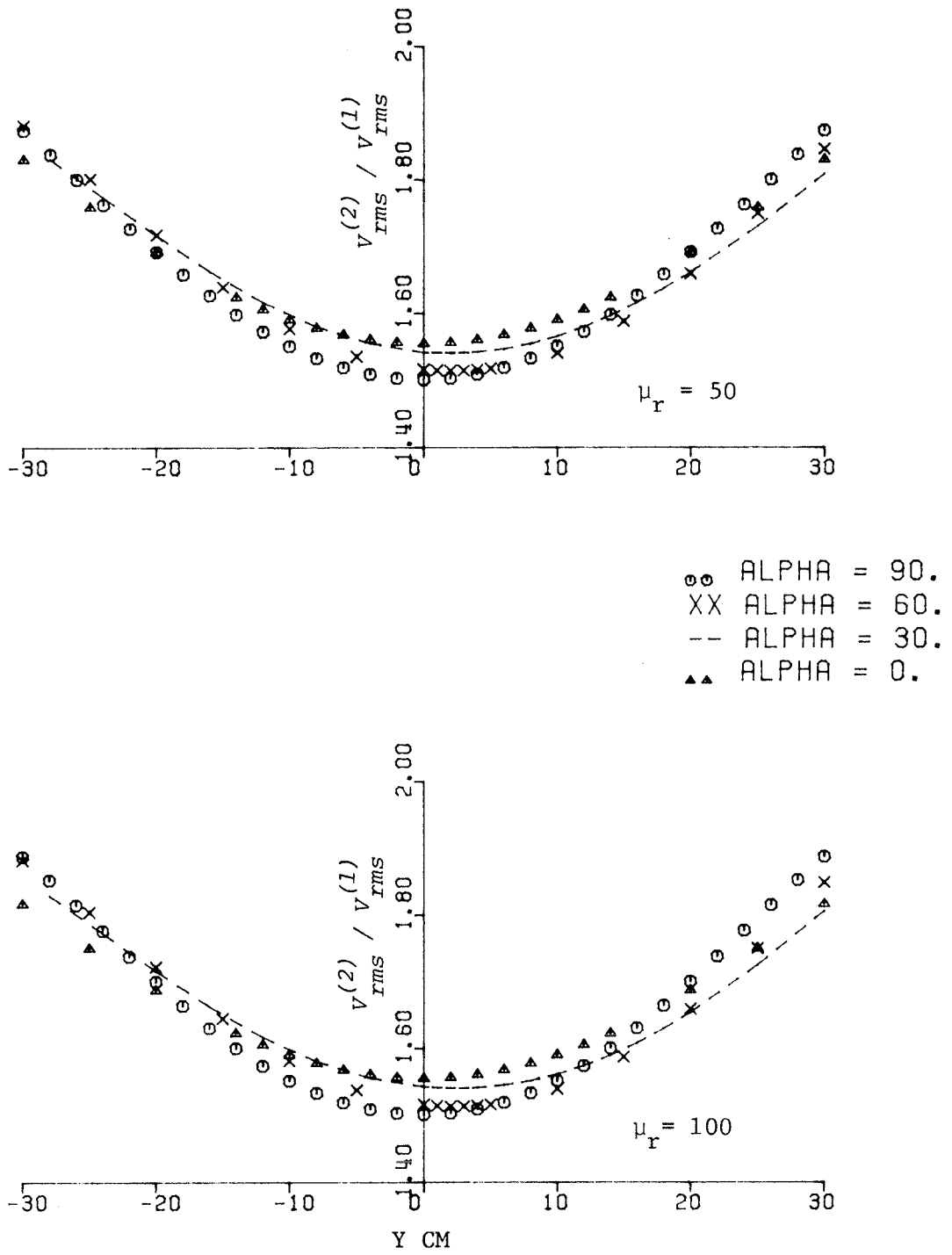

Figure 5.14: The ratio of the received signals (rms) of two loops (RR2/RR1 = 1.411) for spheroids of Fig. 5.10.

These results can again be explained using the magnetostatic approach. The variation of the magnetic flux is maximum along the spheroid axis and results in smaller induced voltage ratios for receiver loops of different sizes. Also, the highest rate of change occurs for vertical spheroids, due to the concentration of flux lines near the z axis.

The ratios of the *rms* voltages, received by two plane loops of different sizes, are shown in Fig. 5.15. Again, variation of signal ratios is relatively independent of the spheroid orientation, and increases at a reducing rate with the vertical distance z. It is expected that the signal ratios will asymptotically approach the ratio of the receiver loop areas, which is about 2.0. The variation of the signal ratios with the spheroid orientation, in this particular case, is most pronounced near the object. It shows the increase in the rate of change with the spheroid tilt angle and is maximum for the vertical case.

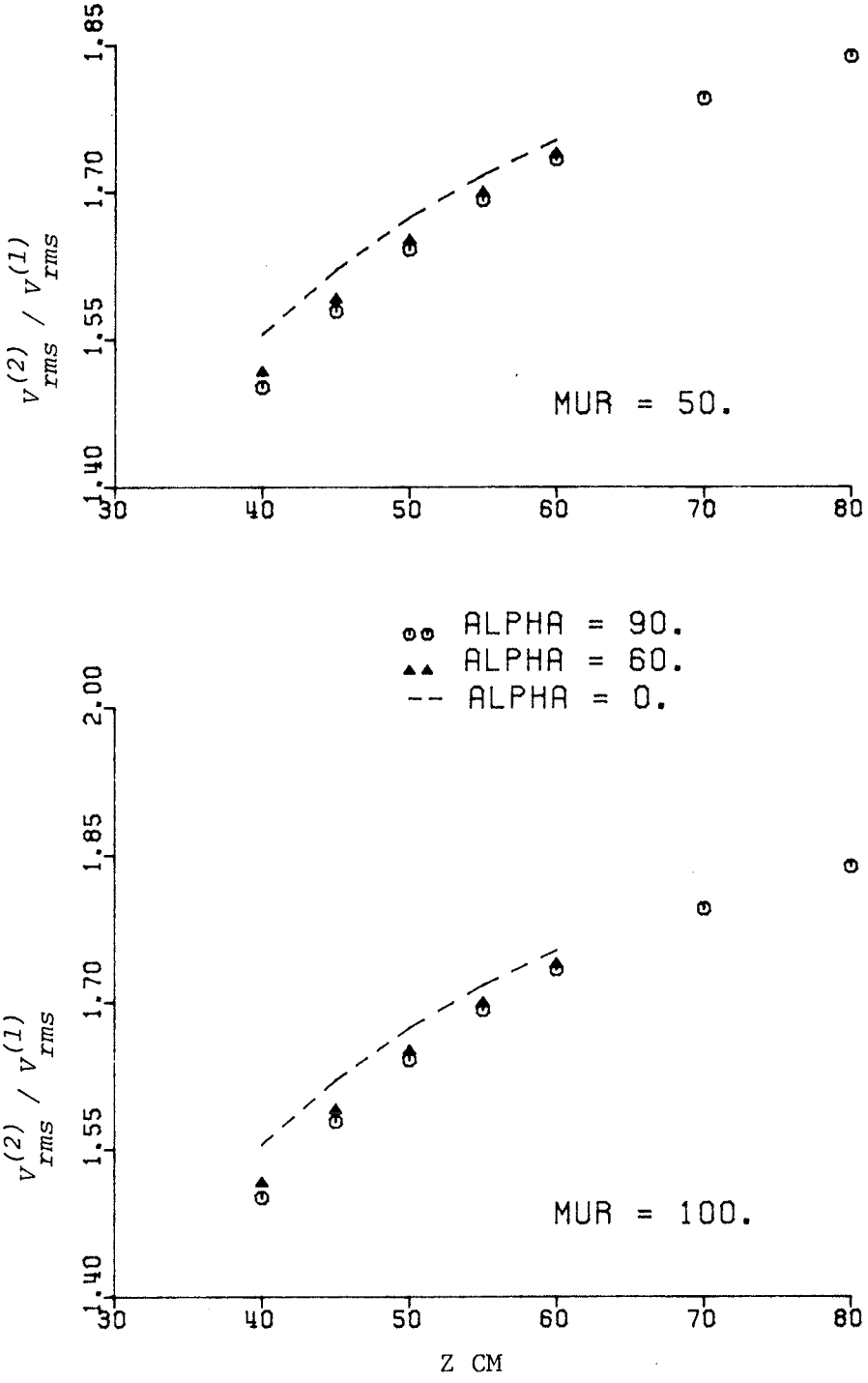

Figure 5.15: Same as Fig. 5.14, but for displacement along the z axis.

5.6 APPLICATION TO TARGET IDENTIFICATION PROBLEM:

5.6.1 Problem Definintion:

Given the incident field and the scattered field from an unknown target, it is desired in the most general case, to retrieve the shape, size, orientation and composition of the target. This is known as inverse scattering or target imaging. Such problems and their solutions have become increasingly important in the past two decades. In military applications, the need to distinguish between friendly, enemy and neutral targets is vital, and is classified as radar targets and normally uses short electromagnetic pulses. On the other hand, commercial and peaceful applications of such a problem are of great interest in geophysics and detection of buried artillery shells in civilian areas. In such cases, long electromagnetic pulses (low-frequency) are most suitable.

For the present case, the problem is restricted to a highly conducting permeable spheroid illuminated by a field generated by a current carrying loop as shown in Fig. 5.1. The primary function of this section is to examine the possibility of obtaining information about such a target from its response with an apriori knowledge of one or more of its parameters.

The solution of this problem may be approached both in the frequency or time domain. Attention will be focused on the time domain approach. This approach, which is the subject of this section uses the basic properties of the transient response to a pulse train of low fundamental frequency in order to obtain information on the spheroid.

5.6.2 Time Domain:

Figure 5.16 shows a simplified diagram of a measuring system which consists of separate transmitting and receiving coils. The transmitter consists primarily of an oscillator generating electromagnetic energy at a certain frequency. Part of this energy is intercepted by the target and reflected back. A comparison of the properties of this reflected energy at different locations, either in space or time, will result in information such as receiver-target distance and target orientation.

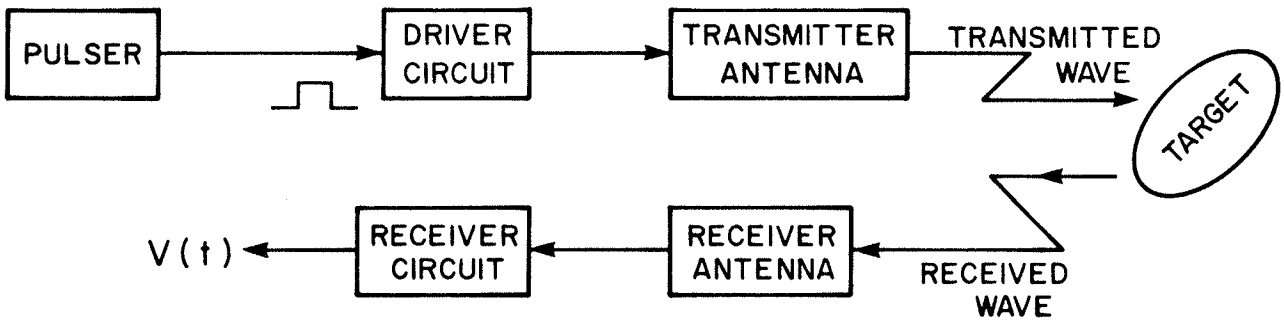

Figure 5.16: Overview of transmitter and receiver antennas.

5.6.3 *Basic Relations:*

Consider the measurment set-up of Fig. 5.16. The pulser generates a train of rectangular pulses with angular frequency ω_o which are fed to a drive circuit including the transmitter coil. The scattered field by the target is intercepted by a receiver coil and is processed through its circuit. The voltage induced in the receiver coil is proportional to the time derivative of the magnetic field component along the axis of the coil, number of coil turns, the cross sectional area and the effective permeability of the core material. In this numerical model, the dependence of the induced voltage on the coil parameters is relaxed, and only the coil radius is included as a parameter. Both the transmitter and receiver coils are represented by two loops as shown in Fig. 5.1. In general, a very large receiver loop has the advantage of a very high signal to noise ratio, since it effectively averages out the local geometric interference. More detail about the driver and receiver circuits, as well as their sensitivities, can be found in a study sponsored by Defence Research Establishment Suffield (*DRES*), Alberta [99]. The study presents, in some detail, a practical guide for the measuring system and the building of a time domain detector. The model used in this chapter is based on the numerical method of *Chapter Four* to generate the frequency domain data in conjuction with the transform technique to calculate the induced voltage $v(t)$.

For a given location of the transmitter, the receiver loop can be moved in both vertical and transverse directions. First, the receiver loop is moved along the vertical direction to establish the signal variation with the separation distance of the transmitter and receiver

loops. The case of offset receiver loop is considered next to relate the signal variation with the target orientation.

5.6.4 *Target Depth:*

To study the response for different separation distances between the receiver center and the object, the ratios of the received signals at different vertical points are computed. Fig. 5.17 shows the results for two different steel permeabilities. It is clear that for any two selected points, the ratio of the signals as a function of time remains constant. The reference signal in this figure is that of the receiver loop at position S_1, coplanar with the transmitter loop. It was found that this linear relationship between the response of the spheroid at different receiver loop locations is true for any object size or orientation. However, if a very small time step is selected, one may find an oscillation about this constant ratio value as described in *Appendix C*.

Figure 5.18 shows the ratios of the signals (peak values) for different locations of the receiver loop. The transmitter loop is located on the z axis with its center at (0.,0.,40.) cm. Again, the reference level is taken as that induced in a receiver loop coplanar with the transmitter loop having a common center. From this figure it is evident that the signal reduction is faster when the receiver loop displacement is along the z axis, which is expected since for this loop location, the flux linkage is maximum and the ratio of the loop distances from the spheroid center is maximum.

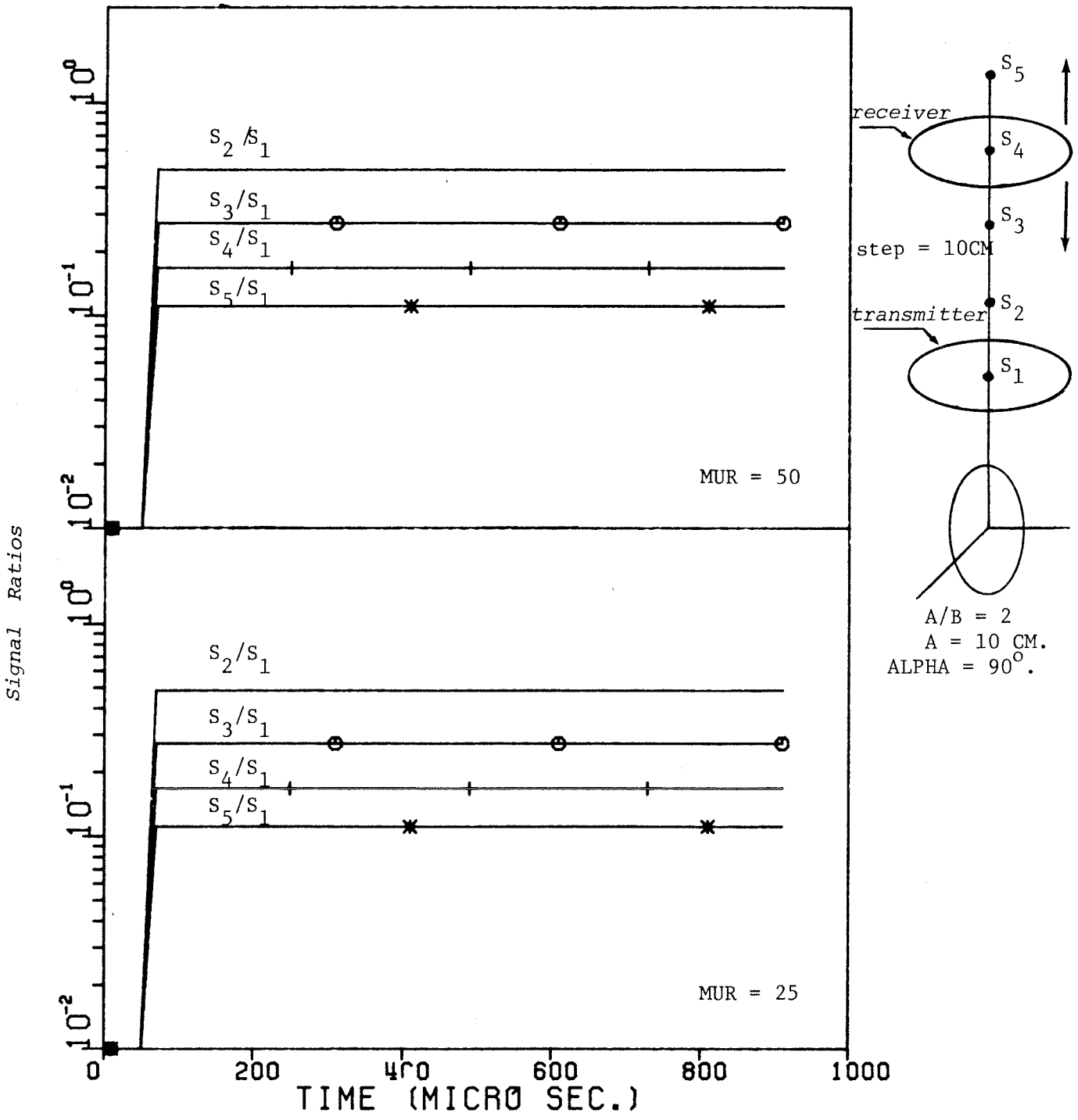

Figure 5.17: Normalized time responses as a function of time for steel spheroids.

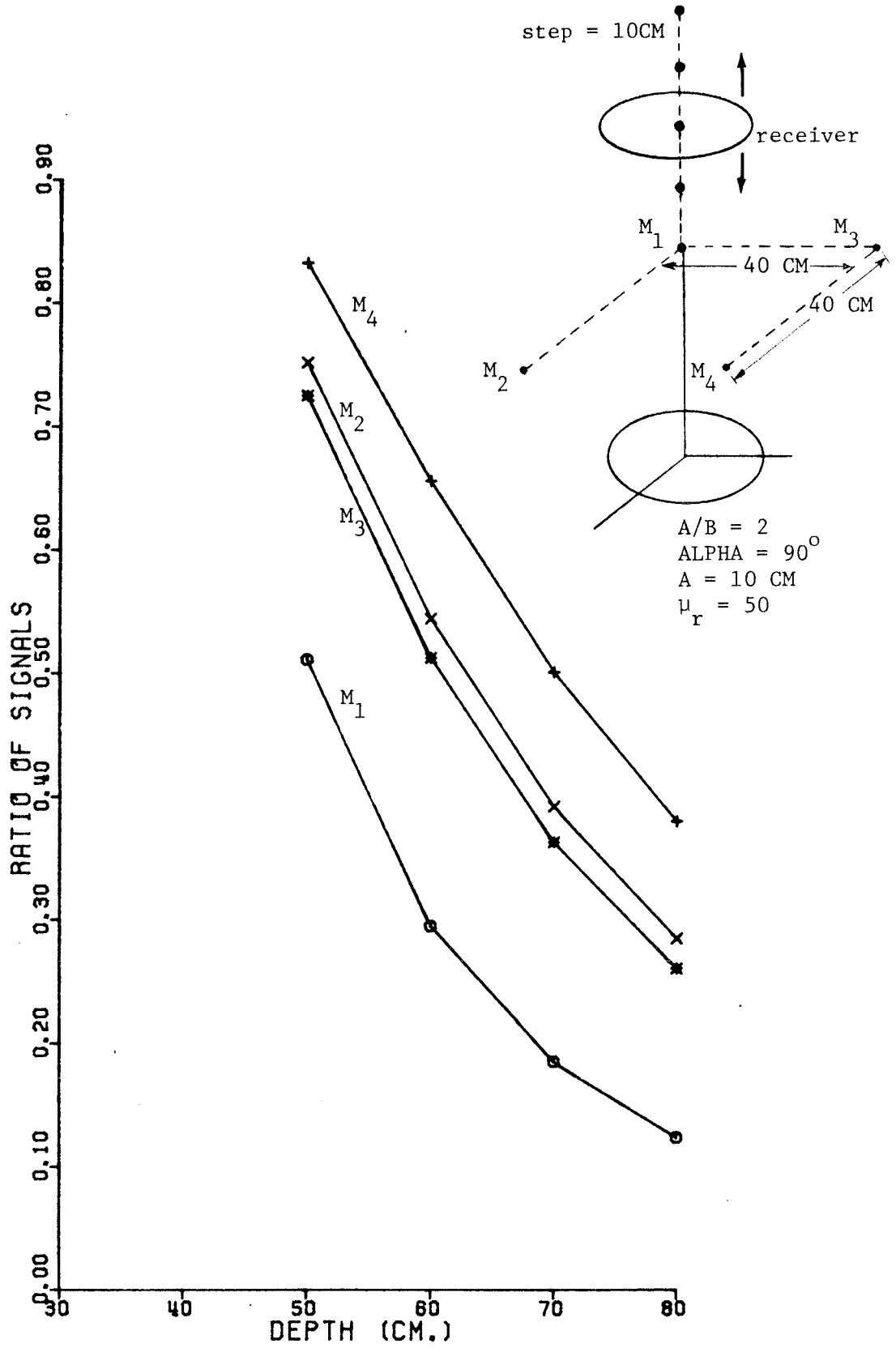

Figure 5.18: Signal ratios (peak values) as a function of the vertical displacement of the receiver loop.

To study the possibility of object depth determination, Table 5.1 is included. It shows a comparison of the quantities S_i/S_1 and $(R_i/R_1)^n$, where

S_1 = reference level at $z = R_1$.

S_i = signal level at $z = R_i$.

It is clear from this table that with $n = 3$, the two ratios are very close with a small error that increases with ALPHA. Thus, from

$$[R_1/R_i]^3 = [R_1/(R_1+\Delta R_i)]^3$$

$$= S_i/S_1 \qquad (5\text{-}19)$$

one finds,

$$R_i = \Delta R_i \cdot \frac{(S_i/S_1)^{1/3}}{1 - (S_i/S_1)^{1/3}} \qquad (5\text{-}20)$$

This means that by selecting $i = 1,2,3,\ldots$ one can determine R_i and by averaging these values, an approximate value for the depth can be obtained. Note that the approximate formula which is given by Equ. (5-20) is not valid when the measuring system is off the z axis. One

limitation of this formula is related to the object size and its orientation. For large objects and vertical orientation cases, it is recommended that the reference level be such that the vertical distance between the transmitter loop and spheroid centers be greater than 5A, where A is the semi-major axis of the spheroid.

Table 5.2 shows the estimated values of the object depth using Equ. (5-20) which indicates the accuracy dependence on the size and the orientation of the spheroid. Generally, the accuracy increases as the separation distance, with respect to the object size, increases. Also, the accuracy improves for flatter positions of the spheroid,i.e. as ALPHA decreases.

TABLE 5.1

RELATIONSHIPS BETWEEN $(R_1/R_i)^3$ AND S_i/S_1^*

ALPHA (deg.)	A (cm)	A/B	$(R_1/R_i)^3$	S_i/S_1	COMMENT
0	10	2	0.5120	0.5112	Transmitter
			0.2963	0.2948	centre at
			0.1865	0.1852	x=y=0,
			0.1250	0.1237	z=40 cm
30	10	2	0.5120	0.5053	
			0.2963	0.2897	
			0.1865	0.1811	
			0.1250	0.1207	
90	10	2	0.5120	0.4861	
			0.2963	0.2726	
			0.1865	0.1681	
			0.1250	0.1109	
0	20	2	0.7023	0.7001	Transmitter
			0.5120	0.5086	centre at
			0.3846	0.3809	x=y=0,
			0.2960	0.2927	z=80 cm
0	10	3	0.5120	0.5148	Transmitter
			0.2963	0.2986	centre at
			0.1865	0.1882	x=y=0,
			0.1250	0.1261	z=40 cm
0	10	1.5	0.5120	0.5066	
			0.2963	0.2904	
			0.1865	0.1817	
			0.1250	0.1210	
90	10	1.5	0.5120	0.4876	
			0.2963	0.2738	
			0.1865	0.1689	
			0.1250	0.1115	

*S_1 = refrence level for receiver centre at (x=y=0, $z=R_1$),

S_i = signal level for receiver centre at (x=y=0, $z=R_i$, i=1,2,3,..).

TABLE 5.2

ESTIMATED OBJECT DEPTHS

Object Geometry	ΔR_i (cm)	S_i/S_1	R Estimated depths (cm)	R Exact depths (cm)	% Error
α = 0 A = 10 cm A/B = 2	10	.5112	39.896	40	-0.26
	20	.2948	39.798	40	-0.5
α = 30 A = 10 cm A/B = 2	10	.5053	39.139	40	-2.15
	20	.2897	39.116	40	-2.21
α = 90 A = 10 A/B = 2	10	0.4861	36.789	40	-8
	20	0.2726	36.88	40	-7.79
α = 90 A = 10 cm A/B = 2	10	0.6166	57.177	60	-4.7
	20	0.4069	57.225	60	-4.6
α = 0 A = 20 cm A/B = 2	10	0.5045	39.037	40	-2.4
	20	0.2876	38.83	40	-2.9
α = 0 A = 20 cm A/B = 2	10	.7001	79.242	80	-0.94
	20	.5086	79.12	80	-1
α = 0 A = 10 cm A/B = 3	10	0.5148	40.36	40	+.9
	20	0.2986	40.31	40	+.77
α = 0 A = 10 cm A/B = 1.5	10	0.5066	39.30	40	+1.7
	20	0.2904	39.21	40	+1.9
α = 90 A = 10 cm A/B = 1.5	10	0.5616	47.15	50	-5.7
	20	0.3464	47.17	50	-5.6

5.6.5 *Object Orientation:*

To establish a procedure to determine the spheroid orientation ALPHA, the receiver loop is displaced on a horizontal plane at fixed hight from the spheroid center. Figures 5.19-5.22 show the variation of the return signal as a function of the displaced transmitter and receiver loops in a horizontal plane. The target is a steel spheroid (σ = 10^7 S/m and μ_r = 100) with axial ratio of 2 and semi-major axis of 20 cm. The basic parameter is taken as the orientation angle ALPHA. In these figures, the vertical axis represents the computed induced voltage V_{rms} in Micro Volts and the horizontal plane represents the common center of the receiver and transmitter loops in centimeters. For tilted spheroids, the peak signal levels move towards the positive y values by changing the spheroid angle ALPHA. The rise in the signal level, from its value on the z axis, is however small and is within about 0.5 percent. Also, for tilted spheroids, the rate of the signal decay with +y is larger than along -y. In all cases but ALPHA = 90°, the rate of signal decay along x axis is larger than that along +y. These results confirm the expectation that the peak signal level must move towards the closer end of the spheroid.

In principle, it seems possible to distinguish between the horizontal or vertical orientation of a spheroid. This can be done by calculating either the peak or *rms* values of the induced voltages at different points in a horizontal plane. The maximum in both cases occurs at a point on the vertical axis passing through the spheroid center. This axis is either the major axis (ALPHA = 90°) or the minor axis (ALPHA = 0°) of the spheroid.

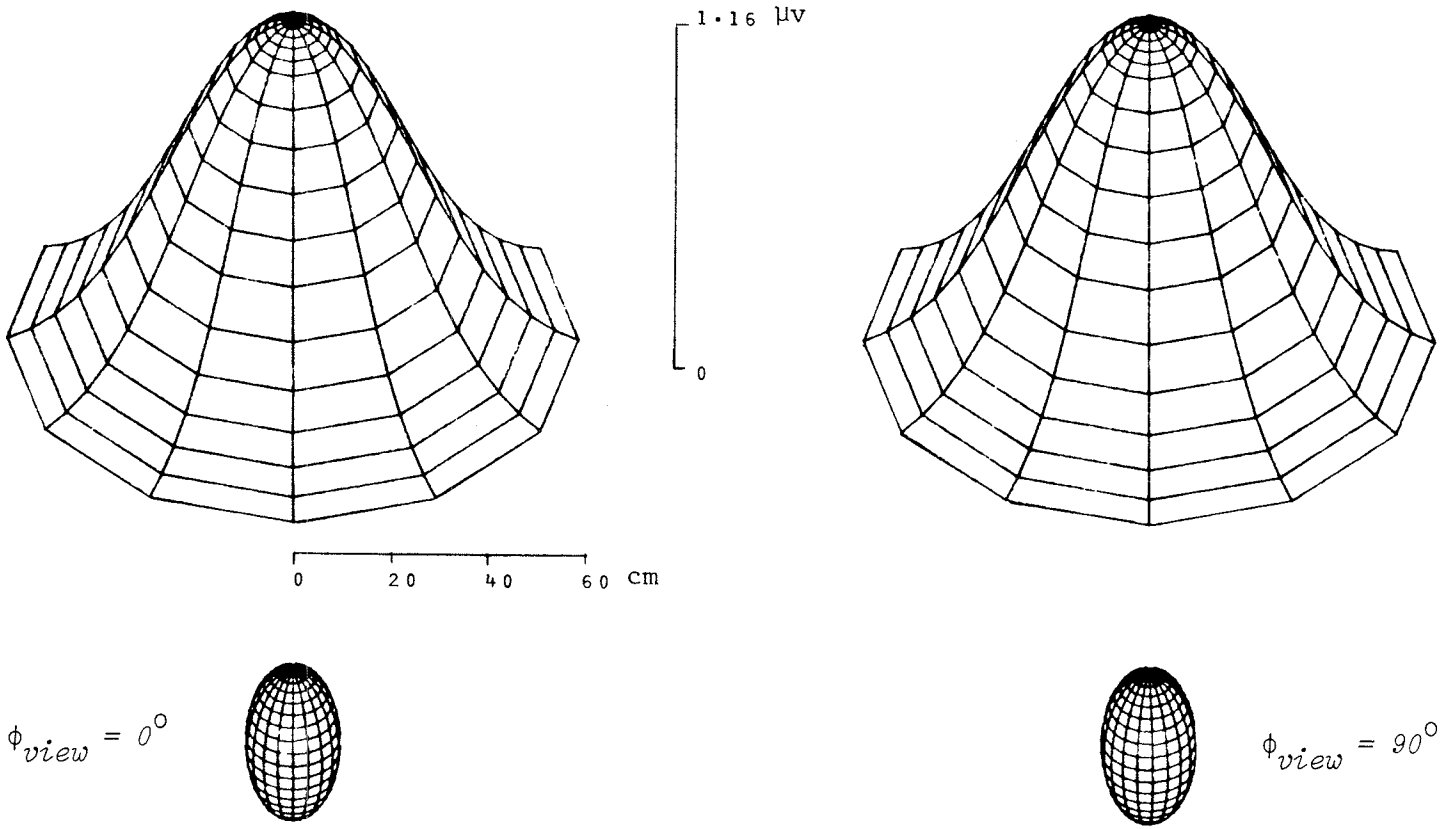

Figure 5.19: Three-dimensional representation of V_{rms} for a vertical steel spheroid with two different view angles.

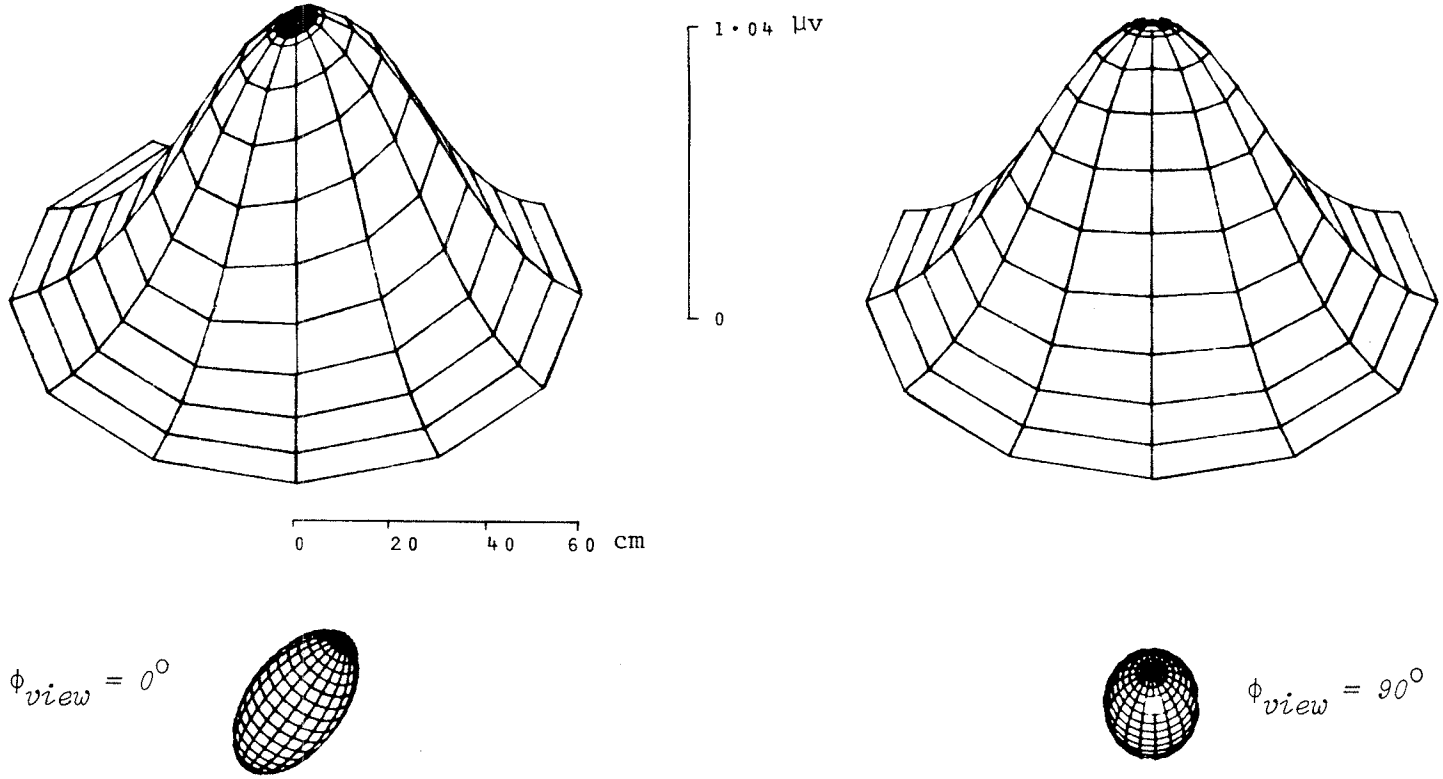

Figure 5.20: Same as Fig. 5.19 except ALPHA = 60.

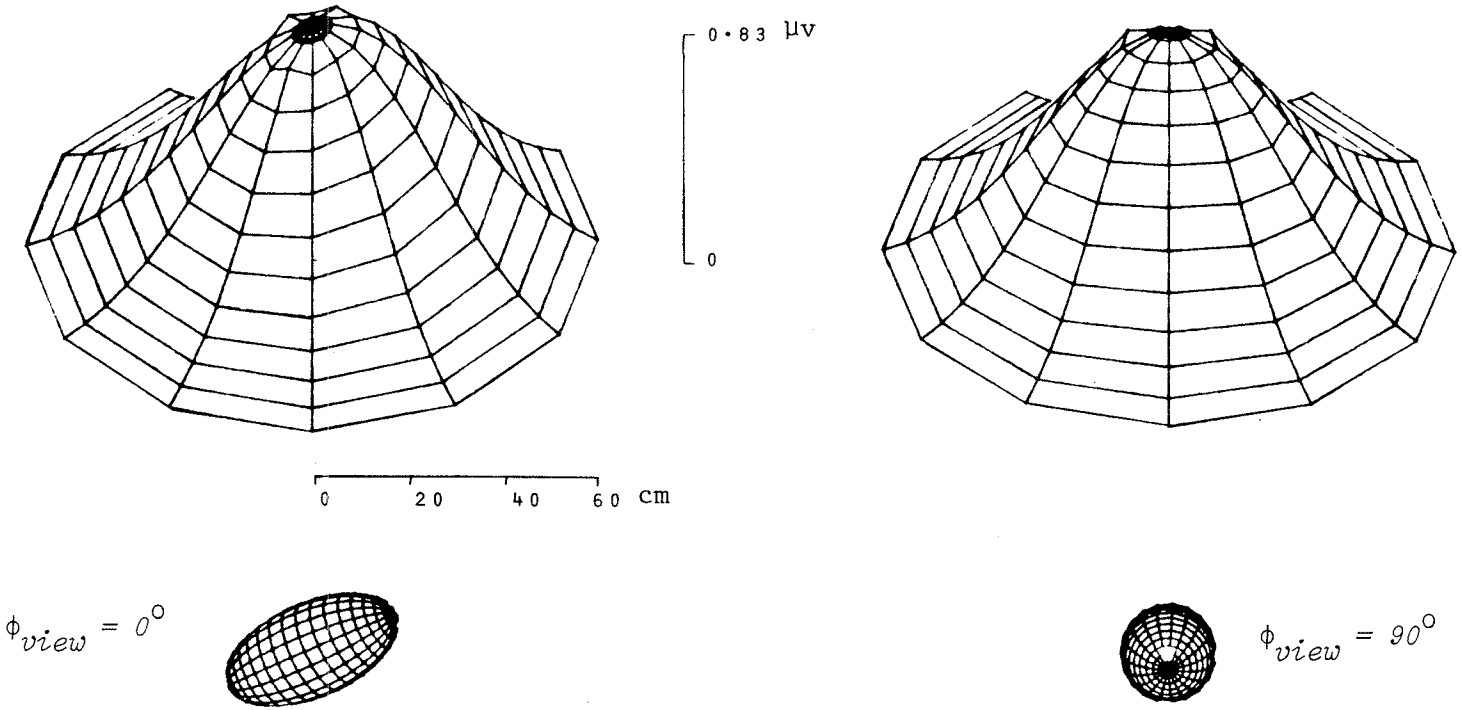

Figure 5.21: Same as Fig. 5.19 except ALPHA = 30.

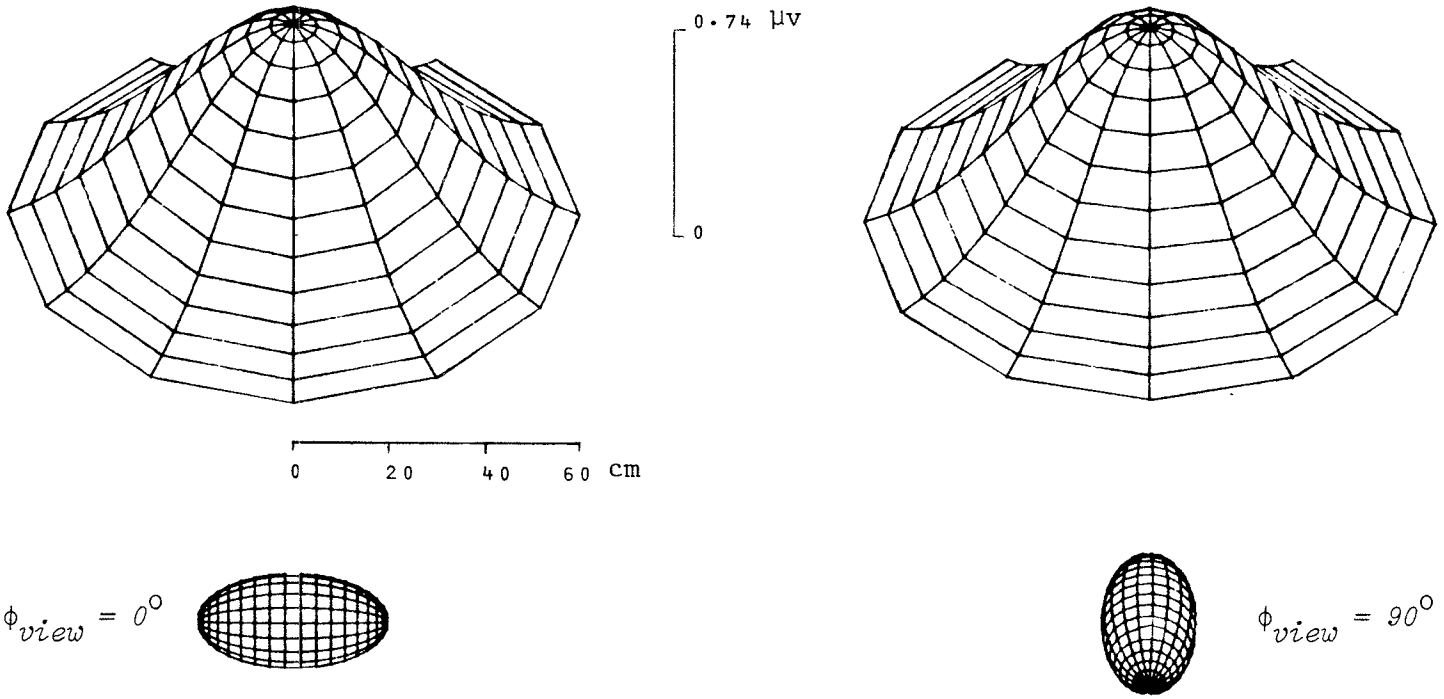

Figure 5.22: Same as Fig. 5.19, but for a horizontal steel spheroid.

By moving the receiver loop along a circular curve centered at that point of maximum, one may discriminate between the vertical and horizontal orientations. If the induced voltage is constant at every point along this circular path, then ALPHA = 90° . On the other hand, if the induced voltage has two planes of symmetry with non-equal values, then ALPHA = 0° . Finally, if there is only one plane of symmetry, then 0° < ALPHA < 90°. In this case, the maximum value of V_{rms} occurs near the closer end of the spheroid. After locating this point, one then rotates the receiver loop slowly until a maximum reading is found. Then the angle between the normal to the loop surface and the z axis gives an indication of the orientation angle. This point is still under investigation.

5.7 SUMMARY:

The transform technique, using the scattered fields in the frequency domain, was used to compute the transient response of imperfectly conducting spheroids. For highly conducting aluminum and steel spheroids, an approximate method was used to solve for surface electric and magnetic currents, which were used to generate the scattered field. Although numerical examples were given only for spheroidal objects, the method can be applied to any highly conducting object.

As an application to low-frequency remote sensing problems, the exciting field was generated by a periodic pulse train of a 500 Hz fundamental frequency and radiated by a small circular loop antenna. Due to the low fundamental and harmonics frequencies, the effect of ground on the scattered field was neglected. The transient responses of small spheroidal objects were then computed for different spheroid parameters and separation distances from the transmitter and receiver loops. By examining the results, it was shown that a two-dimensional field plot on a horizontal plane normally has adequate information to enable one to detect the location and the orientation of the object.

Chapter Six

DISCUSSIONS, CONCLUSIONS AND RECOMMENDATIONS

6.1 DISCUSSIONS AND CONCLUSIONS:

In this thesis, the suitability of using integral equations technique, in conjuction with the method of moment, to analyze the scattering by imperfectly conducting objects were demonstrated. The impedance boundary conditions (*IBC*) were used to reduce the computer storage and execution time requirements. For bodies of revolution, three different integral equations were formulated, the electric field integral equation (*EFIE*), the magnetic field integral equation (*MFIE*) and the combined field integral equation (*CFIE*). It was found that both the *EFIE* and *MFIE* suffered from the internal resonance effect on the numerical results. On the other hand, The *CFIE* gave more stable solution in the vicinity of an internal resonance. In addition, the *CFIE* enjoyed the same superiority as the *MFIE*, over the *EFIE*, in obtaining reasonably accurate solutions, with the same geometrical model of the scattering structure. The reason for this was the fact that the method of moment divides the scatterer surface into sub-areas and assumes some approximation for the unknown currents on each sub-area. Both the *EFIE* and *MFIE* contain a term ($\vec{M}/2$ in the *EFIE* and $\vec{J}/2$ in the *MFIE*) which does not involve integration or equivalently, a term which is independent of the sub-areas' sizes and shapes. For imperfectly conducting objects, $\vec{J}$ is normally more dominant than $\vec{M}$. Hence, the *MFIE*

escapes the surface segmentation effect, since its moment matrix in the numerical solution becomes more diagonally dominant.

For imperfectly conducting bodies of arbitrary shape, a simplified technique was introduced for generating their scattered fields. Although the technique was an approximate one, it overcame the difficulty of selecting smooth basis functions on the body surface and saved computation time. The transient fields of these objects were then computed using the transform technique.

A brief reveiw of the previous work in electromagnetic scattering by imperfectly conducting objects was presented in *Chapter Two*. In the same chapter, the detailed derivation of the impedance boundary conditions and the restrictions which have to be satisfied by the body for their applications were also presented.

In *Chapters Three* and *Four*, the appropriate integral equation was set up to solve for steady state electromagnetic fields scattered by imperfectly conducting and coated objects. For lossy dielectric and coated spheres, comparing the analytic and numerical solutions indicated that representation of these objects' surfaces by impedance ones was reasonable, provided that the signal penetration into the body was small.

The proposed integral equations technique should be of great importance to the basic problem of electromagnetic scattering by arbitrary objects. When a scatterer is neither perfectly conducting nor perfectly dielectric, there is little hope of finding analytic solutions unless the object has a very simple shape. Therefore, numerical techniques in conjuction with the *IBC* provide a method to study many

important problems and to examine any future approximate methods in the field of electromagnetic scattering. Regarding the immediate contribution to numerical analysis, the results presented in *Chapter Three* can be employed for a proper geometrical representation of scatterers and to obtain stable solutions near their internal resonances.

The transform technique, using the numerical results of the steady state solutions was the main topic addressed in *Chapter Five*. The ultimate limitations on this technique were the computer memory size and the required computation time. The time domain data obtained in the same chapter were then processed to relate their behaviour to their source's shape.

The proposed data processing presented at the end of *Chapter Five* can be employed for inverse scattering. It is hoped that this chapter gives one step towards the solution of detection and location of underground objects, using long pulse incident waves.

6.2 *RECOMMENDATIONS:*

The principal recommendations which follow from this study can be summarized as follows:

6.2.1 *Steady State Solutions:*

It is assumed in *Chapter Four* for simplicity that the contribution of the magnetic surface current to the surface fields is negligible. However, in order to improve the accuracy, one should in principle be able to solve either *EFIE* or *MFIE* over arbitrarily-shaped impedance

surfaces without neglecting such contribution. This can be done by a proper selection of the basis functions that are used in the method of moment. One such selection is a tetrahedron shape. This will extend the range of applicability of the *IBC* for objects of arbitrary shape. The extension of the *IBC* method to other numerical methods such as finite elements and extended boundary condition methods can be carried out.

6.2.2 Transient Solutions:

As has been mentioned earlier, the main limitation of the transform technique in generating the transient field is the excessive computation time. An alternative approach would be to solve Maxwell's equations directly in the time domain throughout the volume of the scatterer. This approach is again computer time and memory intensive.

A third approach would be to develop and solve a space-time integral equation for impedance objects. The frequency domain integral equations for objects with *IBC* are given by Equs. (3-17) or (3-21). The space-time integral equations are now obtained by taking the Fourier transform of Equs. (3-17) or (3-21). After the necessary mathematical manipulations, the results for the *MFIE* are

$$\vec{J}(\vec{r},t)/2 = \hat{n} \times \vec{H}^{i}(\vec{r},t) + \frac{1}{4\pi}\hat{n} \times \oint_{S_o} \left(L\vec{J}(\vec{r}',\tau) \times \frac{\vec{R}}{R^2} - L\nabla'_s \cdot \left[Z_{cc}(\tau) * \vec{J}(\vec{r}',\tau) \times \hat{n}(r') \right] \frac{\vec{R}}{R^2} - \frac{\partial}{\partial\tau}\left[Z_p(\tau) * \vec{J}(\vec{r}',\tau) \right] \times \frac{\hat{n}(\vec{r}')}{R} \right) ds' \qquad (6-1)$$

where

$$\vec{R} = \vec{r} - \vec{r}'$$

$$R = |\vec{R}|$$

$$\tau = t - R/c$$

$$Z_{cc}(t) = c\left[\frac{\mu/\mu_o}{\varepsilon/\varepsilon_o}\right]^{\frac{1}{2}} I_o(\alpha t)\exp(-\alpha t)$$

$$Z_p(t) = \frac{2}{c}\left[\frac{\mu/\mu_o}{\varepsilon/\varepsilon_o}\right]^{\frac{1}{2}} \alpha^2 \left[I_o(\alpha t) - \left(1 + \frac{1}{2\alpha}\right) I_1(\alpha t)\right]\exp(-\alpha t)$$

$$\alpha = \frac{\sigma}{2\varepsilon}$$

$$c = 1/\sqrt{\mu_o \varepsilon_o}$$

$$L = 1/R + 1/c\ \frac{\partial}{\partial \tau}$$

$$h(t) * w(t) = \int_{-\infty}^{t} h(t - \tau)\, w(\tau)\, d\tau$$

and $I_o(x)$ and $I_1(x)$ are the modified Bessel functions of argument x and of order zero and one, respectively.

The solution may be carried out numerically in the usual manner, but with more difficulty as was described in [10] for perfectly conducting objects and by stepping on in time. It is interesting to note that the effect of losses is to add an attenuation factor $\exp(-\alpha t)$ to the integrands in Equ. (6-1). Also, it is worthwhile to check whether or not the approximation used in ***Chapter Four*** can be used here as well.

For particular applications such as those of ***Chapter Five***, using quasi-static approximation to obtain the transient field of permeable

conducting objects and their extension to arbitrarily-shaped objects, would be of great value. Another approach would be to replace the object and the transmit and receive loops by an equivalent circuit which includes the effective inductances of the object and loops as well as their mutual coupling.

REFERENCES

[1] D.L. Moffatt, ***Interpretation and Application of Transient and Impulse Response Approximation in Electromagnetic Scattering Problems***, The Ohio State University, OH, Final Rep. Contract F19628-67-C-0239, 1968.

[2] C.L. Bennett et. al., ***Integral Equation Approach to Wideband Inverse Scattering***, Sperry Res. Center, MA, Final Rep. Contract F30602-69-C-0209, 1970.

[3] C.L. Bennett, R.M. Hieronymus and H.M. Mieras, ***Impulse Response Target Study***, Sperry Res. Center, MA, Final Rep. Contract F30602-76-C-0209, 1977.

[4] C.L. Bennett and G.F. Ross, "Time domain electromagnetics and its applications," ***Proc. IEEE***, Vol. 66, pp. 299-318, 1978.

[5] L. Shafai, A. Sebak and A. Mohsen , ***Electromagnetic Response of Artillery Shells***, University of Manitoba, MB, Final Rep. Contract 14-SU.97702-1-3257, 1982.

[6] K.K. Mei, "On the integral equations of thin wire antennas," ***IEEE Trans. Antennas & Propag.***, Vol. AP-13, pp. 374-378, 1965.

[7] J.R. Mautz and R.F. Harrington, "Radiation and scattering from bodies of revolution," ***Appl. Sci. Res.***, Vol. 20, pp. 405-435, 1969.

[8] G.J. Barke and A.J. Poggio, ***Numerical electromagnetic code (NEC)-Method of moments***, Naval Ocean System Center, CA, Tech. Doc. ***116***, 1977.

[9] R. Mittra, "Integral equation methods for transient scattering," in ***Transient Electromagnetic Fields***, Edited by L.B. Felson, Springer-Verlag, NY, pp. 73-128, 1976.

[10] A.J.Poggio and E.K. Miller, "Integral equation solutions of three-dimensional scattering problems," in ***Computer Techniques for Electromagnetics***, Edited by R. Mittra, Pergamon, NY, pp. 159-264, 1973.

[11] J.J. Faran, "Scattering of cylindrical waves by a cylinder," ***J. Acoust. Soc. Am.***, Vol. 25, pp. 155-156, 1953.

[12] S.B. Adler and R.S. Johnson, "New backscattering computation and tables for dielectric and metal spheres," ***Appl. Optics***, Vol. 1, pp. 655-660, 1962.

[13] S. Asano and G. Yamamoto, "Light scattering by a spheroidal particle," *Appl. Optics*, Vol. 14, pp. 29-49, 1975.

[14] A.F. Stevenson, "Solution of electromagentic scattering problems as power series in the ratio (dimension of scatterer) / wavelength," *J. Appl. Phys.*, Vol. 24, pp. 1134-1142, 1953.

[15] G.L. James, *Geometrical Theory of Diffraction for Electromagnetic Waves*, Peter Peregrinus LTD, UK, 1980.

[16] P.W. Barber and C. Yeh, "Scattering of EM waves by arbitrary shaped dielectric bodies," *Appl. Opt.*, Vol. 14, pp. 2864-2872, 1975.

[17] B.H. McDonald and A. Wexler, "Finite element solution of unbounded field problems," *IEEE Trans. Microwave Theory & Tech.*, Vol. MTT-20, pp. 841-847, 1972.

[18] R.F. Harrington and J.R. Mautz , "Theory of characteristic modes for conducting bodies," *IEEE Trans. Antennas & Propag.*, Vol. AP-19, pp. 622-628, 1971.

[19] R.F. Harrington, "Matrix methods for field problems," *Proc. IEEE*, Vol. 55, pp. 136-149, 1967.

[20] --------, *Field Computation by Moment Methods*, Macmillan, NY, 1968.

[21] V.H. Weston, "Theory of absorbers in scattering," *IEEE Trans. Antennas & Propag.*, Vol. AP-11, pp. 578-584, 1963.

[22] K.A. Iskander, L. Shafai, A. Frandson and J.E. Hansen, "Application of impedance boundary conditions to numerical solution of corrugated circular horns," *IEEE Trans. Antennas & Propag.*, Vol. AP-30, pp. 366-372, 1982.

[23] T.B.A. Senior, "Impedance boundary conditions for imperfectly conducting surfaces," *Appl. Sci. Res. (B)*, Vol. 8, pp.418-436, 1961.

[24] --------, "A note on impedance boundary conditions," *Canadian J. Phys.*, Vol. 40, pp. 663-665, 1962.

[25] R.J. Garbacz, "Bistatic scattering from a class of lossy dielectric spheres with surface impedance boundary conditions," *Phys. Rev.*, Vol. 33, pp. A14-A16, 1964.

[26] J.R. Wait and G.M. Jackson, "Calculations of the bistatic scattering cross section of a sphere with an impedance boundary condition," *Radio Sci. J. Res.*, Vol. 69D, pp. 299-315, 1965.

[27] M.G. Andreasen, "Scattering from cylinders with arbitrary surface impedance," *Proc. IEEE*, Vol. 53, pp. 812-817, 1965.

[28] Z. Godzinski, "The surface impedance concept and the structure of radio waves over real earth," *IEE Monograph No. 434E*, pp. 362-373, 1961.

[29] E.S. Cassedy and J. Fainberg, "Back scattering cross sections of cylindrical wires of finite conductivity," *IEEE Trans. Antennas & Propag.*, Vol. AP-8, pp. 1-7, 1960.

[30] K.M. Mitzner, "An integral equation approach to scattering from a body of finite conductivity," *Radio Sci.*, Vol. 2 (New Series), pp. 1459-1470, 1967.

[31] N.G. Alexopoulos and G.A. Tadler, "Accuracy of the Leontovich boundary condition for continuous and discontinuous surface impedances," *J. Appl. Phys.*, Vol. 46, pp. 3326-3332, 1975.

[32] B.M. Thomas, "Bandwidth properties of corrugated conical horns," *Elect. Letters*, Vol. 5, pp. 561-563, 1969.

[33] L. Shafai and J.E. Hansen, "Matrix formulation of corrugated feeds by using impedance boundary conditions," *Elect. Letters*, Vol. 13, pp. 310-311, 1977.

[34] --------, "Correction to matrix formulation of corrugated feeds by using impedance boundary conditions," *Elect. Letters*, Vol. 13, p. 491, 1977.

[35] L. Shafai, K.A. Iskander and J.E. Hansen, "Investigation of scattering by corrugated structures using impedance boundary conditions," *Elect. Letters*, Vol. 14, pp. 144-146, 1978.

[36] J.R. Wait, "Exact surface impedance for a cylindrical conductor," *Elect. Letters*, Vol. 15, pp. 659-660, 1979.

[37] --------, "Exact surface impedance for a spherical conductor," *Proc. IEEE*, Vol. 68, pp. 279-281, 1980.

[38] M. Idemen, "Necessary and sufficient conditions for a surface to be an impedance surface," *Arch. Elec. Ubertragung (Germany)*, Vol. 35, pp. 84-86, 1981.

[39] C.L. Bennett and W.L. Weeks, "Transient scattering from conducting cylinders," *IEEE Trans. Antennas & Propag.*, Vol. AP-18, pp. 627-633, 1970.

[40] A.M. Auckenthaler and C.L. Bennett, "Computer solution of transient and time domain thin-wire antenna problems," *IEEE Trans. Micowave Theory & Tech.*, Vol. MTT-19, pp. 892-893, 1971.

[41] E.P. Sayre and R.F. Harrington, "Time domain radiation and scattering by thin wire," *Appl. Sci. Res.*, Vol. 26, pp. 413-444, 1972.

[42] T.K. Liu and K.K. Mei, "A time-domain integral equation solution for linear antennas and scatterers," *Radio Sci.*, Vol. 8, pp. 797-804, 1973.

[43] G.A. Thiele and G.K. Chan, "Application of the hybrid technique to time domain problems," *IEEE Trans. Antennas & Propag.*, Vol. AP-26, pp. 151-155, 1978.

[44] J.Ch. Bolomey, Ch. Durix and D. Lesselier, "Time domain integral equation approach for inhomogeneous and dispersive slab problems," *IEEE Trans. Antennas & Propag.*, Vol. AP-26, pp. 658-667, 1978.

[45] C.L. Bennett, "The numerical solution of transient electromagnetic scattering problems," in *Electromagnetic Scattering*, Edited by P.L.E. Uslenghi, Academic, NY, pp. 393-428, 1978.

[46] H. Mieras and C.L. Bennett, "Space-time integral equation approach to dielectric targets," *IEEE Trans. Antennas & Propag.*, Vol. AP-30, pp. 2-9, 1982.

[47] T.K. Sarkar, D.D Weiner, V.K. Jain and S.A. Dianat, "Impulse response determination in the time domain: Theory," *IEEE Trans. Antennas & Propag.*, Vol. AP-30, pp. 657-663, 1982.

[48] W.M. Boerner, V.H. Vandenberghe and M.A.K. Hamid, "Determination of the electrical radius ka of a circular cylindrical scatterer from the scattered field," *Canadian J. Phys.*, Vol. 49, pp. 804-819, 1971.

[49] W.M. Boerner and F.H. Vandenberghe, "Determination of electrical radius ka of a spherical scatterer," *Canadian J. Phys.*, Vol. 49, pp. 1507-1535, 1971.

[50] F.H. Vandenberghe and W.M. Boerner, "On the inverse problem of scattering from perfectly conducting prolate spheroid," *Canadian J. Phys.*, Vol. 50, pp. 754-759, 1972.

[51] E.M. Kennaugh and R.L. Cosgriff, "The use of impulse response in electromagnetic scattering problems," *IRE Nat'l Conv. Rec.*, Pt. I, pp. 72-77, 1958.

[52] Y. Das and W.M. Boerner, "On radar shape estimation using algorithms for reconstruction from projects," *IEEE Trans. Antennas & Propag.*, Vol. AP-26, pp. 274-279, 1978.

[53] Special Issue on Inverse Methods in Electromagnetics, *IEEE Trans. Antennas & Propag.*, Vol. AP-29, pp. 185-397, 1981.

[54] C.L. Bennett, "Time domain inverse scattering," *IEEE Trans. Antennas & Propag.*, Vol. AP-29, pp. 213-219, 1981.

[55] R. Barakat, "Diffraction of plane waves by an elliptic cylinder," *J. Acoust. Soc. Am.*, Vol. 35, pp. 1990-1996, 1963.

[56] B.P. Sinha and R.H. MacPhie, "Electromagnetic scattering by prolate spheroids for plane waves with arbitrary polarization and angle of incidence," *Radio Sci.*, Vol. 12, pp. 171-184, 1977.

[57] C. Flammer, *Spheroidal Wave Functions*, Stanford University Press, CA, 1957.

[58] B.P. Sinha and R.H. MacPhie, "Accurate computation of eigenvalues for prolate spheroidal wave functions," *IEEE Trans. Antennas & Propag.*, Vol. AP-21, pp. 406-407, 1973.

[59] --------, "On the computation of the prolate spheroidal radial functions of the scond kind," *J. Math. Phys.*, Vol. 16, pp. 2378-2381, 1975.

[60] E.K. Miller and A.J. Poggio, "Moment-method techniques in electromagnetic from an application viewpoint," in *Electromagnetic Scattering*, Edited by P.L.E. Uslenghi, Academic, NY, pp. 315-358, 1978.

[61] M.G. Andreasen, "Scattering from bodies of revolution," *IEEE Trans. Antennas & Propag.*, Vol. AP-13, pp. 303-310, 1965.

[62] F.K. Oshiro and K.M. Mitzner, "Digital computer solution of three-dimensional scattering problems," in *Symposium Dig., 1967 IEEE Int. Antennas & Propag. Symp.*, pp. 257-263, 1967.

[63] P.L.E. Uslenghi, " Computation of surface currents on bodies of revolution," *Alta Freq. (Italy)*, Vol. 39, pp. 213E-224E, 1970.

[64] J.R. Mautz and R.F. Harrington, "H-field, E-field and Combined-field solutions for conducting bodies of revolution," *Arch. Elec. Ubertragung (Germany)*, Vol. 32, pp. 159-164, 1978.

[65] J.F. Shaeffer, "EM scattering from bodies of revolution with attached wires," *IEEE Trans. Antennas & Propag.*, Vol. AP-30, pp. 426-431, 1982.

[66] S.M. Rao, D.R. Wilton and A.W. Glisson, "Electromagnetic scattering by surfaces of arbitrary shape," *IEEE Trans. Antennas & Propag.*, Vol. AP-30, pp. 409-418, 1982.

[67] P.C. Waterman, "Matrix formulation of electromagnetic scattering," *Proc. IEEE*, Vol. 53, pp. 805-812, 1965.

[68] --------, "Scattering by dielectric obstacles," *Alta Freq. (Italy)*, Vol. 38, pp. 348-352, 1969.

[69] M.H. Lean, *Electromagnetic Field Solution With the Boundary Element Methods*, PH.D. Dissertation, Univ. of Manitoba, MB, 1981.

[70] K.K. Mei, "Unimoment method of solving antenna and scattering problems," *IEEE Trans. Antennas & Propag.*, Vol. AP-22, pp. 760-766, 1974.

[71] S.-K. Chang and K.K. Mei, "Application of the unimoment method to electromagnetic dielectric cylinders," *IEEE Trans. Antennas & Propag.*, Vol. AP-24, pp. 35-42, 1976.

[72] J. Van Bladel, *Electromagnetic Fields*, McGraw-Hill, NY, pp. 354-355, 1964.

[73] S. Silver, *Microwave Antenna Theory and Design*, McGraw-Hill, NY, p. 89, 1949.

[74] A. Sebak and L.Shafai, "Performance of various integral equation formulation for numerical solution of scattering by impedance objects," *Canadian J. Phys.*, in Press, 1984.

[75] R.F. Harrington, *Time-Harmonic Electromagnetic Fields*, McGraw-Hill, NY, pp. 213-214, 1965.

[76] C.E. Baum, "The singularity expansion method," in *Transient Electromagnetic Fields*, Edited by L.B. Felsen, Springer-Verlag, NY, pp. 129-179, 1976.

[77] D.L. Knepp and J. Goldhirsh, "Numerical analysis of electromagnetic radiation properties of smooth conducting surfaces," *IEEE Trans. Antennas & Propag.*, Vol. AP-20, pp. 383-388, 1972.

[78] N.B. Alberstsen, J.E. Hansen and N.E. Jansen, "Computation of radiation from wire antennas on conducting bodies," *IEEE Trans. Antennas & Propag.*, Vol. AP-22, pp. 200-206, 1974.

[79] J.J.H. Wang, "Numerical analysis of three-dimensional arbitrarily-shaped scatterers by trilateral surface cell modelling," *Radio Sci.*, Vol. 13, pp. 947-952, 1978.

[80] E.K. Miller and F.J. Deadrick, "Some computational aspects of thin-wire modelling," in *Numerical and Asymptotic Techniques in Electromagnetics*, Edited by R. Mittra, Springer-Varlag, NY, pp. 89-127, 1975.

[81] A. Sebak, L. Shafai and A. Mohsen, "Generation of scattering data of imperfectly conducting objects from perfectly conducting ones," in *Symposium Dig., 1982 IEEE Int. Antennas & Propag. Symp.*, pp. 513-514, 1982.

[82] --------, "Generation of field scattered by imperfectly conducting objects from the solution of a perfectly conducting object," *Elect. Letters*, Vol. 19, pp. 25-27, 1983.

[83] A. Sebak and L. Shafai, "Scattering by imperfectly conducting and impedance spheroids: A numerical approach," *Radio Sci.*, Vol. 19, pp. 258-266, 1984.

[84] A.F. Stevenson, "Electromagnetic scattering by an ellipsoid in the third approximation," *J. Appl. Phys.*, Vol. 24, pp. 1143-1151, 1953.

[85] J.R. Wait, "Propagation of very-low-frequency pulses to great distances," *J. Res. Nat. Bur. Stand.*, Vol. 61, pp. 187-203, 1958.

[86] R.E. Kleinman, "Far field scattering at low frequencies," *Appl. Sci. Res.*, Vol. 18B, pp. 1-8, 1967.

[87] T.B.A. Senior, "Low-frequency scattering by a dielectric body," *Radio Sci.*, Vol. 11, pp. 477-482, 1976.

[88] J.R. Mautz and R.F. Harrington, *A New E-Field Solution for a Conducting Surface Small or Comparable to the Wavelength*, Tech. Rep. 17, Dept. Elec. & Computer Eng., Syracuse University, NY, 1982.

[89] V.H. Weston, "Pulse return from a sphere," *IEEE Trans. Antennas & Propag.*, Vol. AP-7, pp. 543-551, 1959.

[90] E.M. Kennaugh, "The scattering of short electromagnetic pulses by a conducting sphere," *Proc. IEEE*, Vol. 49, p. 380, 1961.

[91] E.M. Kennaugh and D.L. Moffatt, "Transient and impulse response approximations," *Proc. IEEE*, Vol. 53, pp.893-901, 1965.

[92] J. Rheinstein, "Scattering of short pulses of electromagnetic waves," *Proc. IEEE*, Vol. 53, pp. 1069-1070, 1965.

[93] --------, "Backscattering from spheres: A short pulse view," *IEEE Trans. Antennas & Propag.*, Vol. AP-16, pp. 89-97, 1968.

[94] E.M. Kennaugh and D.L. Moffatt, "On the axial echo area of the cone-sphere shape," *Proc. IEEE*, Vol. 50, p. 199, 1962 and Vol. 51, p. 232, 1963.

[95] D.L. Moffatt and E.M. Kennaugh, "The axial echo area of a perfectly conducting prolate spheroid," *IEEE Trans. Antennas & Propag.*, Vol. AP-13, pp. 401-409, 1965.

[96] S.K. Chaudhuri, "A time domain synthesis of electromagnetic backscattering by conducting ellipsoids," *IEEE Trans. Antennas & Propag.*, Vol. AP-28, pp. 523-530, 1980.

[97] J.R. Wait, "Criteria for locating an oscillating magnetic dipole buried in the earth," *Proc. IEEE*, Vol. 59, pp. 1033-1035, 1971.

[98] R. Kemp, *Theoretical Report for Pulsed Eddy Current Metal Detector*, Final Report, Plessy Co. Ltd., U.K., 1970.

[99] R.H. Chesney, *Feasibilty of Discriminating Between Buried Metallic Spheroids By Classification of Their Electromagnetic Response*, M.Sc. Thesis, Univ. of Britch Columbia, BC, 1982.

[100] J.A. Stratton, *Electromagnetic Theory*, McGraw-Hill, NY, pp. 563-566, 1941.

[101] M.A. Abramowitz and I.A. Stegum (Editors), *Handbook of Mathematical Functions*, Dover, NY, pp. 331-478, 1972.

Appendix A

SCATTERING BY A SPHERE: CLASSICAL SOLUTIONS

A.1 EXACT SOLUTION:

The eigenfunction solution for the sphere is given by Stratton [100]. The method consists of expanding the incident plane wave, the scattered wave and the interior wave in terms of spherical wave functions. The wave functions are $\vec{M}_{mn} = \nabla \times U_{mn} \vec{r}$ and $\vec{N}_{mn} = \nabla \times \vec{M}_{mn}$ where $U_{mn} = \hat{B}_n(kr)/kr \; P_n^m(\cos\theta) \; \exp(jm\phi)$ are solutions to the Helmholtz equation in spherical coordinates (r,θ,ϕ). The $P_n^m(\cos\theta)$ are the associated Legendre functions and $\hat{B}_n(kr)$ are the Riccati-Bessel functions given by [101]. The boundary conditions are then applied and the coefficients of like functions equated. A collection of the pertinent equations is given here. The geometry is still that of Fig. 3.1, except that the object is a sphere. The sphere is of radius a and is characterized by a complex wave constant k', given by $k'^2 = \omega^2\mu\varepsilon(1 - \frac{j\sigma}{\omega\varepsilon})$ where ε,μ,σ are the permittivity, permeability and conductivity of the sphere material, respectively.

A linearly polarized plane electromagnetic wave is incident from the direction of the negative z axis, and without loss of generality, the incident fields can be written in the form,

$$\vec{E}^i = E_o \exp(-jkz) \hat{x}$$

$$= E_o \sum_{n=1}^{\infty} a_n \left[\vec{m}_{o1n}^{(1)} + j\vec{n}_{e1n}^{(1)} \right] \qquad \text{(A-1)}$$

and

$$\vec{H}^{i} = E_o/Z_o \sum_{n=1}^{\infty} a_n \left[\vec{m}_{e1n}^{(1)} - j\vec{n}_{o1n}^{(1)} \right] \tag{A-2}$$

where

$$a_n = (-j)^n \frac{2n+1}{n(n+1)} \tag{A-3}$$

$$2(\vec{m},\vec{n})_{e1n}^{(i)} = (\vec{M},\vec{N})_{1n}^{(i)} + (\vec{M},\vec{N})_{-1n}^{(i)} \tag{A-4}$$

$$2(\vec{m},\vec{n})_{o1n}^{(i)} = (\vec{M},\vec{N})_{1n}^{(i)} - (\vec{M},\vec{N})_{-1n}^{(i)} \tag{A-5}$$

with $\theta = 180°$ representing the backscattering direction and $\theta = 0°$ the forward one. The time-dependent $exp(j\omega t)$ is assumed and suppressed. The superscript (1) in Equs. (A-1) and (A-2) refers to the appearance of the first kind Riccati-Bessel function which is finite at the origin and is therefore used in the incident as well as the interior waves. The fourth kind Riccati-Bessel function $\hat{H}_n^{(2)}(kr)$ appears in the scattered wave expression, since it is outward traveling and is finite at infinity. The scattered fields can be written in the form,

$$\vec{E}^{s} = E_o \sum_{n=1}^{\infty} \left[A_n \vec{m}_{o1n}^{(4)} + jB_n \vec{n}_{e1n}^{(4)} \right] \tag{A-6}$$

and

$$\vec{H}^{s} = E_o/Z_o \sum_{n=1}^{\infty} \left[B_n \vec{m}_{e1n}^{(4)} - A_n \vec{n}_{o1n}^{(4)} \right] \tag{A-7}$$

In the interior, $\vec{E}^{t}$ and $\vec{H}^{t}$ have similar expressions, except that ε_o, μ_o, k are replaced by $\varepsilon'=\varepsilon+\sigma/j\omega$, μ, k', respectively, and the expansion coefficients are C_n, D_n and the eigenfunctions contain Riccati-Bessel functions of the first kind. At the boundary $r = a$ the boundary conditions are given by

$$\hat{r} \times \left\{ \vec{E}^{i} + \vec{E}^{s} - \vec{E}^{t} \right\} = 0 \tag{A-8}$$

$$\hat{r} \times \left\{ \vec{H}^{i} + \vec{H}^{s} - \vec{H}^{t} \right\} = 0 \tag{A-9}$$

which give a set of four equations in the unknowns A_n, B_n, C_n and D_n which can be solved directly.

For the far scattered field, the asymptotic values of the radial function as $r \to \infty$ can be used, and the field components are given by

$$E_{\theta}^{s} = jE_o \cos\phi \frac{\exp(-jkr)}{kr} \sum_{n=1}^{\infty} a_n j^n \left[B_n \frac{dP_n^1(\cos\theta)}{d\theta} + C_n \frac{P_n^1(\cos\theta)}{\sin\theta} \right] \tag{A-10}$$

$$E_{\phi}^{s} = -jE_o \sin\phi \frac{\exp(-jkr)}{kr} \sum_{n=1}^{\infty} a_n j^n \left[B_n \frac{P_n^1(\cos\theta)}{\sin\theta} + C_n \frac{dP_n^1(\cos\theta)}{d\theta} \right] \tag{A-11}$$

where

$$B_n = - \frac{\hat{J}_n'(ka) - \Delta_n \hat{J}_n(ka)}{\hat{H}^{(2)}{}'(ka) - \Delta_n \hat{H}^{(2)}(ka)} \tag{A-12}$$

and

$$C_n = - \frac{\hat{J}_n'(ka) - \delta_n \hat{J}_n(ka)}{\hat{H}^{(2)}{}'(ka) - \delta_n \hat{H}_n^{(2)}(ka)} \tag{A-13}$$

with

$$\Delta_n = \frac{Z_c}{Z_o} \cdot \frac{\hat{J}_n'(k'a)}{\hat{J}_n(k'a)} \tag{A-14}$$

$$\delta_n = \frac{Z_o}{Z_c} \cdot \frac{\hat{J}_n'(k'a)}{\hat{J}_n(k'a)} \tag{A-15}$$

and

$$Z_c = \sqrt{\frac{j\omega\mu}{j\omega\varepsilon + \sigma}} \tag{A-16}$$

A.2 IMPEDANCE BOUNDARY CONDITION SOLUTION:

In this case, only external fields are assumed to exist, and the relation between the tangential field components at $r = a$ are given by an impedance factor. The expressions for the far field components can be obtained from the standard Mie series solution (see, for example, Wait and Jackson [26]) and an application of the boundary conditions of the form

$$\vec{E} - (\hat{r} \cdot \vec{E})\hat{r} = Z_s(\hat{r} \times \vec{H}) \tag{A-17}$$

at the sphere surface with Z_s being the surface impedance. The results for the scattered field components are similar to those given by (A-10) through (A-13) but with Δ_n replaced by (jZ_s/Z_o) and δ_n by (jZ_o/Z_s) in (A-12) and (A-13), respectively.

This result can be obtained directly from the exact solution as a special case. For highly conducting objects for which $|k'| >> 1$, Δ_n become mode independent. In the limiting case of $|k'| >> 1$ and $\mathrm{Im}(k') >> 1$, one may find

$$\hat{J}'_n(k'a)/\hat{J}_n(k'a) \to (j) \tag{A-18}$$

Using this limiting value in Equs. (A-14) and (A-15), the exact solution can be reduced to that of the impedance boundary conditions.

Appendix B

FIELDS RADIATED BY A CIRCULAR CURRENT LOOP

Consider a circular loop of radius c carrying a current I. A general method to obtain its electromagnetic fields is to find the magnetic vector potential $\vec{A}$ and determine the electric and magnetic fields using the following equations:

$$\vec{E} = \frac{-j}{\omega\varepsilon_0} \nabla \times \nabla \times \vec{A} \tag{B-1}$$

and

$$\vec{H} = \nabla \times \vec{A} \tag{B-2}$$

At an observation point (r,θ,ϕ), $\vec{A}$ is given by,

$$\vec{A} = \frac{1}{4\pi} \int_0^{2\pi} \frac{\vec{I}(\vec{r}\,') \exp(-jk|\vec{r}-\vec{r}\,'|)}{|\vec{r}-\vec{r}\,'|} \, dl \tag{B-3}$$

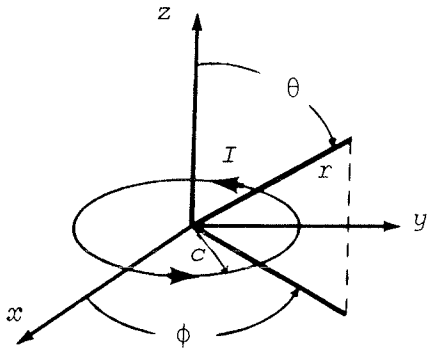

where

$$dl = c \, d\phi' \tag{B-4}$$

$$\vec{I}(\vec{r}\,') = I_{\phi'} \hat{\phi}' = -I \sin\phi' \hat{x} + I \cos\phi' \hat{y} \tag{B-5}$$

and

$$\frac{\exp(-jk|\vec{r}-\vec{r}\,'|)}{|\vec{r}-\vec{r}\,'|} = -kh_0^{(2)}(k|\vec{r}-\vec{r}\,'|) \tag{B-6}$$

where $h_0^{(2)}(x)$ is the ***2nd*** kind spherical Hankel function of argument x and zero order. Substituting the expansion of $h_0^{(2)}(k|\vec{r}-\vec{r}'|)$ given in [75], and using the orthogonality properties of the trigonometric functions $cos(n\phi)$ and $sin(n\phi)$ one finds

$$\vec{A} = A_\phi \hat{\phi} \tag{B-7}$$

where

for $r > c$:

$$A_\phi = \frac{-jI}{2kr} \sum_{n=1}^{\infty} \left[\frac{2n+1}{n(n+1)} \hat{J}_n(kc) \hat{H}_n^{(2)}(kr) P_n^1(cos\theta) \right] \tag{B-8}$$

for $r < c$:

$$A_\phi = \frac{-jI}{2kr} \sum_{n=1}^{\infty} \left[\frac{2n+1}{n(n+1)} \hat{J}_n(kr) \hat{H}_n^{(2)}(kc) P_n^1(cos\theta) \right] \tag{B-9}$$

and $\hat{J}_n(u)$ and $\hat{H}_n^{(2)}(u)$ are the Riccati-Bessel and 2nd kind Riccati-Hankel functions, respectively, and $P_n^1(v)$ is the associated Legendre function [101].

A substitution of Equ. (B-8) in Equ. (B-1) or Equ. (B-2) gives for

$r > c$:

$$E_\phi = \frac{-IZ_o}{2r} \sum_{n=1}^{\infty} \left[\frac{2n+1}{n(n+1)} \hat{J}_n(kc) \hat{H}_n^{(2)}(kr) P_n^1(0) P_n^1(cos\theta) \right] \tag{B-10}$$

$$H_\theta = \frac{jI}{2r} \sum_{n=1}^{\infty} \left[\frac{2n+1}{n(n+1)} \hat{J}_n(kc) \hat{H}_n^{(2)'}(kr) P_n^1(0) P_n^1(cos\theta) \right] \tag{B-11}$$

$$H_r = \frac{-jI}{2kr^2} \sum_{n=1}^{\infty} \left[\frac{2n+1}{n(n+1)} \hat{J}_n(kc) \hat{H}_n^{(2)}(kr) P_n^1(0) \cdot \left(\frac{dP_n^1(cos\theta)}{d\theta} + cos\theta \frac{P_n^1(cos\theta)}{sin\theta} \right) \right] \tag{B-12}$$

The expressions for $r < c$, can be obtained by an interchange of r and c in the arguments of the Riccati functions.

Appendix C

GIBB'S PHENOMENON

In *Section 5.2* a formal series representing an even function $f(t)$ was given. It was in the form of Fourier series and was given by

$$f(t) = A_0 + \sum_{n=1,3,..}^{\infty} A_n \cos(2n\pi t/T) \qquad \text{(C-1)}$$

This expression for $f(t)$ is uniformly and absolutely convergent under the following conditions: 1) $f(t)$ is a continuous function with a period T, 2) $f(t)$ is a piecewise continuous in the interval $[-T/2, T/2]$, and 3) $f(-T/2.) = f(T/2)$.

Since the incident wave-form used in *Chapter Five* is a pulse train, we shall examine the limit of the finite summation in Equ. (C-1) at a point of its discontinuity. Let

$$S_N = A_0 + \sum_{n=1,3,..}^{N} A_n \cos(2n\pi t/T) \qquad \text{(C-2)}$$

The function $S_N(t)$ is shown in Fig. C.1. With increasing N, only the time scale changes while the ripple remains. This behaviour of $S_N(t)$ near a discontinuity of $f(t)$ is called Gibb's phenomenon.

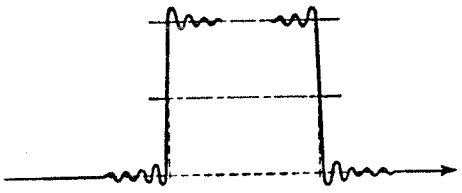

Figure C.1: The oscillatory decay which characterizes the Gibb's phenomenon.

In the limit as $N \to \infty$, these ripples are compressed into a single vertical line at the point of discontinuity. For large, but finite values of N, the overshoot with the adjacent ripples occupies a negligible space in the fundamental range, so that practically speaking one may say that no residual discrepancy between the series and the function remains. Nevertheless, from a mathematical standpoint the phenomenon is worth noticing, since it illustrates the failure of the series in approaching its ideal form in the limit as $N \to \infty$.

It must be admitted, of course, that a discontinuity in the function $f(t)$ offers an extreme test of the partial sum $S_N(t)$ to approximate this function. In other words, for a continuous function, the partial sum $S_N(t)$ with the same number of terms yields a vastly improved degree of approximation.

EXAMPLE

An RL circuit is shown in Fig. C.2 with an applied voltage $v(t)$. For simplicity let $v(t)$ be a single pulse of width $t_o = T/2$.

Direct Solution:

The voltage across the inductor is given by

$$v_l^{(d)}(t) = L \frac{di(t)}{dt} \qquad \text{(C-3)}$$

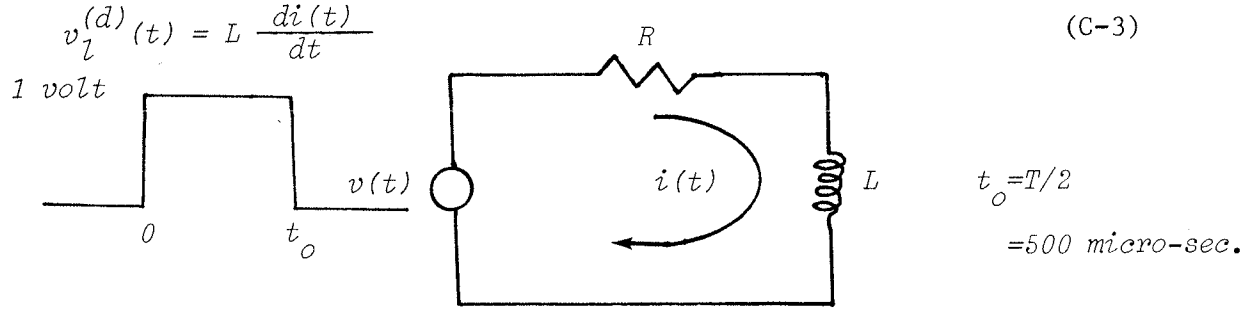

Figure C.2: RL circuit with pulse excitation.

where the current $i(t)$ is given by the transformation

$$I(s) = \frac{V(s)}{R + sL} \tag{C-4}$$

where

$$V(s) = 1/s \cdot [\ 1 - exp(-t_o s)\ ] \tag{C-5}$$

Using inverse Laplace transformation of Equ. (C-4) yields

$$i(t) = 1/R \left([\ 1 - exp(-R/L\ t)\ ]\ u(t) - [\ 1 - exp(-R/L(t-t_o))\ ]\ u(t-t_o) \right) \tag{C-6}$$

$$v_l^{(d)}(t) = exp(-R/L\ t)\ u(t) - exp(-R/L(t-t_o))\ u(t-t_o) \tag{C-7}$$

Series Solution:

A good approximation for the input voltage is given by

$$v(t) = Re \sum_{n=1}^{N} A_n\ exp(-jn\omega_o t) \tag{C-8}$$

where N is finite. The approximation to $v_l^{(s)}(t)$ is obtained from

$$v_l^{(s)}(t) = Re \sum_{n=1}^{N} \frac{jn\omega_o L}{jn\omega_o L + R}\ A_n\ exp(jn\omega_o t) \tag{C-9}$$

The above derivation has been conducted in terms of one pulse, but the results are easily extended to the case of periodic rectangular pulses. Fig. C.3 presents $v_l^{(d)}(t)$ and $v_l^{(s)}(t)$ for a periodic rectangular excitation wave. It is clear from the extended scale (i.e.,

using very fine increments for t), that $v_l^{(s)}(t)$ is oscillating at the initial and final parts of the pulse. It is interesting to note that, although $v_l^{(s)}(t)$ has the same order of oscillation at the beginning and end of the pulse, the effect on $v_l^{(s)}(t)$ is less near the end. This is because of the finite number of terms which has been used in Equ. (C-8), which means neglecting the higher order harmonics that contribute to the initial part.

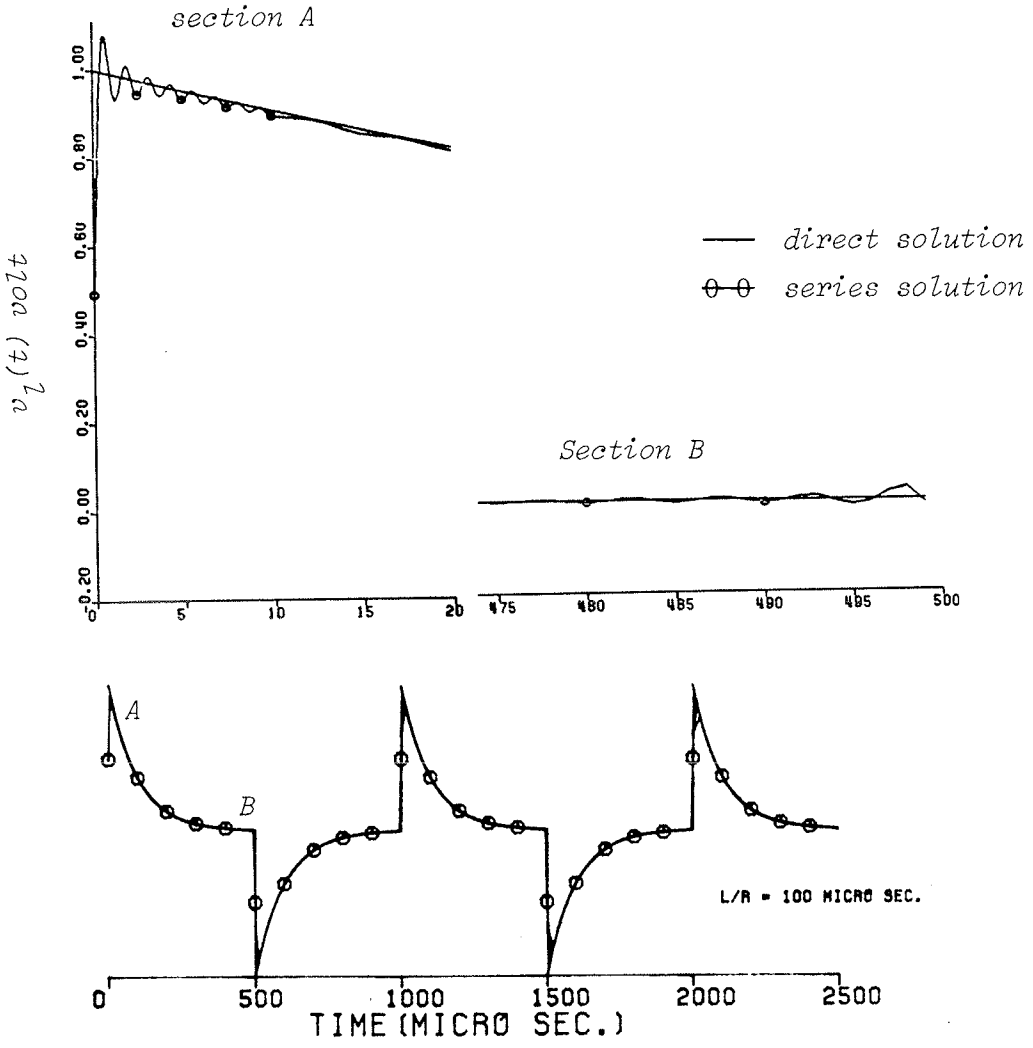

Figure C.3: Induced voltage across L for a pulse train excitation.

Appendix D

SYMBOLS

Unless otherwise stated, the symbols most commonly used in this thesis have the following meaning.

α	orientation angle of spheroid,
	scalar introduced on page 30,
δ	skin depth, signal penetration level,
∇	gradient operator,
$\nabla_s \cdot$	surface divergence operator,
∇X	curl operator,
ε	permittivity of body material $(\varepsilon = \varepsilon_r \varepsilon_o)$,
ε_o	permittivity of free space,
ε'	complex permittivity of body material
ε_r	stands for $(\varepsilon/\varepsilon_o)$,
Ψ	magnetic scalar potential,
κ_u, κ_v	principal curvatures,
λ	wavelength in free space,
μ	permeability of body material,
μ_o	permeability of free space,
μ_r, MUR	stands for (μ/μ_o) ,
Φ	electric scalar potential,
ρ, ϕ, z	circular cylindrical coordinates,
σ	conductivity of body material,
τ	retarded time,

ω	(angular) frequency,
ω_o	(angular) fundamental frequency,
$\theta, \theta^i, \phi, \phi^i$	polar angles,
$\|Q\|$	magnitude of Q,
$\int\!\!\!\!\!\!-$	Cauchy principle value integral of,
a, a, A	radius of sphere, semi-major axis of spheroid,
$\vec{A}$	electric vector potential,
AL	aluminum,
ALPHA	angle between spheroid semi-major axis and y axis,
a_{mn}, b_{mn}	expansion coefficients
b, B	semi-minor axis of spheroid,
CFIE	abbreviated form for combined field integral equation,
DR	z coordinate of receive loop center,
DT	z coordinate of transmit loop center,
EFIE	abbreviated form for electric field integral equation,
$\vec{E}^i$	incident electric field,
Equ(s).	stands for equation(s),
$\vec{E}^s$	scattered electric field,
$\vec{F}$	magnetic vector potential,
Fig(s).	stands for figure(s),
G	free space Green's function,
$\vec{H}^i$	incident magnetic field,
$\vec{H}^s$	scattered magnetic field,
IBC	abbreviated form for impedance boundary condition(s),
Im	imaginary part of,
j	square root of (-1),
$\vec{J}$	effective electric surface current,

J_u, J_v u and v components of $\vec{J}$,

k wavenumber in free space,

k' wavenumber in body material,

$\vec{M}$ effective magnetic surface current,

MFIE abbreviated form for magnetic field integral equation,

MV,mv millivolt

$\hat{n}$ outward unit normal to a scatterer surface,

N number of segments along a generating curve,

number of patches on a surface,

R distance between source point r' and observer point r,

Re real part of,

RR radius of receive loop,

RT radius of transmit loop,

S,S scattering cross section,

So, S_o stands for surface of body material,

ST steel,

S/m siemens per meter,

t time,

$\hat{t}, \hat{t}_1, \hat{t}_2$ surface unit vectors,

x,y,z rectangular Cartesian coordinates,

Z_o characteristic impedance of free space,

Z_s, Z_c surface impedance of body material,

$\bar{\bar{Z}}$ impedance dyadic,

$v(t), V(T)$ induced voltage in a receive loop,

V_{rms} root-mean-square of $v(t)$ or $V(T)$.